READING BETWEEN THE LINES OF THE DUPLEX THEORY

THE IMPACT OF RELATIVE SPIKE TIMING ON SPATIAL CODING MECHANISMS IN LOW AND HIGH FREQUENCY NEURONS OF THE AUDITORY BRAINSTEM

Barbara Beiderbeck

Graduate School of
Systemic Neurosciences
LMU Munich

Dissertation at the
Graduate School of Systemic Neurosciences
Ludwig-Maximilians-Universität München

January, 2022

1st Supervisor
PD Dr. Michael Pecka
Department Biology II
Division of Neurobiology
Ludwig-Maximilians-University Munich

2nd Supervisor
Prof. Dr. Benedikt Grothe
Department Biology II
Division of Neurobiology
Ludwig-Maximilians-University Munich

First Reviewer: PD Dr. Michael Pecka
Second Reviewer: Prof. Dr. Christian Leibold
External Reviewer: PD Dr. Thomas Künzel

Date of Submission: 11th January 2022
Date of Defense: 16th March 2022

Table of Contents

Abstract

Back in 1907, Lord Rayleigh suggested in his pioneering studies that interaural level differences (ILDs) are used for the localization of high frequency sounds and interaural time differences (ITDs) are used for localization of low frequency sounds (Rayleigh 1907) which was later termed the 'Duplex theory' in sound localization. Over the last century, the duplex theory came up against its limits with the presence of ILDs between low frequency sounds in the near-field and ITDs in the envelope of modulated high-frequency sounds. The goal of this doctoral thesis was to further read between the lines of the Duplex theory by studying in study 1 the role of precisely-timed inhibition in the LSO (lateral superior olive), a nucleus in the auditory brainstem of mammals that is equipped to decode ILDs and on the other hand in study 2 to study the role of effective envelope information (created through non-linear cochlear filtering) in low frequency MSO (medical superior olive) neurons, another nucleus in the auditory brainstem of mammals that is well-known for its modulation by ITDs. In the LSO, by disentangling amplitude effects from effects specifically related to input timing, we demonstrate that the timing of inhibition controls spiking with microsecond precision throughout high frequency click trains, resulting in input timing-specific modulation of neuronal output. Furthermore, our data reveal that spiking is facilitated when contralateral inputs are functionally leading excitation within a precise time window. Importantly, our data suggest that post-inhibitory facilitation (PIF) can support ILD maintenance when excitatory inputs are weak. In addition, *in vitro* whole-cell recordings in mature LSO neurons confirm a reduction in the firing threshold due to prior hyperpolarization giving rise to PIF of otherwise sub-threshold synaptic events. This facilitatory effect based on microsecond precise differences between excitation and inhibition could therefore promote spatial sensitivity of faint sounds. In study 2, since low frequency neurons in the MSO are sensitive to both fine structure and effective envelopes, our goal was to disentangle the contribution of effective envelopes and stimulus fine structure on ITD sensitivity through methodological post-hoc analyses. In order to identify the impact of effective envelopes (ergo the "effective energy" within the spectral content) we presented a battery of frozen broadband noise stimuli at various ITDs. Specifically, these stimuli share the same spectral contents (i.e., same carrier frequencies) but vary in their respective envelopes (i.e., their

amplitude fluctuations across the stimulus). Our data reveal that the interplay of effective envelopes and temporal fine structure of the stimulus not only impacts relative spike timing but also dynamically affects overall ITD sensitivity in low frequency MSO neurons. Importantly, each event within the effective envelope that the neuron responds to (i.e., fast energy rise within the relevant sound spectrum with regard to the neuron's tuning) can contain a unique spectral composition. Since it is unlikely that all four functional inputs to the MSO exhibit identical tuning, the strength of individual functional inputs to the MSO and therefore the underlying coincidence mechanism can vary between events. Interestingly, within each stimulus, we were able to identify specific events where spike timing was neatly matching the temporal displacement of the monaural envelope across ITDs. The findings of this study show that effective envelopes play a crucial role for binaural integration in low frequency MSO neurons with strong evidence for its regulation through pre- and short-time adaptation which suggests that the tuning of relative inputs (inhibition/excitation) could be individually adapted across the stimulus. Specifically, we detected spiking phenomena in MSO neurons that can be attributed to effects of preceding inhibition similar to our findings for the LSO.

1 Introduction

While the visual system allows parallel processing of spatial information along retinal receptor cells, sound localization in mammals does not arise from a direct relationship between the external location of a sound source and the sensory receptive fields that ultimately react to the physical features of the sound wave itself, e.g., to its intensity, entailed frequencies/envelope, onset and duration.
Sound localization therefore implies a considerable computational challenge for the mammalian brain and depends on monaural and binaural information.

1.1 Sound localization in the horizontal plane and the Duplex Theory of binaural hearing

"That child will either be very clever or be an idiot." - John Holden Strutt on seeing his first grandson (John William Strutt, Lord Rayleigh)

Inter alia, mammals can compare differences in the movement of the two eardrums to localize sound in the horizontal plane. In simple terms, there are two major interaural differences of the physical dimensions of the acoustic stimulus that can be encoded binaurally:

1. The head can create an acoustic shadow that attenuates the sound pressure wave when it travels to the further ear, which results in amplitude differences of the acoustic stimulus between the two ears, the so-called interaural level differences (ILDs) (Fig. 1a). However, since the head functions as a low-pass filter, the magnitude of such ILDs strongly depends on the spectral content of the stimulus. Wavelengths that are equal to or shorter than the diameter of the head are individually affected by the shadowing effect of the head. On the other hand, low-frequency sounds can travel around the head nearly unhindered, creating only a small ILD that becomes negligible. The attenuating effect, by inference, depends on the head size: the smaller the head size, the higher the cut-off frequency for ILD-detection.
2. If a sound source is off midline, the sound pressure wave has further to travel to reach the far ear than the near ear. The result is a difference in the arrival of the sound at the two ears, the so-called interaural time difference (ITD) (Fig 1b).

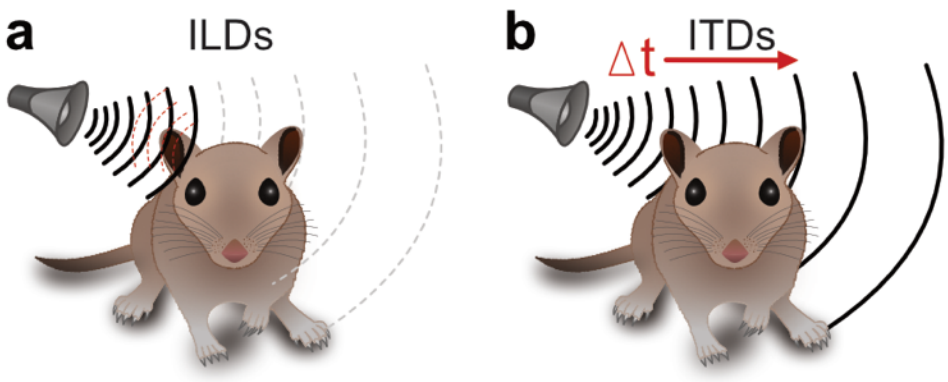

Figure 1: Sensitivity to ILDs and ITDs.
a The acoustic head shadow produces location-specific ILDs between the ears
b ITDs are defined by the time that a sound pressure wave takes to travel from one ear to the other.

This has been experimentally observed around 150 years ago, amongst others by the British physicist and future Nobel Laureate John William Strutt, known as Lord Rayleigh. In his first lecture “on the perception of sound direction” in 1876 he proposed the use of ILDs as the “binaural ratio” for sound localization. At this time, it was considered that ITDs were too small to be detected by the auditory system. The breakthrough began with the work of Thompson (1878) using mistuned low-frequency forks demonstrating that small interaural phase differences were indeed detectable and contradicting the ‘acoustic law’ by Ohm and Helmholtz that suggested the ear to be “phase insensitive”. Nearly 30 years later in 1907, Lord Rayleigh re-evaluated the binaural cues for sound localization and argued that ILDs are used for the localization of high frequency sounds and ITDs are possibly used for the localization of low frequency sounds (Rayleigh 1907). This theory that was later called the “duplex theory” was further validated by other scientists at this time (Moore and Fry 1907; Klemm 1920; von Hornbostel and Wertheimer 1920; Stevens and Newman 1936). Today, we know that the classic view of the duplex theory has its limitations, e.g. with regard to ILDs of low frequency sounds in the near-field (Shinn-Cunningham, Santarelli, and Kopco 2000) as well as ITDs in the envelope of modulated high frequency sounds (Bernstein and Trahiotis 1985). Nevertheless, the duplex theory is still cited as a backbone of sound localization in various textbooks and publications.

1.2 From mechanical energy to electrical potentials

Georg von Békésy's replies in a questionnaire sent to him by the Academy of Science 1956:
"Major interest?" – "Art."
"Major influences which determined the selection of your particular field of science?"
– "Pure accident."

In order to encode ITDs and ILDs in the brain acoustic signals need to be converted into electrical potentials, the neuronal readout.

A sound pressure wave is generated by back-and-forth vibrations of small molecules in the air resulting in high-pressure regions where particles are densely packed (compressions) and low-pressure regions (rarefactions) where particles are spread apart. Furthermore, the sound pressure wave is mainly characterized by 3 dimensions: its frequency components (the number of cycles per second in the vibrations), its intensity (which reflects how densely packed the molecules are during compression), and its duration (from long pure tones or noise bursts to transients like clicks). The information about these dimensions needs to be transferred through the ear into the brain with maximal precision to provide detailed ITD and ILD information. The ear consists of three major departments: The outer ear (including the tympanic membrane), the middle ear (air-filled) and the inner ear (fluid-filled). When sound waves are funnelled into the ear canal they impinge onto the tympanic membrane. The thin and filigree membrane is thereby picking up the vibrations of the sound pressure wave which are further conducted by the middle ear bones. When sound is transmitted from one medium to another (here from the air-filled middle ear to the fluid-filled inner ear), the transfer of sound energy needs to be maximized to prevent reflection at the surface of the new medium. The middle ear bones act as highly specialized levers guiding the pressure wave towards the oval window that has a smaller surface area than the tympanic membrane. Since pressure is equal to force over area the pressure increases maintaining optimal signal transmission to the new fluid-filled medium of the inner ear (impedance matching). The cochlea, which is coiled around a central axis, is a fluid filled bony structure within the inner ear divided into several compartments by a membranous structure, the cochlear duct. The bottom layer of the cochlear duct, the so-called 'basilar membrane' is narrow at the base (where the pressure wave enters the cochlea through the oval window) and becomes broader towards the tip of the cochlear (the apex), while its stiffness and thickness decreases with further

distance from its base (Wever et al. 1971; Webster and Webster 1980; Naidu and Mountain 2007; Hudspeth 1985). Vibrations propagate along the basilar membrane from the base to the apex in the form of a traveling wave that oscillates at the frequency of stimulation, but not as a simple sinusoidal wave. The amplitude changes as it traverses along the basilar membrane and where it is highest depends on the frequency of the stimulus and the stiffness along the length of the basilar membrane (von Békésy 1947). Hence, the basilar membrane is a set of mechanical filters along its longitudinal axis with each filter having its own resonance frequency. In simple terms, the basilar membrane acts as a frequency spectrum analyzer: For high frequencies, the basilar membrane resonates at the base, and for low frequencies the basilar membrane resonates at the apex (Zhang et al. 2007). Realistically, natural stimuli contain numerous frequency components and will therefore lead to complex vibrations on several sites along the basilar membrane at once resulting in entirely different filtered waveforms depending on the characteristic frequency filter band at different cochlear sites. The mechanical force that is generated by the displacements of the basilar membrane is transduced into electrical signals by inner and outer hair cells, a group of cells that is located on top of the basilar membrane (Hudspeth 1989). The deflection of their ciliary bundles during basilar membrane vibration leads to ion-influx into the cells resulting in a flow of transducer current (Hudspeth 1982; Denk et al. 1995). The generated receptor potential in outer hair cells causes the cell to contract at the frequency of the basilar membrane oscillation, providing active mechanical amplification to the system (Brownell et al. 1985). Generated potentials in inner hair cells facilitate the release of neurotransmitters at their synaptic end enabling the generation of action potentials (APs) that are transmitted into the brain through auditory nerve fibers (ANFs) (Russell and Sellick 1978; Dallos 1985; Dallos, Santos-Sacchi, and Flock 1982) with firing rates of up to 300 Hz (Rose et al. 1967; Kiang 1965; Johnson 1980). In dependency on the capacitance and resistance of the hair cell membrane (Palmer and Russell 1986) it has been shown that ANFs lock their impulses to a preferred phase range within a pure tone cycle (Rose et al. 1967). Such phase-locking to pure tones has been shown for frequencies up to 1000 Hz were phase-locking becomes progressively more inaccurate (Kiang 1965; Johnson 1980; Palmer and Russell 1986). Beyond that, ANFs can phase-lock to the envelope of high-frequency sounds for modulation frequencies up to 250 Hz (Dreyer and Delgutte 2006).

1.3 The auditory brainstem

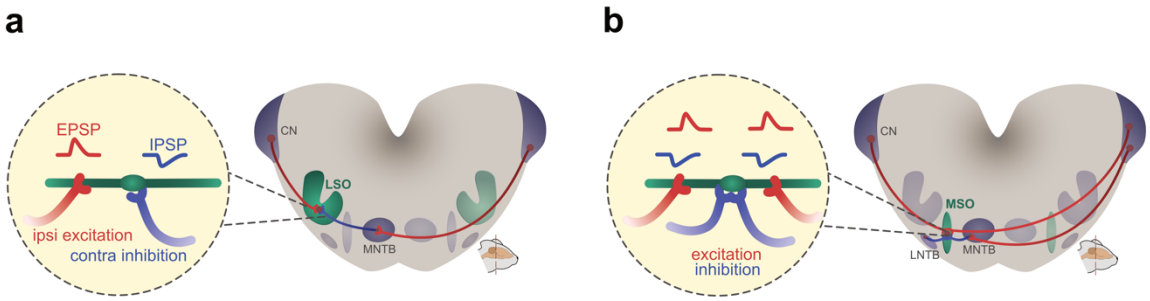

Figure 2: Projections to the Medial and Lateral Superior Olive.
Computation in both the Lateral Superior Olive (LSO) and Medial Superior Olive (MSO) involve gauging of relative excitatory and inhibitory postsynaptic potentials (EPSPs and IPSPs):
a Neurons in the LSO receive excitatory input from neurons in the ipsilateral cochlear nucleus (CN) and indirect inhibitory input from neurons in the contralateral CN via the ipsilateral Medial Nucleus of the Trapezoid Body (MNTB).
b Neurons in the MSO receive binaural excitatory input from neurons in the ipsilateral and contralateral CN and binaural inhibitory input from neurons in the ipsilateral Lateral Nucleus of the Trapezoid Body (LNTB) and indirectly from neurons in the contralateral CN via the ipsilateral MNTB.

1.3.1 From monaural to binaural innervation

Carrying the electrical output from inner hair cells, auditory nerve fibers root in the cochlear nucleus (CN) – the first brain structure of the auditory pathway (De No 1933). The CN is subdivided into several compartments comprising several neuronal subtypes with different morphology and temporal discharge patterns (Oertel 1999; Rhode and Smith 1985; Osen 1969; Cant and Morest 1984). One important group of cells in the CN for sound localization in the horizontal plane are the bushy cells (Schofield and Cant 1991; Smith et al. 1991; Smith, Joris, and Yin 1993). This group is further subdivided into two types: Spherical bushy cells (SBCs) and globular bushy cells (GBCs). SBCs receive their inputs through the endbulbs of Held (first described by Hans Held in 1893), huge nerve endings of about three myelinated ANFs per cell (Brawer and Morest 1975; Ryugo and Fekete 1982; Ryugo and Sento 1991). On the other hand, terminals that contact GBCs are smaller modified endbulbs comprising inputs of between 4 and 40 ANFs per cell (Tolbert, Morest, and Yurgelun-Todd 1982;

Smith and Rhode 1987; Ostapoff and Morest 1991; Nicol and Walmsley 2002). Both SBCs and GBCs transmit the temporal features of their inputs with high precision which is essential for coupling neuronal activity to acoustic events such as amplitude modulation and sound localization cues. The response patterns of SBCs and GBCs are similar to the discharge pattern of ANFs (that exhibits a pronounced onset followed by rapid adaptation): SBCs exhibit a pure primary-like response pattern, GBCs exhibit a sharp onset followed by a notch and a rapidly adapting response (‘primary-like with notch response) (Rhode and Smith 1986). Interestingly, by collecting phase-locked input from several ANFs, firing in bushy cells is even more temporally aligned and more consistent compared to ANF responses (Joris, Smith, and Yin 1994; Joris et al. 1994; Joris et al. 2006; Wever and Bray 1930; Joris and Smith 2008).

It follows that bushy cells are the bottleneck feeding temporally precise monaural inputs into the superior olivary complex (SOC), a complex that is located on each hemisphere of the auditory brainstem.

As mentioned before, the duplex theory (i.e., the spectral segregation for the use of ITDs and ILDs) was widely accepted, and scientists have been searching for the anatomical and physiological basis of two parallel pathways that are thought to encode ITDs and ILDs. Early anatomical studies revealed two prominent structures of the SOC as the first major site for convergence of binaural information in the ascending auditory pathway: The Medial Superior Olive (MSO) and the Lateral Superior Olive (LSO).

1.3.2 The Medial Superior Olive

The MSO comprises a thin sheet of cells with a predominantly bipolar morphology characterized by two distinct dendrites facing into opposite directions (Ollo and Schwartz 1979; Rautenberg, Grothe, and Felmy 2009; Scott, Mathews, and Golding 2005; Smith 1995). SBCs from both sides provide binaural, glutamatergic inputs with axon terminals ending on the closer dendrite of either side respectively (Stotler 1953; Goldberg and Brown 1968; Lindsey 1975; Cant and Casseday 1986; Yin and Chan 1990; Smith, Joris, and Yin 1993) (Fig. 2b). Consequently, most neurons in the MSO exhibit an ‘EE’-type response phenotype. In 1969, Goldberg and Brown found that the output of MSO neurons can be modulated by differences in the relative phase of low frequency tones (they found most MSO neuros to be tuned to low frequencies below

1 kHz) (Goldberg and Brown 1969). They argued their findings could have parallels with a hypothetical model by Jeffress (Jeffress 1948). In ‘line’ with this model, MSO neurons could be regarded as coincidence detectors, firing maximally when receiving bilateral information simultaneously resulting in a peak-shaped rate curve as a function of ITD. The model explains that coincidence is established by precise setups of bilateral delay lines within each frequency channel with systematically varying relative axonal conduction times compensating for distinct ITDs respectively. Since the system is based on hardwired settings, the model predicts that maximal neuronal activity at certain ITDs can directly be converted into a map of auditory space.

However, it was shown for small mammals that the peaks of the ITD functions (best ITDs) are typically clustered at contralateral leading ITDs outside their physiologically relevant range (McAlpine, Jiang, and Palmer 2001; Hancock and Delgutte 2004; Pecka et al. 2008) (Fig. 3).

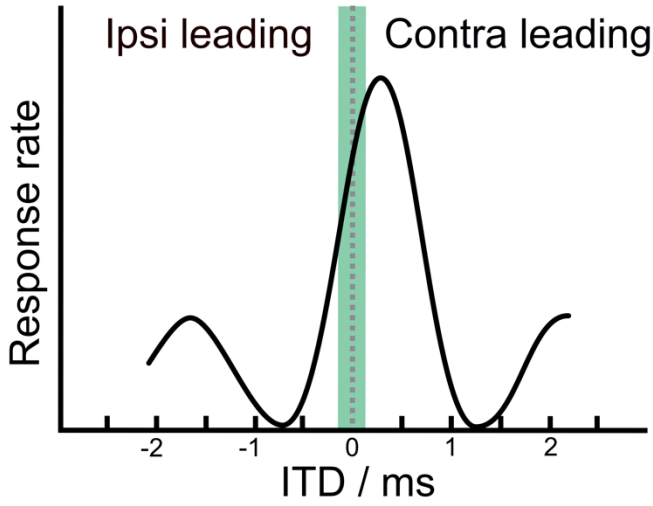

Figure 3: Schematic ITD function. ITD Tuning function of a neuron in the MSO. The peak of this function is typically positioned at contra-leading ITDs outside the physiological range of the animal (green-shaded area).

Applying Jeffress’ model, this would mean that they map ITDs that are much larger than the required time for a sound pressure wave to travel from one ear to the other (for gerbils +/- 120 µs (Maki and Furukawa 2005; Brand et al. 2002)). Furthermore, it was shown, that best ITDs systematically increased with decreasing characteristic frequencies (CF) (McAlpine, Jiang, and Palmer 2001; Brand et al. 2002; Hancock and Delgutte 2004). More specifically, best ITDs were found to be approximately equivalent to an interaural phase difference (IPD) of 45° with respect to the neuron’s individual CF (Brand et al. 2002; McAlpine and Grothe 2003). Taken together, peak

ITDs appear to be restricted to a narrow ITD-range often outside of the physiological range which is different from the theoretical model by Jeffress, suggesting a full 'spatial map' represented by distinct peak responses per ITD within each frequency channel. Interestingly, the dependency of best ITD on CF causes the slope of the ITD function rather than its peak to be positioned near midline ITDs within the physiological range (regardless of the neuron's CF). In other words: The greatest change in discharge rate per ITD and therefore the greatest sensitivity to the change in ITD falls within a range that mammals are most probable to experience.

These findings lead to a controversy about Jeffress' model based on peak responses of narrowly tuned neurons and suggests a rate code strategy based on two broadly tuned orthogonal channels in each brain hemisphere (one MSO per hemisphere) (McAlpine, Jiang, and Palmer 2001; Pecka et al. 2008).

However, it remains puzzling how the causal relationship between CF and best ITD is constructed.

1.3.3 Glycinergic inhibition in the MSO

Apart from excitatory inputs, early studies have also revealed that the MSO is additionally influenced by inhibition (Goldberg and Brown 1969; Yin and Chan 1990) which may have important implications for ITD tuning:

MSO neurons receive ipsilateral input from a group of periolivary cells known as the Lateral Nucleus of the Trapezoid Body (LNTB) (Kuwabara and Zook 1992; Grothe and Sanes 1993) as well as inputs from principle cells in the ipsilateral Medial Nucleus of the Trapezoid Body (MNTB) (Cant and Hyson 1992) (Fig. 2b). LNTB and MNTB neurons receive excitatory projections from GBCs. Whilst LNTB neurons receive GBC inputs from the same hemisphere, the MNTB is innervated by GBCs from the contralateral side, therefore providing indirect contralateral inputs to the MSO. The output of LNTB and MNTB neurons is glycinergic (Adams and Mugnaini 1990; Spirou and Berrebi 1997) and elicits inhibitory postsynaptic potentials (IPSPs) in MSO neurons (Grothe and Sanes 1993; Magnusson et al. 2005; Chirila et al. 2007; Couchman, Grothe, and Felmy 2010; Fischl et al. 2012).

It was shown that contralateral IPSPs can develop at MSO cell somata slightly earlier than contralateral excitatory postsynaptic potentials (EPSPs) despite the longer

anatomical pathway and the additional synapse at the MNTB (Grothe and Sanes 1994; Grothe and Park 1998; Dodla, Svirskis, and Rinzel 2006; Roberts, Seeman, and Golding 2013). By iontophoretically blocking glycinergic inputs *in vivo*, firing rates in fact increased at the left-hand slope of the ITD function, shifting the maximal firing rates towards zero and moving the slope away from the physiological range (Brand et al. 2002; Pecka et al. 2008). It was therefore suggested that the temporal margin of inhibition is able to delay the net excitation (Myoga et al. 2014) therefore setting a delayed time window for neuronal excitability.

Together, these findings suggest strong evidence that temporal interactions between excitation and inhibition are critical for ITD processing and became an important game changer in the debate on MSO processing.

However, the fact that the MSO receives both inhibition and excitation from each side complicates the interpretations of *in vivo* data, resulting in controversial discussions about the underlying mechanisms (Brand et al. 2002; Pecka et al. 2008; Roberts, Seeman, and Golding 2013; van der Heijden et al. 2013; Franken, Bremen, and Joris 2014; Myoga et al. 2014; Plauška, Borst, and van der Heijden 2016).

1.3.4 The MNTB – “fires faster than its shadow”

Despite the longer contralateral pathway and the additional synapse at MNTB principal neurons, inhibitory inputs can arrive slightly earlier at the MSO than excitatory inputs. This is the result of highly specialized adaptations (Joris and Trussell 2018; Borst and Soria van Hoeve 2012) that contribute to reliable, fast and temporally precise signaling at the calyx of Held synapse:

Strong myelination and well defined internodal lengths allow for high conduction velocities in GBC axons that terminate in the MNTB (Morest 1968; Ford et al. 2015). Most principle neurons in the MNTB are contacted by a single, giant terminal, the calyx of Held that was first described by the neuromorphologist Hans Held (Held 1893). There is a high number of Na^+ channels at the last axonal heminode with a negative activation voltage that contributes to fast repolarization following calyceal APs allowing for high sustainability (Kim, Kushmerick, and von Gersdorff 2010; Leão et al. 2005). Additionally, a whole battery of low-threshold activated K^+ channels not only assists to maintain the resting potential (Huang and Trussell 2011) but also prevents firing during repolarization and therefore contributes to high temporal fidelity (Ishikawa et al. 2003).

The synapse is driven by a large number of vesicle releases (up to 100 vesicles per AP) (Borst and Sakmann 1996) that give rise to suprathreshold glutamatergic EPSPs (Banks and Smith 1992; Forsythe and Barnes-Davies 1993). A single calyceal input is sufficient to trigger an AP in MNTB principle neurons which minimizes the jitter in the arrival time in comparison to multiple inputs (Borst and Soria van Hoeve 2012). On the postsynaptic side, MNTB neurons express distinct sets of potassium channels to promote short APs and high frequency firing: KV1 channels suppressing multiple firing in response to a giant calyceal EPSC (Forsythe 1994; Dodson, Barker, and Forsythe 2002), KV2 channels support the recovery of inactivated Na^+ channels during repetitive spiking (Johnston et al. 2008) and KV3 channels minimizing AP duration (Wang et al. 1998). MNTB neurons show a minimum response latency of 3-5 ms which is only slightly longer than their precursors in the CN (Grothe and Sanes 1994; Grothe and Park 1998; Smith, Joris, and Yin 1998; Kopp-Scheinpflug et al. 2008; Roberts, Seeman, and Golding 2013; Sommer, Lingenhöhl, and Friauf 1993) and they exhibit temporally reliable and sustained firing rates in a phase-locked manner (Pecka et al. 2008; Franken et al. 2015; Goldwyn et al. 2017) up to 300 Hz (Spirou, Brownell, and Zidanic 1990; Kopp-Scheinpflug et al. 2008; Lorteije et al. 2009; Sonntag et al. 2009). Glycinergic projections to the MSO originating in the less studied LNTB are suggested to be less temporally precise than inputs from the MNTB (Roberts, Seeman, and Golding 2014).

1.3.5 The ‘textbook’ ILD processor

Rayleigh argued that ITDs are possibly used for the localization of low frequency sounds and ILDs are used for the localization of high frequency sounds (Rayleigh 1907). As outlined in section 3.2, the MSO was found to cover ITD processing of low frequency sounds leaving the question how the ‘ideal’ ILD processor could look like to complete the physiological manifestation of the duplex theory.

ILDs result from relative frequency-dependent modifications of a sound that are predominately based on the ‘shadowing’ effect of the head and possible amplifications by the specialized anatomical properties of the pinna to optimally tunnel sound towards the eardrum (Wiener, Pfeiffer, and Backus 1966; Phillips et al. 1982; Irvine 1987). A neuronal correlate of an acoustic ILD cue therefore requires a binaural structure that subtracts the relative inputs from either side.

1.3.6 The Lateral Superior Olive: Why it is not a 'textbook' ILD integrator

Such a neuronal correlate for binaural subtraction was suggested to be present in the LSO, predominantly enclosing high frequency neurons (Guinan, Norris, and Guinan 1972; Tsuchitani 1977; 1997). Principle neurons in the LSO receive a subset of the same excitatory and inhibitory inputs as the MSO: They receive direct ipsilateral inputs by glutamatergic terminals from the ipsilateral SBCs and indirect contralateral inputs by glycinergic terminals of the ipsilateral MNTB (Stotler 1953; Harrison and Warr 1962; Warr 1966; Browner and Webster 1975; Cant and Casseday 1986; Cant and Hyson 1992) (Fig. 2b) generating excitatory and inhibitory postsynaptic potentials respectively (Finlayson and Caspary 1989; Caspary and Faingold 1989; Sanes 1990; Wu and Kelly 1991; Glendenning et al. 1991). LSO neurons exhibit a sigmoidal discharge rate along the ILD axis (Boudreau and Tsuchitani 1968; Tsuchitani and Boudreau 1969) (Fig. 4): They fire maximally when glutamatergic inputs are strong (given by acoustic stimuli located on the ipsilateral side) and minimally when APs are maximally suppressed by glycinergic inhibition (given by sound sources located on the contralateral side), allegorizing inhibition as the neural equivalent of 'subtraction'.

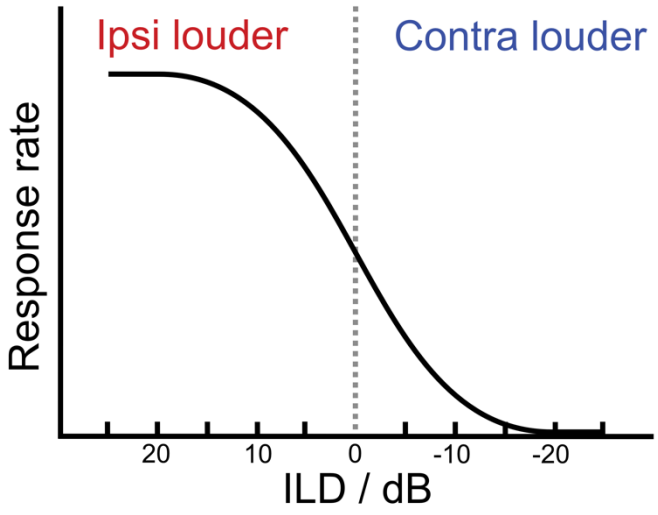

Figure 4: Schematic ILD function. Neurons in the LSO respond maximally when acoustic stimuli are loud on the ipsilateral side in comparison to the contralateral side and vice versa, LSO neurons are maximally suppressed when acoustic stimuli are in relation louder on the contralateral side.

At first sight, this renders the LSO to be the 'ideal' candidate for ILD processing. However, the anatomical and functional properties of the LSO pathway do not fully account for simple gauging of relative spike rates. Relative intensity differences encoded as relative neuronal activity is an integral quantity. Therefore relative

subtraction would require a temporal integration window of several ms (Brown and Tollin 2016). By theory, such timeframes would not require the existence of a highly temporally reliable calyx of Held (discussed in 3.4).

Additionally, the precursor cells to the LSO exhibit a temporally precise and reliable onset response. However, at high frequencies, they exhibit rather low firing rates with primary-like (SBCs) or primary-like with notch responses (GBCs, MNTB) and increased spontaneous activity (Smith, Joris, and Yin 1998) providing a stochastic nature for neuronal subtraction that could not account for experimentally determined limits of ILD sensitivity ranging from 0.5 to 4 dB (Yost and Dye 1988; Tollin, Koka, and Tsai 2008). Moreover, recent *in vivo* patch clamp findings have shown that LSO principal cells exhibit transient responses characterized by onset firing and it has been revealed that their ILD-sensitivity is restricted to the stimulus onset (0-10 ms) whilst being absent in the ongoing segment of the stimulus (Franken, Joris, and Smith 2018). The outcome of this study raises doubts about the long believed integrating role of LSO principal cells over longer time periods.

Interestingly, the comparison of the timing of the excitatory and inhibitory inputs in the LSO is an integral part of ILD computation: In theory, ILDs can be regarded as relative energy per time interval. This energy is reflected by amplitude modulations of the physical stimulus, i.e., the instantaneous envelope of the stimulus. Such instantaneous differences in energy entail a change in the relative arrival times of the respective inputs at the LSO (Grothe and Park 1995; Park et al. 1996). This phenomenon has been described as the so-called latency hypothesis (Jeffress 1948; Yin, Hirsch, and Chan 1985; Pollak 1988; Tsuchitani 1988; Irvine, Park, and Mattingley 1995; Joris and Yin 1995). These internal level-to-time conversions include stimulus dependent temporal changes of synaptic potentials: An increase in the stimulus amplitude gives rise to synaptic potentials with steeper slopes and shorter latencies (Sanes 1990).

The latency shifts of synaptic inputs can vary by ~1 ms / 10 dB at stimulus onset (Park et al. 1996; Kiang 1965; Irvine, Park, and McCormick 2001; Heil and Neubauer 2001). Thus, physiologically experienced ILDs can give rise to relative EPSPs and IPSPs being in – or out of temporal register (Park et al. 1996; Kiang 1965; Irvine, Park, and McCormick 2001; Franken et al. 2015). The importance of timing is further emphasized by the fact that LSO neurons are also sensitive to ITDs (Finlayson and Caspary 1991; Wu and Kelly 1991; Joris and Yin 1995; Park et al. 1996; Tollin and Yin 2005; Ashida, Kretzberg, and Tollin 2016). The resolution of such internally created delays would

require – in contrast to the theory for 'ILD-only' computation – small temporal integration windows and temporally precise inputs which could explain the need of a calyx in the LSO pathway. Furthermore, earlier *in vivo* studies revealed that the effective time window for AP suppression lasts only a few hundreds of microseconds (Park et al. 1996; Irvine, Park, and McCormick 2001). This high temporal precision of inhibition *in vivo* is coherent with recent *in vitro* findings revealing similar decay times of EPSCs and IPSCs in the LSO that match the results for IPSPs in the MSO (Grothe and Sanes 1994; Myoga et al. 2014; Couchman, Grothe, and Felmy 2010; 2012; Franken et al. 2015).

Taken together, the LSO is well equipped for being a coincidence detector similar to the MSO.

1.3.7 "Same Same…" The LSO as archetypical proxy for the MSO

Early mammals that arose more than 200 million years ago were relatively small with middle-ear ossicles having an effective transmission range of mid-to high frequencies up to 20 kHz (Rosowski and Graybeal 1991; Grothe and Pecka 2014). The physiological characteristics of early mammals therefore met the requirements to experience significant ILDs that are primarily detected in the LSO (Erulkar 1972). Later adaptations, e.g., an increase in the body (and therefore head size) gave rise to more readily detectable interaural distances applying a selective pressure towards new ITD-dependent niches. The evolutionary evidence therefore leads to the suggestion that the MSO likely derived from LSO neurons.

As outlined in 1.3.4 and 1.3.6 the LSO circuit based on coincidence detection of glutamatergic and glycinergic inputs is tuned for high temporal fidelity and belongs to the most temporally precise circuits in the brain despite the longer inhibitory pathway via the MNTB. Interestingly, as the MSO and the LSO share a subset of inputs (ipsilateral glutamatergic inputs and contralateral glycinergic inputs) it is highly likely that they share similar coding principles whereby the MSO developed further refinements towards pure ITD/IPD sensitivity. These refinements include an additional inhibitory input from the ipsilateral side which makes it reasonable to speculate that synaptic inhibition plays an essential role in the MSO circuit.

Considering the LSO as an archetypical proxy for the MSO could reflect the cellular blueprint for the underlying interplay of well-timed inhibitory and excitatory inputs and its implications on ITD tuning.

1.3.8 "…But Different" Fine structure and envelope sensitivity in the MSO

It is a well-known phenomenon in the auditory brainstem that neurons can lock their activity to a particular phase of a stimulus. More specifically, the highest probability for spiking usually occurs at the rising slope of any complex stimulus (Dietz et al. 2014) which typically includes the temporal fine structure (TFS) and the overall envelope of a signal.

As mentioned earlier, neurons in the LSO respond predominantly to high frequency sounds, intrinsically limiting the ability for phase-locking to the envelope of the stimulus since phase-locking is limited to frequencies below 2-3 kHz (Johnson 1980).

Neurons in the MSO, however, are often tuned to low frequencies below 1 kHz which theoretically allows for phase locking to both TFS and envelope of the stimulus. In fact, relatively high-CF MSO neurons can exhibit comparable sensitivity to envelope ITDs (Batra, Kuwada, and Stanford 1993; Griffin et al. 2005).

Nevertheless, since the head functions as a low-pass filter (outlined in 1.1) disparities in interaural amplitudes of the physical acoustic waveform are less prevalent with low carrier frequencies.

In the cochlea, however, complex broadband signals are decomposed by non-linear filtering along the basilar membrane resulting in a series of narrowband signals with unique envelope patters (Fletcher 1940; Ruggero 1973; Moore 1986; Palmer 1987), that can individually drive neuronal activity. Such cochlear filters are level-dependent (Ruggero et al. 1997; Moore 1998) and their filter bandwidth decreases with increasing center frequencies (Moore 1998; Pickles 1982; Joris and Yin 1992), therefore cochlear filters are not constant entities.

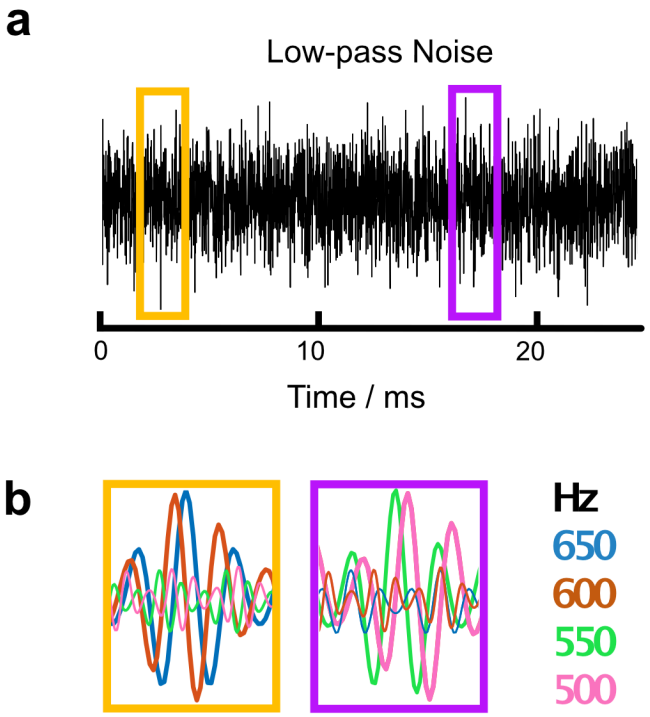

Figure 5: Schematic of the effective envelope and potential changes in instantaneous spectral energy.
a Schematic. Non-linear cochlear filtering decomposes a complex low-pass signal into a series of narrowband signals whose spectral energy can change instantaneously. Yellow and magenta boxes highlight the effective stimulus at different times.
b Left and middle panel: Within a specific frequency band (schematically 500-650 Hz) the instantaneous spectral energy can vary over time (color-coded relative to boxes in (a); frequencies color-coded as per right panel). Right panel: Schematic frequencies; color-coded.

In addition, ANFs and subsequent neurons can phase-lock to the waveform of this effective envelope ($envelope_{effect}$), and therefore transmit its temporal pattern along the auditory pathway (Joris and Yin 1992; Joris 2003; Palmer 1982). Importantly, the $envelope_{effect}$ serves as energy source that determines the instantaneous spectral energy within a frequency band that is relevant for the MSO neuron and thereby can affect the neuronal drive of its inputs relative to their specific frequency tuning (Fig. 5). On top of that, the activity of ANFs in response to rapid events in these $envelope_{effect}$ can also depend on dynamic factors, such as ITD, short time depression, facilitation or spike time plasticity (Wang and Manis 2008; Yang and Xu-Friedman 2008; Fortune and Rose 2001). Therefore, by theory, the neuronal drive can strongly depend on the TFS, the $envelope_{effect}$ and/or various intrinsic factors.

In fact, it was shown that envelope components can bias ITD sensitivity at low frequencies (Bernstein and Trahiotis 1985).

In addition, studies in the inferior colliculus (IC) and the dorsal nucleus of the lateral lemniscus (DNLL) (inter alia upstream targets of MSO neurons) revealed rate and delay asymmetries in noise-delay functions (NDFs) of low-CF and mid-CF neurons that cannot be exclusively explained by IPD-dependent components (Joris 2003; Agapiou and McAlpine 2008). These components could partially be reflected by cochlear filtering.

It has also been shown previously that stimuli require high binaural coherence to be perceived to derive from a single sound source (Jeffress, Blodgett, and Deatherage 1962; Blauert and Lindemann 1986; Blauert 1997). Therefore, due to cochlear filtering, the question arises how coherent both signals are within a specific frequency band at a given time window.

In summary, to what extend ITD sensitivity to low frequency broadband stimuli is biased by envelopes$_{effect}$ is not fully understood.

1.4 Goals of this study and author contributions to the individual studies

This thesis is subdivided into two studies representing 2 independent studies that were conducted.

1.4.1 Study 1:

Precisely timed inhibition facilitates action potential firing for spatial coding in the auditory brainstem

As discussed in 3.6, relative differences in input timing are a concomitant consequence of ILD computation. To gain better insight into the functional relevance of relative input timing during binaural spatial processing, I performed extracellular single-cell recordings in the LSO of Mongolian gerbils *in vivo*. By disentangling amplitude effects from effects specifically related to input timing, we demonstrate that inhibition controls spiking with microsecond precision throughout high frequency click trains, resulting in input timing-specific modulation of neuronal output. Furthermore, our data reveal that spiking is facilitated when contralateral inputs are functionally leading excitation within a precise time window. Importantly, our data suggest that post-inhibitory facilitation (PIF) can support ILD maintenance when excitatory inputs are weak. In addition*, in vitro* whole-cell recordings (conducted by Prof. Dr. Michael Myoga and Dr. Alexander Callan and Dr. Nicolas Müller) in mature LSO neurons

confirm a reduction in the firing threshold due to prior hyperpolarization giving rise to PIF of otherwise sub-threshold synaptic events. This facilitatory effect based on microsecond precise differences between excitation and inhibition could therefore promote spatial sensitivity of faint sounds.

Study 1 is published: (Beiderbeck et al. 2018)

1. These authors contributed equally: Barbara Beiderbeck, Prof. Dr. Michael H. Myoga.

2. These authors jointly supervised this work: Prof. Dr. Benedikt Grothe, PD Dr. Michael Pecka.

Affiliations

1. Department Biology II, Division of Neurobiology, Ludwig-Maximilians-Universität Munich, Planegg-Martinsried, 82152, Germany
   Barbara Beiderbeck, Prof. Dr. Michael H. Myoga, Dr. Alexander R. Callan, Prof. Dr. Benedikt Grothe & PD Dr. Michael Pecka

2. Graduate School of Systemic Neurosciences, Ludwig-Maximilians-Universität Munich, Planegg-Martinsried, 82152, Germany
   Barbara Beiderbeck & Dr. Alexander R. Callan

3. Max Planck Institute of Neurobiology, Am Klopferspitz 18, Martinsried, 82152, Germany
   Prof. Dr. Michael H. Myoga & Prof. Dr. Benedikt Grothe

4. Department of Biology, Animal Physiology Group, University of Kaiserslautern, Kaiserslautern, 67653, Germany
   Dr. Nicolas I. C. Müller & Prof. Dr. Eckhard Friauf

Contributions

B.B. performed *in vivo* experiments and histology, analyzed the *in vivo* data and contributed to writing the paper. M.H.M. designed and performed *in vitro* experiments and pharmacology, analyzed *in vitro* data and contributed to writing the paper. N.M. designed and performed *in vitro* experiments. A.R.C. performed *in vitro* experiments. E.F. designed *in vitro* experiments and contributed to writing the paper. B.G. conceived the experiments and contributed to writing the paper. M.P. conceived and designed the experiments, analyzed the *in vivo* data and wrote the paper.

Corresponding authors
Correspondence to B.G. or M.P.

1.4.2 Study 2:

Pushing the envelope – The impact of the effective envelope on low frequency MSO neurons

In study 1 we have investigated how the temporal relationship between inputs can affect neuronal output in the LSO. Such changes in temporal input composition can result from naturally occurring ILDs that independently affect the strength, latency and duration of excitatory and inhibitory inputs (as outlined in 1.3.6). With MSO neurons inherently being tuned to low frequencies that (given the relatively small head of a rodent) give rise to only minuscule ILDs, naturally occurring intensity-to-time conversions (as observed in the LSO) are negligible in the MSO. Most studies in the MSO are conducted using single pure tone stimuli or single frozen low-pass noise tokens naively assuming that relative input strengths are (and remain) constant. Following stimulation with low-pass noise each event within the $envelope_{effect}$ that the neuron responds to (i.e., fast energy rise within the relevant sound spectrum with regard to the neuron's tuning) can contain a unique spectral composition that can vary over time. Being a biological system, it is unlikely, that all for functional inputs to the MSO share identical frequency tuning. Hypothetically, such instantaneous differences in spectral energy could individually affect the neuronal drive of the four functional inputs if slight differences in their frequency tuning do exist. Moreover, not only changes in frequency tuning might lead to such an effect, but also inherent differences in the gain function between intensity and latency. Furthermore, such differences could individually offset adaptational effects on MSO inputs. Hence, instantaneous integration of the four functional inputs might be dynamic in the MSO not only throughout the duration of the stimulus but also between different complex stimuli (Fig. 6). To investigate this hypothesis, I conducted extracellular single-cell recordings in low frequency MSO neurons of Mongolian gerbils with CFs ranging from 267-1600 Hz (mean CF over all neurons: 837 Hz)) which represents one of the lowest-frequency datasets that have been recorded in the MSO *in vivo*. In order to identify stimulus dependent changes in input strength and/or timing, I presented a battery of frozen broadband noise stimuli at various ITDs. Specifically, these stimuli share the same

spectral contents (i.e., same carrier frequencies) but vary in their respective envelopes (i.e., their amplitude fluctuations across the stimulus). Our data reveal that the interplay of $envelopes_{effect}$ and the instantaneous spectral energy not only impacts relative spike timing but also dynamically affects overall ITD sensitivity in low frequency MSO neurons. In addition, within each stimulus, we were able to identify specific events where spike timing was neatly matching the temporal displacement of the monaural envelope across ITDs. The findings of this study show that $envelopes_{effect}$ play a crucial role for binaural integration in low frequency MSO neurons with strong evidence for its regulation through pre- and short-time adaptation which suggests that the tuning of relative inputs (inhibition/excitation) could be individually adapted across the stimulus. Specifically, we detected spiking phenomena in MSO neurons that can be attributed to effects of preceding inhibition similar to our findings for the LSO.

Study 2 is not published.

These authors jointly supervised this work: PD Dr. Michael Pecka, Prof. Dr. David McAlpine, Prof. Dr. Benedikt Grothe

Affiliations

1. Department Biology II, Division of Neurobiology, Ludwig-Maximilians-Universität Munich, Planegg-Martinsried, 82152, Germany
   Barbara Beiderbeck, Prof. Dr. Benedikt Grothe & PD Dr. Michael Pecka

2. Graduate School of Systemic Neurosciences, Ludwig-Maximilians-Universität Munich, Planegg-Martinsried, 82152, Germany
   Barbara Beiderbeck

3. Department of Linguistics, Macquarie University, North Ryde, NSW 2109, Australia
   Dr. Jason Mikiel-Hunter, Prof. Dr. David McAlpine

Contributions

B.B. performed *in vivo* experiments and histology, analyzed the *in vivo* data and wrote the manuscript presented in this thesis. J. M.-H. analyzed the *in vivo* data and contributed to the design of the experiments. M.P., D.M.A. and B.G. designed and conceived *in vivo* experiments.

Corresponding authors
Correspondence to M.P.

2 Material and Methods

2.1 Ethical approval for animal experiments.

All experiments were approved in accordance with the stipulations of the German animal welfare law (Tierschutzgesetz) (AZ 55.2-1-54-2532-53-2015). Animals were housed in groups of 4 to 6 individuals with 12 h light/dark cycles.

2.2 *In vivo* extracellular single-cell recordings (Study 1 and Study 2)

2.2.1 Anesthesia

Adult Mongolian gerbils (*Meriones unguiculatus* 3-7 months of age) of both sexes (study 1: n=15; study 2: n=12 and additional n=3 for add-on recordings of tonal adapter stimuli) were injected with a solution of ketamine (20 %, Medistar GmbH) and xylazine (2 %, Bayer AG) diluted in 0.9 % NaCl solution (50 µl g^{-1} body weight). Anesthesia was maintained with a continuous subcutaneous application of the same solution (2.4 µl/min per 100 g body weight) using an automatic syringe pump (Univentor Ltd.). The hind leg withdrawal reflex was routinely checked to monitor anesthesia.

2.2.2 Pre-experimental procedures

Access to the ear canal was enabled by making two incisions of both sides of the tragus. The animal was then places on a thermostatically controlled heating pad (Fine Science Tools GmbH) to maintain the body temperature at 38 °C using a rectal probe. The scalp was cut to reveal the dorsal part of the skull. Anterior to bregma, a metal rod was attached onto the skull using UV-sensitive dental-restorative material (Charisma, Heraeus Kulzer GmbH). The neck muscles at the recording site (caudal to lambda, behind the sinus transversus) were partially removed to reveal the skull posterior to lambda. The animal was then transferred to a custom-made stereotactic setup (Schuller, Radtke-Schuller, and Betz 1986) in a sound-attenuated chamber where it was placed onto another thermostatically controlled heating pad. The head of the animal was fixated by the attached metal rod. An electrocardiogram was monitored and a custom-made oxygen mask was placed on the mouth of the animal. For the

reference electrode a small craniotomy was performed between bregma and lambda. To enable access to the LSO (study 1) and MSO (study 2), a craniotomy and durotomy was performed behind the sinus transversus. For the prevention of micro-bleedings and dehydration the revealed surface of the brain was regularly rinsed and covered with physiological NaCl solution (0.9 %).

Earphones were placed on the ear canals and the head of the animal was then stereotactically aligned relative to lambda.

2.2.3 Acoustic stimulus creation and extracellular single-cell recording

2.2.3.1 LSO recordings / Study 1

In study 1 calibrated custom-made electrostatic earphones were placed on the ear canals. Earphones were calibrated using a condenser microphone (Type 4138, ¼ in., adapter Type 2669, Brüel & Kjaer) for frequency responses between 15 to 90 kHz.

Acoustic stimuli were generated digitally using MATLAB (MathWorks) at a sampling rate of 192 kHz. The stimulus signal was converted into an analogue signal (RX6, Tucker Davis Technologies), attenuated (PA5, Tucker Davis Technologies) and conveyed to custom-made electrostatic earphones.

To identify responsive neurons white noise bursts (duration: 200 ms; rise/fall at stimulus onset/offset: 5 ms cosine window) were presented. LSO neurons were identified by their characteristic 'EI' response, i.e., stimulation of the ipsilateral ear evoked neuronal spiking whilst neuronal firing appears to be increasingly suppressed with increased stimulus intensity on the contralateral ear. ILD-response functions (data not shown) were recorded using a set of binaural correlated noise stimuli with varying ILDs for each side respectively (ipsilateral: 19-84 dB SPL; contralateral: 49-74 dB SPL; 5 repetitions). The neuron's CF was determined audio-visually using a cassette of tonal pure tone stimuli 20 dB above threshold (5 repetitions).

Temporal resolution of binaural processing was quantified using a train of 6 consecutive 50 µs clicks that were presented binaurally. Click trains were presented at various inter-click-intervals (ICIs; 5-1 ms, 1 ms increments) and binaural click trains were presented at five different composite timing delays (cTDs) generated by applied ITDs of -400 to 400 µs (200 µs increments). The ILD, i.e., the relative intensity on each

ear was individually adjusted relative to maximal responsiveness during monaural stimulation on the ipsilateral side and significant modulation of neuronal response rate with varying cTDs during binaural stimulation (mean ILD was 0.7 dB ± 6.1 dB s.e.m.)
To test the impact of changes in ipsilateral stimulus intensity on ILD coding, response rates of 7 LSO neurons (n=3) to binaural white noise tokens (duration: 50 ms) with various contralateral stimulus intensities were compared for 3 different ipsilateral stimulus intensities.
All stimulus combinations were presented in a pseudo-randomized order.
For extracellular-single cell recordings, APs of single LSO neurons were recorded using glass electrodes (Sigma-Aldrich) filled with 5 units/µl horseradish peroxidase (HRP) diluted in 10% NaCl solution (resulting tip resistance of ~8-12 MΩ). Using a motorized micromanipulator (Mitutoyo) and a piezo-drive (Inchworm controller 8200, EXFO Burleigh Products Group) for remote control, the position of the recording electrode was normalized relative to the 3-dimensional coordinates of lambda and was lowered into the brain tissue with a relative angle of 20°. Extracellular voltage and voltage changes during APs were measured by a pre-amplifier (Electro 705, World Precision Instruments), amplified (TOE 7607, Toellner Electronic), filtered (Hum Bug Noise Eliminator, Quest Scientific Instruments), converted and delivered to the computer via a real-time processor (RP2, Tucker Davis Technologies). Here, neuronal responses were analyzed online using the spike-analysis software 'BrainWare' (Jan Schnupp, Tucker Davis Technologies) allowing audio-visual control and refinements of recordings. Single-units were tested by visual inspection and online sorting. A signal-to-noise ratio of the spike waveform of > 5 was required for recorded neurons to be included for further analysis.

2.2.3.2 MSO recordings / Study 2

In study 2 calibrated earphones (ER-4 microPro, Etymotic Research) were placed on the ear canals. Earphones were calibrated using a condenser microphone (Type 4138, ¼ in., adapter Type 2669, Brüel & Kjaer) for frequency responses up to 10 kHz.
Acoustic stimuli were generated digitally using MATLAB (MatWorks) at a sampling rate of 192 kHz. Stimulus presentation was controlled in AudioSpike (HörTech) using a sound card interface (Fireface UFX, RME-Audio).
To identify responsive neurons white noise bursts (duration: 200 ms; rise/fall at stimulus onset/offset: 5 ms cosine window) were presented. MSO neurons were

identified by their characteristic ‘EE’ response, i.e., stimulation of the ipsilateral and contralateral ear evoked neuronal spiking.

Noise delay functions (NDFs) were recorded using a set of 10 distinct frozen and binaurally correlated white noise tokens (duration: 100 ms, 5 ms cos-ramps) at varying ITDs from -1.75 ms to +1.75 ms (50 µs increments; 3 repetitions per noise token and ITD) that have been presented 30 dB above threshold.

The neuron’s CF was determined audio-visually using a cassette of tonal pure tone stimuli 20 dB above threshold (5 repetitions).

Tonal ITD functions were recorded by presenting 50 ms tonal tokens (5 tonal tokens at and/or around CF) at ITD ranges from either ± 1.08 ms or ± 1.42 ms (50 µs increments respectively) 30 dB above threshold (5 repetitions).

Tonal adapter stimuli were recorded by presenting a 100 ms long tonal adapter at CF either monaurally (ipsi- or contralaterally) or binaurally followed by NDFs as described above (here 6 repetitions per noise token and ITD).

All stimulus combinations were presented in a pseudo-randomized order.

For extracellular-single cell recordings, APs of single MSO neurons were recorded using glass electrodes (Sigma-Aldrich) filled with 5 units/µl horseradish peroxidase diluted in 10% NaCl solution (resulting tip resistance of ~5-12 MΩ). Using a motorized micromanipulator (either Mitutoyo or Scientifica) and a piezo-drive (either Inchworm controller 8200, EXFO Burleigh Products Group or Scientifica) for remote control, the position of the recording electrode was normalized relative to the 3-dimensional coordinates of lambda and was lowered into the brain tissue with a relative angle of 20°. Extracellular voltage and voltage changes during APs were measured by a pre-amplifier (Electro 705, World Precision Instruments), filtered (Hum Bug Noise Eliminator, Quest Scientific Instruments), converted and delivered to the computer via a sound card interface (Fireface UFX, RME-Audio). Here, neuronal responses were analyzed online using the spike-analysis software ‘AudioSpike’ (HörTech) allowing audio-visual control and refinements of recordings. Single-units were tested by visual inspection and online sorting. A signal-to-noise ratio of the spike waveform of > 5 was required for recorded neurons to be included for further analysis.

2.2.4 Histology

2.2.4.1 Iontophoretical HRP injection

For histological identification of the recording site, HRP was released from the electrode iontophoretically by applying a current of 1 µA for 3-8 minutes.

2.2.4.2 Intracardial perfusion and PFA fixation

After conclusion of an experiment, the animal was intraperitoneally (2 µl g^{-1}) injected with a lethal dose of Narcoren (Pentobarbital 160 mg ml^{-1}). The thorax was cut open and the sternum was lifted using a clamp forceps to reveal the heart. A cannula was inserted into the left ventricle while the right atrium was cut open to allow blood efflux. The animal was perfused with Ringer-solution (containing NaCl (0.9 %), heparin (100 µl ml^{-1}) and 5 mM Phosphate-buffered saline (PBS) in H_2O) for approximately 10 minutes (until the remaining blood in the system was washed out) followed by a perfusion with 4 % paraformaldehyde (PFA in PBS pH 7.4) for another 10-25 minutes. For further fixation the brain was removed from the skull and incubated in 4 % PFA for 1-2 days at 4 °C.

2.2.4.3 Slicing and Staining

Following fixation, the brain was washed three times à 10 minutes in PBS (0.02 M) and was then embedded in 4 % agarose for optimized stability during slicing. Using a vibratome device and a razor blade (Leica Biosystems, Wilkinson) 50-80 µm thick coronal sections of the respective area in the auditory brainstem were prepared.
Labelling of the recording site was accomplished using a 3, 3′-diaminbenzidine (DAB) substrate kit for peroxidase (Vector Laboratories). Substrate solution was produced in accordance with the following standard protocol:

Amount	**Chemical**
5.0 ml	Distilled water
4 drops	DAB Stock Solution
2 drops	Hydrogen Peroxidase Solution

Table 1: Substrate solution for DAB staining.

Brain slices were incubated in 500 µl of substrate solution for 2-10 minutes, then slices were rinsed twice with distilled water and third time with 0.02 M PBS. Slices were transferred onto glass objective slides where they were air-dried at room temperature. Empty wells were neutralized using sodium hypochlorite and distilled water. Neutral Red staining was accomplished using the following standard protocol:

Incubation time [min]	**Chemical**
8	Neutral red solution (1 g neutral red + acetate buffer 0.2 M pH 4.8 + 100 ml distilled water)
10 sec	Distilled water
10 sec	Distilled water
10 sec	Distilled water
2.5	70% ethanol
2.5	96% ethanol
2.5	96% ethanol
2.5	100% isopropanol
2.5	100% isopropanol
2.5	Xylol
2.5	Xylol
2.5	Xylol

Table 2: Protocol for Neutral Red staining.

Objective slides were mounted with DePeX mounting medium (Serva Electrophoresis GmbH).

2.2.4.4 Overview images

Overview images of respective recording sites were acquired using an Olympus virtual slide fluorescence microscope (brightfield, 10× magnifications, Olympus BX61VS, Olympus Corp.). For LSO neurons, 13 of 17 recording sites and for MSO neurons, 11 of 15 recording sites in total could be confirmed histologically. In the remaining cases,

no distinct DAB counterstaining was found but recording sites could be reconstructed from the track of the recording electrodes.

2.2.5 *In vivo* data analysis

2.2.5.1 LSO recordings / Study 1

Data were analyzed using custom-made programs in MATLAB (MathWorks). For further analysis a mean spike rate of >1 spike per repetition (calculated over 20 repetitions) at the cTD/ICI combination which elicited the maximal spike rate and significant cTD sensitivity was required. The ICI which evoked the largest response modulation rate between the peak and the trough of the cTD function was defined as the best ICI. Significance of cTD tuning was assumed if the mean response rate modulation (for all six clicks at best ICI) was at least two times larger than the standard deviation of the response rate during monaural (ipsilateral) stimulation at the same ICI. For population analysis, cTD functions at best ICI of each neuron were re-centered to its respective min-cTD, resulting in a prolonged relative cTD axis (Δt re min-cTD) from +800 to –800 µs (Fig. 9a,b). To compare slope steepness (Fig. 15e), ILD-response functions were fitted with broken stick (i.e., piecewise linear) regressions. To compare separability based on ILD-response functions, the standard separation D was calculated as described previously (Sakitt 1973):

$$D_n = |mu_n + 1 - mu_n| / (sqrt(sigma_n + 1 \times sigma_n)),$$

where mu_n + 1 and mu_n are the mean values of the responses to two ILD values while sigma_n + 1 and sigma_n are their standard deviation. Depending on normality of the distribution, population average data are shown by the mean ± s.e.m., or the median and the 25 and 75% confidence intervals (interquartile range). Accordingly, parametric or nonparametric tests were used to determine statistical significances (see text and figure legends).

2.2.5.2 MSO recordings / Study 2

Data were analyzed using custom-made programs in MATLAB (MathWorks). MSO neurons that showed significant ITD sensitivity (across all 10 noise tokens; 3 repetitions per noise, hence 30 repetitions overall) were included in this study.

The threshold for separation between “epoch-spikes” and “non-epoch-spikes” in 3.2.2 onwards was set in a way that >90 % of the summed coincident spikes across ITDs are considered to be spikes that are aligned with monaural timing of the envelope (Fig. 20b). Epoch-components that contained >1 spike were included in further analysis of epoch-spike related noise-delay-functions ($NDFs_{Epoch}$). Individual best ITDs NDF_{Epoch} per noise token protocol have been identified through the peak of each individual Gauss-fitted NDF_{Epoch}/noise.

2.3 *In vitro* LSO recordings (Study 1)

In vitro whole-cell recordings were conducted by Prof. Dr. Michael Myoga and Dr. Alexander Callan and Dr. Nicolas Müller (section derived from (Beiderbeck et al. 2018)).

2.3.1 Slice preparation and setup

LSO slice preparation and electrophysiology: In vitro experiments were conducted in Mongolian gerbils (*Meriones unguiculatus*) aged 31-38 days and of either sex (19 animals). Gerbils were anesthetized with isoflurane (Zoetis) and decapitated. Brains were removed from the skull and transferred into ice-cold dissecting solution containing in mM: 93 N-methyl-D-glucamine, 93 HCl, 30 NaHCO3, 25 glucose, 20 HEPES [4-(2-hydroxyethyl)-1-piperazineethanesulfonic acid], 10 MgCl2, 5 L- ascorbic acid, 3 myo-inositol, 3 Na-pyruvate, 2.5 KCl, 1.2 NaH2PO4, 0.5 CaCl2 (pH 7.4 when oxygenated with 95% O2 and 5% CO2). Using a VT1200S vibratome (Leica), 200 µm thick transverse slices were prepared. Brain slices were incubated at 35 ºC for 30 minutes in dissecting solution and for another 30 minutes in an oxygenated perfusion saline containing in mM: 125 NaCl, 25 NaHCO3, 25 glucose, 3 myo-inositol, 2.5 KCl, 2 Na-pyruvate, 2 CaCl2, 1.25 NaH2PO4, 1 MgCl2, and 0.4 L-ascorbic acid (pH 7.4). Recordings were performed in perfused oxygenated saline (1 ml min−1). Temperature was measured near the slice and maintained at 35 ± 1 °C by an SF-28 in-line heater (Warner Instruments) and a PH-1 bath chamber heater (Biomedical Instruments). Tissue was imaged under an upright Axioskop microscope (Zeiss) with infrared Dodt gradient contrast optics. LSO neurons were identified visually and whole-cell

recordings were performed using borosilicate glass electrodes and a patch-clamp amplifier (EPC10/2; HEKA Elektronik).

2.3.2 Synaptic stimulation

The internal solution for synaptic stimulation contained the following in mM: 122 Cs-MeSO4, 10 HEPES, 10 Na2-phosphocreatine, 5 QX-314 [N-(2,6-dimethylphenylcarbamoylmethyl) triethylammonium chloride], 4 MgCl2, 4 Na2- ATP, 3 Na-L-ascorbate, 0.2 Cs-EGTA (cesium ethylene glycol tetraacetic acid), 0.4 Na2-GTP, and 0.03 Alexa Fluor 633, adjusted to pH 7.25 and 297 mOsm. Voltage- clamp recordings at –70 mV were made with electrodes of 2–3 MΩ tip resistances, and series resistance (4–7 MΩ) was compensated to a residual of 1.5–2 MΩ on the amplifier. Termination criteria involved a change of >10% of the uncompensated series resistance. Synaptic stimulation was performed with borosilicate glass electrodes (3–4 MΩ) filled with saline and placed at a distance of 50–150 µm relative to the recorded neuron. Lateral (excitatory) and medial (inhibitory) inputs were activated every 2 s with brief (0.2 ms) 10–50 V bipolar pulses generated by a Model 2100 isolated pulse generator (A-M Systems).

2.3.3 Conductance-clamp

The internal solution for synaptic stimulation contained the following in mM: 145 K-gluconate, 15 HEPES, 5 Na2- phosphocreatine, 3 Mg2-ATP, 0.3 Na2-GTP, and 0.05 Alexa Fluor 592, adjusted to pH 7.25 and 320 mOsm. Current-clamp recordings were made with electrodes of 2–3 MΩ tip resistances, and series resistance (4–6 MΩ) was 100% balanced on the bridge of the amplifier. The liquid junction potential was estimated to be 15 mV and subtracted offline. All reported membrane voltages reflect this subtraction. Selected synaptic conductance waveforms were delivered to an SM-1 conductance injection amplifier (Cambridge Conductance), which calculates instantaneous current commands [I(t)] by equation (Denève and Machens 2016):

$$I(t) = G(t)[V(t) - E_{rev}]$$

This calculation was performed independently for excitatory [reversal potential (E_{rev}) = 5 mV] and inhibitory (E_{rev} = –85 mV) synaptic conductance waveform templates [G(t)], while simultaneously measuring the membrane potential [V(t)]. Ramps (1 nS increments) of excitatory conductance (G_e) templates were applied to determine the AP conductance threshold. Then the same conductance ramps were performed in the presence of an inhibitory conductance (Gi) template of 20, 50 or 80 nS, varying the relative timing difference (rTD) of inhibitory to excitatory event onset. Templates were delivered as single events in 0.5 ms rTD steps between –1 to 10 ms (n = 19 recordings) or as six events at 5 ms inter-stimulus intervals (ISIs) in 0.25 ms rTD steps between 0 and 4.75 ms (Fig. 12b,c; Fig. 13a, n = 9 neurons). These protocols were repeated six times for each condition tested.

2.3.4 AP current measurement

Electrodes had the same internal solution and specifications as during conduction-clamp recordings. In voltage clamp, neurons were held at their resting membrane potential of -67 ± 6 mV (n = 10 recordings; a subset of the 19 recordings). IPSP waveform templates with varying start points of abrupt interluded suprathreshold voltage were presented (- 45 to -15 mV, duration: 3 ms; after 0 (no inhibition) to 10 ms of IPSP waveform (IPSP time) in 0.25 ms increments, 6 repetitions).

2.3.5 *In vitro* data analysis

Data were acquired at 100 kHz. Data from voltage-clamp recordings (2.3.3) were filtered (8 kHz including a shallow three-pole Bessel filter). Data analysis was performed offline using Igor Pro (Wavemetrics) and MATLAB (MathWorks).

For single-event experiments, analysis of AP probability was performed at the largest Ge ramp step that failed to generate an AP on any trial for excitation alone. AP jitter was determined as the standard deviation of spike timing across all six events at each individual rTD and was normalized to the jitter observed under excitation-only conditions. Exclusion criteria involved the occurrence of < 3 spikes per rTD (Fig. 13c).

3 Results

3.1 Study 1:

Precisely timed inhibition facilitates action potential firing for spatial coding in the auditory brainstem

For study 1, I performed *in vivo* experiments and histology, analyzed the *in vivo* data and contributed to writing the paper. Prof. Dr. Michael H. Myoga designed and performed *in vitro* experiments and pharmacology, analyzed *in vitro* data and contributed to writing the paper. Dr. Nicolas I. C. Müller designed and performed *in vitro* experiments. Dr. Alexander R. Callan performed *in vitro* experiments. Prof. Dr. Eckhard Friauf designed *in vitro* experiments and contributed to writing the paper. Prof. Dr. Benedikt Grothe conceived the experiments and contributed to writing the paper. PD Dr. Michael Pecka conceived and designed the experiments, analyzed the *in vivo* data and wrote the paper (Beiderbeck et al. 2018).

3.1.1 The impact of input timing for binaural processing in the LSO

As described in 1.3.4 and 1.3.6, the LSO is well equipped for gauging of both input strength (amplitude) as well as input timing. Neuronal response rates during ILD processing depend on the relative amplitudes and the temporal overlap of integrated EPSPs and IPSPs. During free-field ILD processing, if a sound source is located off-midline, it will not only be louder on one ear than the other, it will also arrive slightly earlier at the ear that is closer to the sound source resulting in an external ITD. In addition, the higher the intensity of an acoustic stimulus at a particular ear, not only the underlying PSP amplitudes will be the larger. More specifically, high intensity stimuli also result in PSPs having steeper rising slopes, shorter latencies and longer durations than less intense signals (Sanes 1990) (Fig. 6a (right panel)). These additional temporal features may influence the temporal interference of individual inputs at LSO somata. However, the cellular mechanisms underlying its sensitivity to

relative input timing and the functional relevance of precisely timed inhibition for binaural spatial processing in the LSO *in vivo* has not yet been fully understood but has also received surprisingly little attention (Grothe and Pecka 2014; Park et al. 1996).

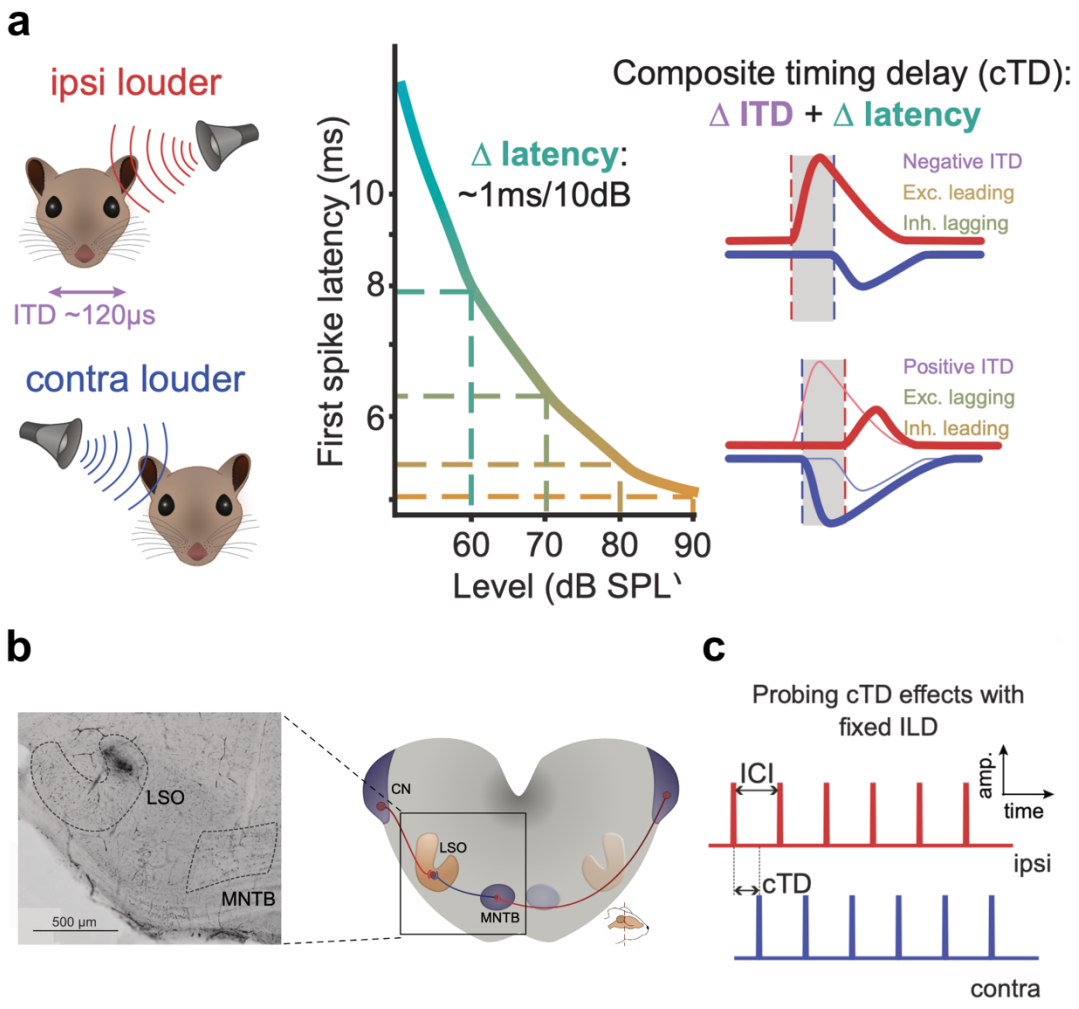

Figure 6: Relative input timing in dependence of stimulus intensity and experimental stimulus design. a Higher absolute sound intensity cause PSPs with larger amplitude, and also shorter latencies. The graph (middle panel) illustrates these level-dependent changes in first spike latency of an auditory nerve fibre (adapted from (Heil and Neubauer 2001)). Together with the location-specific ITD (in the range of <120 µs), these latency changes largely determine the range of input timing changes associated with changes in the location of a sound source (right panel). Thus, ILD computation also involves gauging of the relative timing of EPSPs and IPSPs. **b** Left: The recording site of the example neuron in c and d has been histologically located in the medial limb of the LSO, scale bar; 500 µm. Right: Neurons in the LSO receive excitatory inputs from the ipsilateral CN and indirect inhibitory inputs from the contralateral CN via the ipsilateral MNTB. **c** The stimulus consisted of a battery of individual click-trains consisting of six consecutive clicks (50 µs per click) that are presented at various ICIs in the range of 1-5 ms (1 ms steps). Click-trains were either presented monaurally to the ipsilateral ear only or binaurally at various cTDs in the range of ± 400 µs in 200 µs steps (positive cTDs indicate contra-leading conditions). (Adapted from (Beiderbeck et al. 2018); Modified. *Nature Communications* articles

For the following study, I conducted extracellular recordings from single LSO neurons in anesthetized Mongolian gerbils. In order to investigate neuronal sensitivity in dependence of input timing without being confused by intensity-dependent changes in PSP amplitudes, I presented binaural individual click-trains of 6 consecutive clicks at fixed relative sound intensities between the two ears (the ILD was individually selected for each neuron, see Material and Methods) with each train being spaced with a specific inter-click interval (ICI; 1-5 ms, 1 ms increments). In addition, in order to replicate the combined changes in input timing (external ITD and latency shifts of PSPs as depicted in Fig. 5a (middle panel)), binaural stimuli were presented with “composite timing delays” (cTDs) (Fig. 6c and 7a (bottom schematic)) in the range of ± 400 µs in 200 µs steps. Clicks were used to test the temporal sensitivity of the integration between excitation and inhibition for multiple, repetitive events. Since clicks invoke robust responses of typically 1 spike per click using this stimulus paradigm allows for assessment of the temporal sensitivity of binaural integration with very high resolution, not only at the onset of the stimulus but also throughout the battery of consecutive clicks (ergo: This allows further evaluation of how this sensitivity changes with later clicks in the train) including its functional time course through repeating this paradigm with various ICIs.

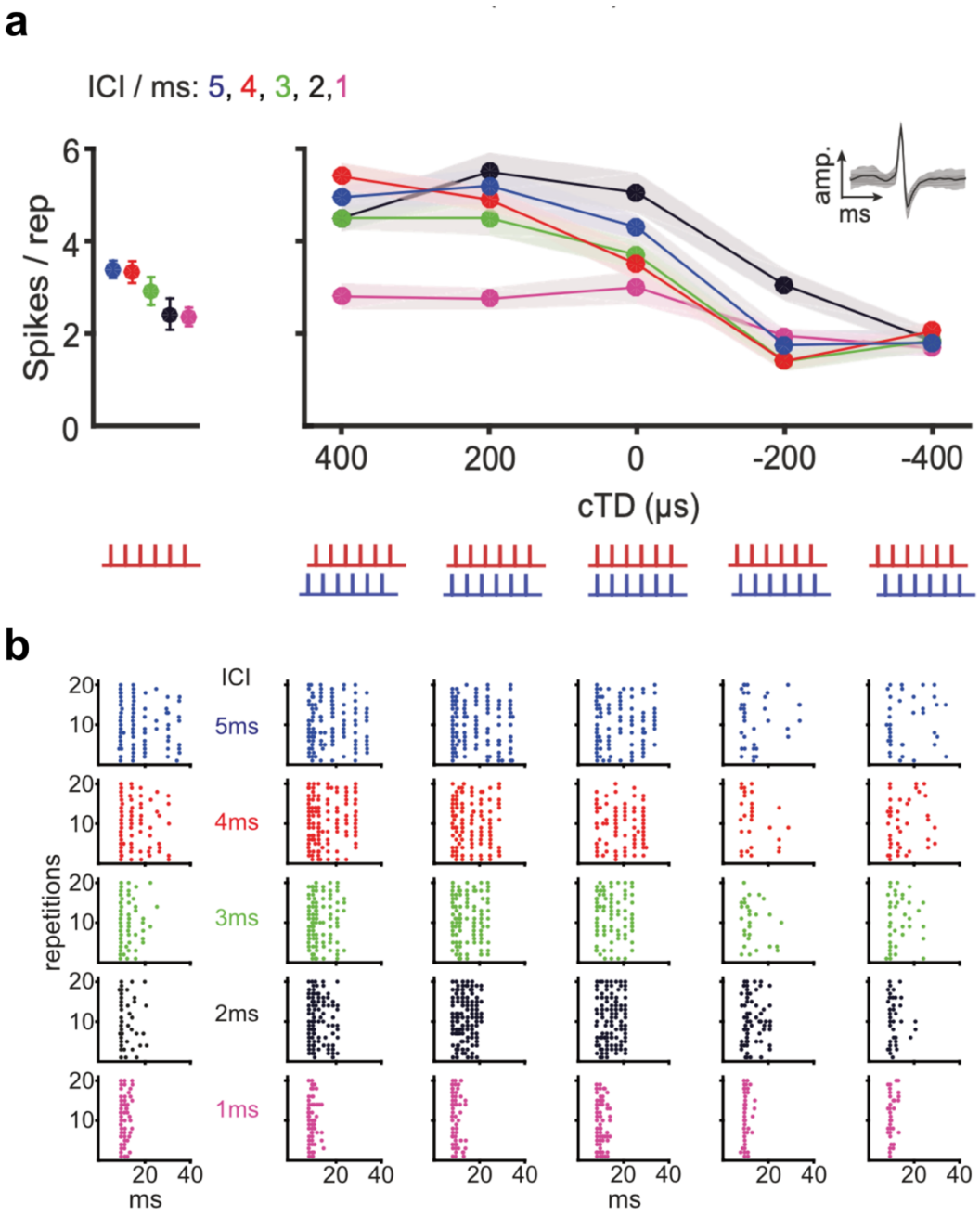

Figure 7: LSO example neuron. a Left: Mean spike rates and standard error of the mean (s.e.m.) per repetition of an LSO example neuron (CF: 24.3 kHz) to monaural (ipsilateral) presentation of acoustic click-trains at various ICIs (20 repetitions, 74 dB SPL); ICIs in the range of 1-5 ms (1 ms increments) are color-coded. Right: Mean spike rates and s.e.m. (shaded area) of binaural cTD response functions of the same neuron as in (c) (ipsi: 74 dB SPL, contra 79 dB SPL, 20 repetitions). Inset represents spike waveform. Note that maximal response rates at +200 µs and +400 µs cTD surpass mean rates during monaural (ipsilateral) stimulation. **b** Dot-raster displays from the same example neuron as in (a) during monaural (left panel, 20 repetitions, ipsilateral stimulation) or binaural (remaining panels, 20 repetitions) presentation of individual click-trains at various ICIs ranging from 1-5 ms (as described in (a)). For binaural panels, each column of figures (across ICIs) represents the neuronal responses at a particular cTD (from left to right: +400 µs (contra-leading) to -400 µs (ipsi-leading) (step size: 200 µs). (Adapted from (Beiderbeck et al. 2018); Modified. *Nature Communications* articles are published open access under a CC BY license (Creative Commons Attribution 4.0 International License). The CC BY license allows for maximum dissemination and re-use of open access materials. Under Creative Commons, authors retain copyright in their articles.)

Figure 7a (left panel) depicts mean response rates over 20 repetitions to monaural click-trains at various ICIs (re. color coding in Fig. 7 b) that have been presented to the ipsilateral (excitatory) ear only. Neuronal response rates decreased with decreasing ICI and spike probability seemed to be decreased for later clicks in the train (Fig 7b). During binaural stimulation, response rates were modulated by cTD, i.e., relative input timing. In addition, for all ICIs tested, minimal response rates during binaural stimulation fell below the mean response rate during monaural-only presentation of the stimulus. This can be explained by the additional inhibitory inputs coinciding and interfering with excitatory inputs at a certain cTD ("Min-cTD"). Conversely, neuronal responses were maximal at contra-leading cTDs of 200-400 µs ("Max-cTD"). Interestingly, however, highest response rates at Max-cTD under binaural stimulation exceeded monaural response rates at every tested ICI (Fig. 7a (left panel) vs. (right panel)). A population analysis (n=17 LSO neurons from 12 animals, CFs 15-36 kHz) revealed similar results with regard to response modulation in dependence of ICI (under monaural stimulation) or in dependence of both ICI and cTD under binaural stimulation. Here, both ICI and cTD had a significant impact on neuronal response rates (two-way analysis of variance (ANOVA), $P(ICI) < 0.0001$, $F(4, 64) = 22.48$; $P(cTD) < 0.0001$, $F(8,128) = 9.59$) (Fig. 8). In line with expectations of maximal suppression at Min-cTD, response rates at Min-cTD ("Min-rates") for each ICI were consistently lower than response rates under monaural (ipsilateral) stimulation only. The unexpected significant increase in response rate at respective Max-cTDs that has been observed in the example neuron in Fig. 7 was consistent across the population sample except for ICIs of 1 ms (Fig. 8e). To rule out involvement of potentially unknown contralateral excitatory inputs to the LSO that may cause increase in firing rates at certain cTDs we repeated the stimulus-patterns but increased the contralateral stimuli by +5 dB SPL in a subset of 9 LSO neurons. This increase in contralateral intensity led to a decrease of in Max-rates (Fig. 8f, see figure description for further information) which is in line with the current textbook knowledge of related input projections to the LSO (i.e., exclusively inhibitory inputs from the contralateral side). Therefore, we can draw the conclusion that spike enhancement was not caused by potential contralateral excitatory inputs and spike enhancement is not only dependent on ICI and cTD but also on the pre-selected ILD for the neuron (please note: fixed ILDs were chosen based on maximal response modulation through cTDs, see Material and Methods). The question arises if spike enhancement is consistent

throughout the click-train or whether the time course of inhibition and potential summation effects may affect the response to clicks that appear later in the click-train in a different way. To assess this, spikes (typically one spike per click) were binned in accordance to their occurrence along the stimulus. (n = 15 neurons, 11 animals, Fig. 8g/h). Binned results reveal under monaural (ipsilateral) stimulation not only a consistent decrease in response rate with decreasing ICIs, but also a decrease in spike probability with subsequently later clicks in the click-train (Fig. 8g, two-way ANOVA, P(click) < 0.0001, F(5, 400) = 124.1; P(ICI) = 0.017, F(4, 80) = 3.2; interactions: P < 0.0001, F(20, 400) = 2.76). However, under binaural stimulation at appropriate Max-cTDs, it appears that, in particular, response rates to later clicks in the train are affected by an spike enhancing mechanism (two-way ANOVA, P(click) = 0.032, F(5, 400) = 2.47; P(ICI) = 0.49, F(4, 80) = 0.87; Interactions: P = 0.28, F(20, 400) =1.16). Thus, it seems dependent on the relative timing between ipsilateral and contralateral inputs the LSO, inhibitory inputs in the LSO either decreased or facilitated spiking to excitatory inputs in the LSO.

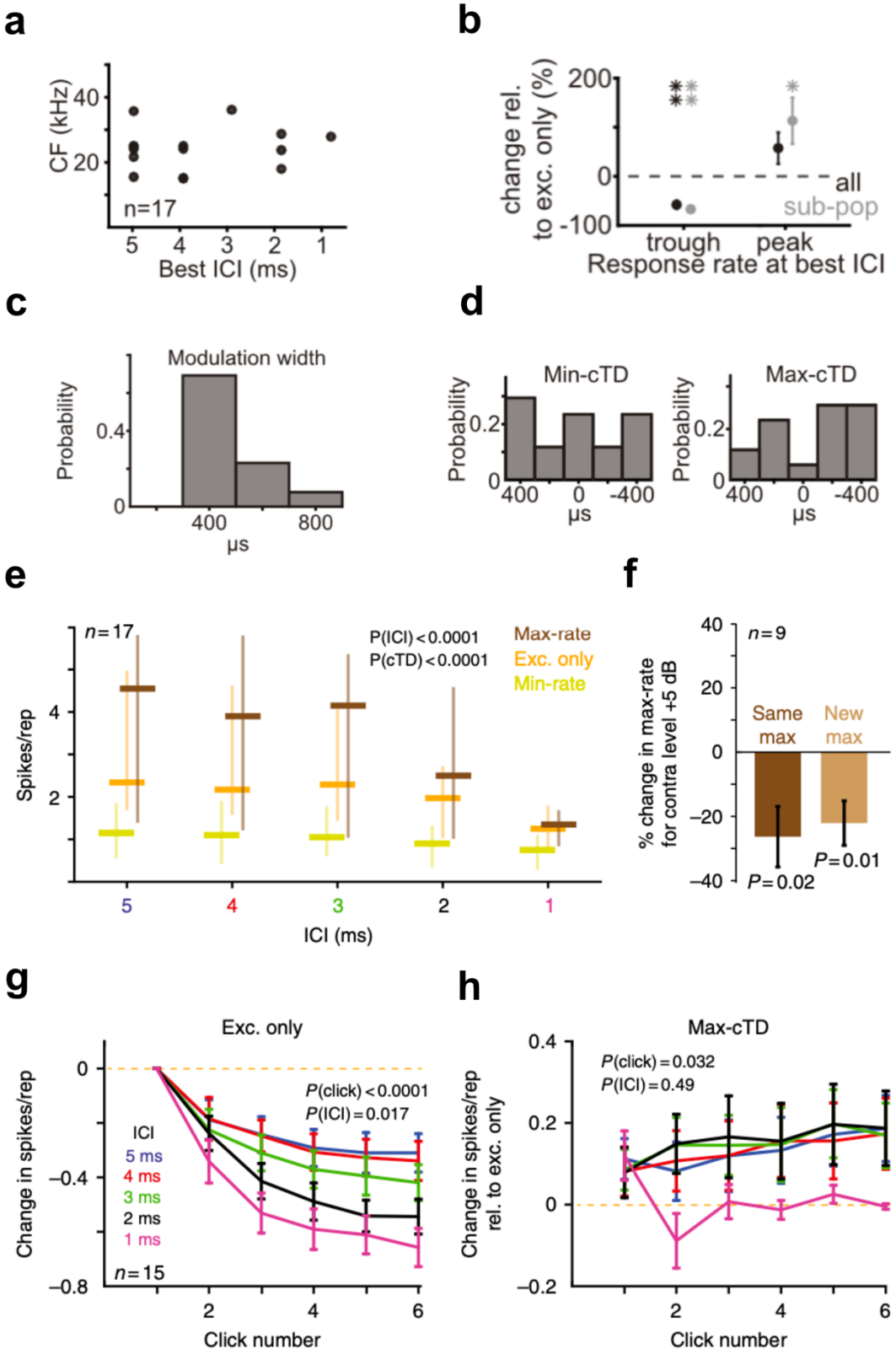

Figure 8: General quantification and further assessment of spike enhancement for individual subsequent clicks within the click-train. a Best ICIs of individual neurons did not depend on CF, but were biased towards larger ICIs, as 13/17 neurons had best ICIs of 5 ms or 4 ms. **b** Change of mean binaural response rates at best ICI and at Min-cTD relative to monaural (ipsilateral) stimulation for all

recorded neurons (black, n = 17) and a subset of neurons for which absolute response rates at Min-cTD fell below their monaural mean response rate (grey, n=15). Min-rates were significantly lower than corresponding mean response rates under monaural stimulation (57.8 % ± 8.3 %, p=0.000003, Student's t-test, and -66.9 % ± 6.1 %, p=0.000003, Student's t-test, respectively). At Max-cTD, binaural mean response rates seem to be increased in the entire population (black, 57.6 % ± 31.9 %, p=0.09, Student's t-test) which becomes significant for the subpopulation of neurons whose binaural absolute response rates superseded the response rates during monaural (ipsilateral) stimulation (grey; n = 15; 113.5 % ± 47.1 %, p=0.04, Student's t-test). Data points are presented as mean ± s.e.m. **c** Modulation width. The Median width between Min- and Max-cTD was 400 µs. **d** Both, Min-cTDs (left panel) and Max- cTDs (right panel) varied across the population. **e** Median and interquartile ranges of response rates to click-trains of 6 consecutive clicks that were presented either monaurally (ipsilaterally, orange), or binaurally at Min-cTD (yellow) or Max-cTD (brown) are shown for the entire population sample at various ICIs (x-axis, color-coded as in (g)). Both, cTD and ICI significantly modulated response rates under binaural stimulation (n = 17, two-way ANOVA: p(ICI) < 0.0001, p(cTD) < 0.0001). **f** Increased stimulus-levels on the contralateral ear (ipsilateral stimulation unchanged) resulted in reduced Max-rates, at both, the original Max-cTD at the original ILD (dark brown, mean change ± s.e.m.: −26.34 ± 9.4%, P = 0.02, t-test, n = 9 neurons) and the potentially new Max-cTD for the new ILD (light brown, −22.11 ± 6.9%, P = 0.01, t-test, n = 9 neurons). **g** Single-click analysis (n=15). Binned mean spike rates to monaural (ipsilateral) stimulation for each click (x-axis) and each ICI (color-coded) were normalized to the mean response rates to the 1st click of the click-train. Mean response rates decreased with both, with subsequently later clicks in the click-train and with decreasing ICIs (two-way ANOVA, P(click) < 0.0001, F(5, 400) = 124.1; P(ICI) = 0.017, F(4, 80) = 3.2). Interactions between click-order and ICI were also significant (P < 0.0001, F(20, 400) = 2.76). **h** Binaural mean response rates at Max-cTD were significantly higher than monaural mean response rates (ipsilateral stimulus presentation) across all subsequent clicks for all ICIs > 1 ms (two-way ANOVA, P(click) = 0.032, F(5, 400) = 2.47; P(ICI) = 0.49, F(4, 80) = 0.87). (Adapted from (Beiderbeck et al. 2018); Modified. *Nature Communications* articles are published open access under a CC BY license (Creative Commons Attribution 4.0 International License). The CC BY license allows for maximum dissemination and re-use of open access materials. Under Creative Commons, authors retain copyright in their articles.)

3.1.2 Preceding inhibition facilitates spiking *in vivo*

We have seen in 3.1.1 that binaural response rates in the LSO are significantly modulated by changing the relative timing (cTDs) or frequency (ICIs) of ipsilateral and contralateral inputs. More specifically, it appears that each neuron has specific 'sweet spot', i.e., specific combinations of cTD and ILD where spiking in response to both ipsilateral (excitatory) and contralateral (inhibitory) stimulation is enhanced compared to ipsilateral-only (excitatory-only) stimulation. Since both cTDs and ILDs have a combined impact on the relative arrival times of individual inputs, we can assume that spike enhancement might be related to the relative timing of EPSPs and IPSPs. Noteworthy, a similar mechanism for facilitation through precisely timed inhibition has been previously observed *in vitro* in juvenile MSO neurons (Dodla, Svirskis, and Rinzel 2006). In this study, spike facilitation was observed when inhibition was leading excitation in a temporally precise manner. Since the LSO is hypothesized to be the evolutionary blueprint of the MSO (Grothe and Pecka 2014) and since both nuclei

share the same subset of inputs (as outlined in 1.3.7) we therefore sought to test whether the observed 'sweet spots' in the LSO underly a similar mechanism *in vivo*. To test this hypothesis, we required a relational reference for the input timing between excitation and inhibition. In general, spiking can only we suppressed if inhibition and excitation are in temporal register, thus respective Min-ITDs for each neuron represent maximal temporal coincidence between excitation and inhibition. Since Min-cTDs were widely distributed across neurons, we re-centered the cTD-spike rate function of each individual neuron (at its best ICI) to the min-cTD (n = 17 neurons from 12 animals). Hence, positive values of the new normalized *Δt*-spike rate function (Min-cTD = 0 µs *Δt*) represent conditions where inhibitory inputs are functionally leading excitation and vice versa (Fig. 9b).

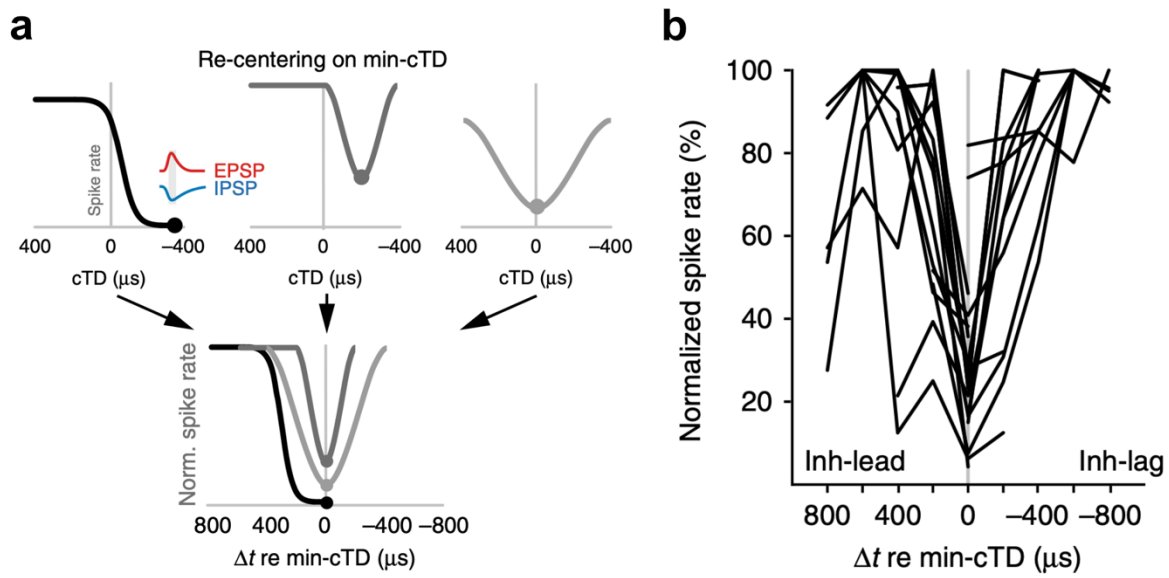

Figure 9: Normalization of cTD functions relative to maximal functional coincidence of excitation and inhibition. a Schematic of the re-centering of cTD functions from individual neurons (at individual best ICI) relative to their respective Min-cTD (representing maximal coincidence of excitation and inhibition; as per schematic inset in top left panel) resulting in an extended *Δt*-axis (± 800 µs). b Normalized cTD functions (*Δt* re Min-cTD (µs)) of each LSO neuron at best ICI (as described in (a); n = 17 neurons from 12 animals). (Adapted from (Beiderbeck et al. 2018); Modified. *Nature Communications* articles are published open access under a CC BY license (Creative Commons Attribution 4.0 International License). The CC BY license allows for maximum dissemination and re-use of open access materials. Under Creative Commons, authors retain copyright in their articles.)

Relative to functional coincidence of the re-centered *Δt*-spike rate function our data reveal that significant spike enhancement occurred exclusively when inhibition was functionally leading excitation by 400 or 600 µs (Fig. 10a (left panel); n = 17 neurons from 12 animals; median increase: 120.6 and 16.3%, P = 0.00007 and P = 0.003 respectively; Wilcoxon signed rank test). Interestingly, this increase in spiking not only was preserved throughout the entire click train, but was even more pronounced for subsequently later clicks of the click train (Fig. 10a (right panel); n = 15 neurons from 11 animals, P = 0.01 at *Δt* = 600 µs and P = 0.002 at *Δt* = 400 µs, Friedman's test). In addition, we also observed significant shifts of spike timing as a function of *Δt* that appears nearly periodic which could result from excitatory and inhibitory inputs arriving in and out of temporal register. More specifically, spikes occurred significantly earlier when inhibition led excitation by 600 µs (n = 15 neurons from 11 animals; median: 96.6 µs, p=0.002; Wilcoxon signed rank test;) or 800 µs (median: 85.7 µs, p=0.0006; Wilcoxon signed rank test) which coincides with the functional inhibitory lead for highest spike enhancement (Fig. 10b (left panel)). Similar trends of bidirectional spike timing shifts as a function of *Δt* were observed for individual clicks (Fig. 10b (right panel). Moreover, we observed a decrease in temporal jitter across *Δts* with highest reduction at *Δt* = 600 µs (Fig. 10c (left panel); n = 15 from 11 animals; median: -46.2%, p=0.0005; Wilcoxon signed rank test), which again coincides with the functional inhibitory lead for highest spike enhancement and spike time reduction. The reduction in jitter and therefore increase in temporal precision tended to be higher for later clicks in the train (Fig. 10c (right panel)). Noteworthy, the observed effects of precisely timed inhibition were present at all ICIs tested (Fig. 11; n = 17 neurons from 12 animals for spike rate; n = 15 neurons from 11 animals for spike timing and jitter; paired Wilcoxon signed rank test).

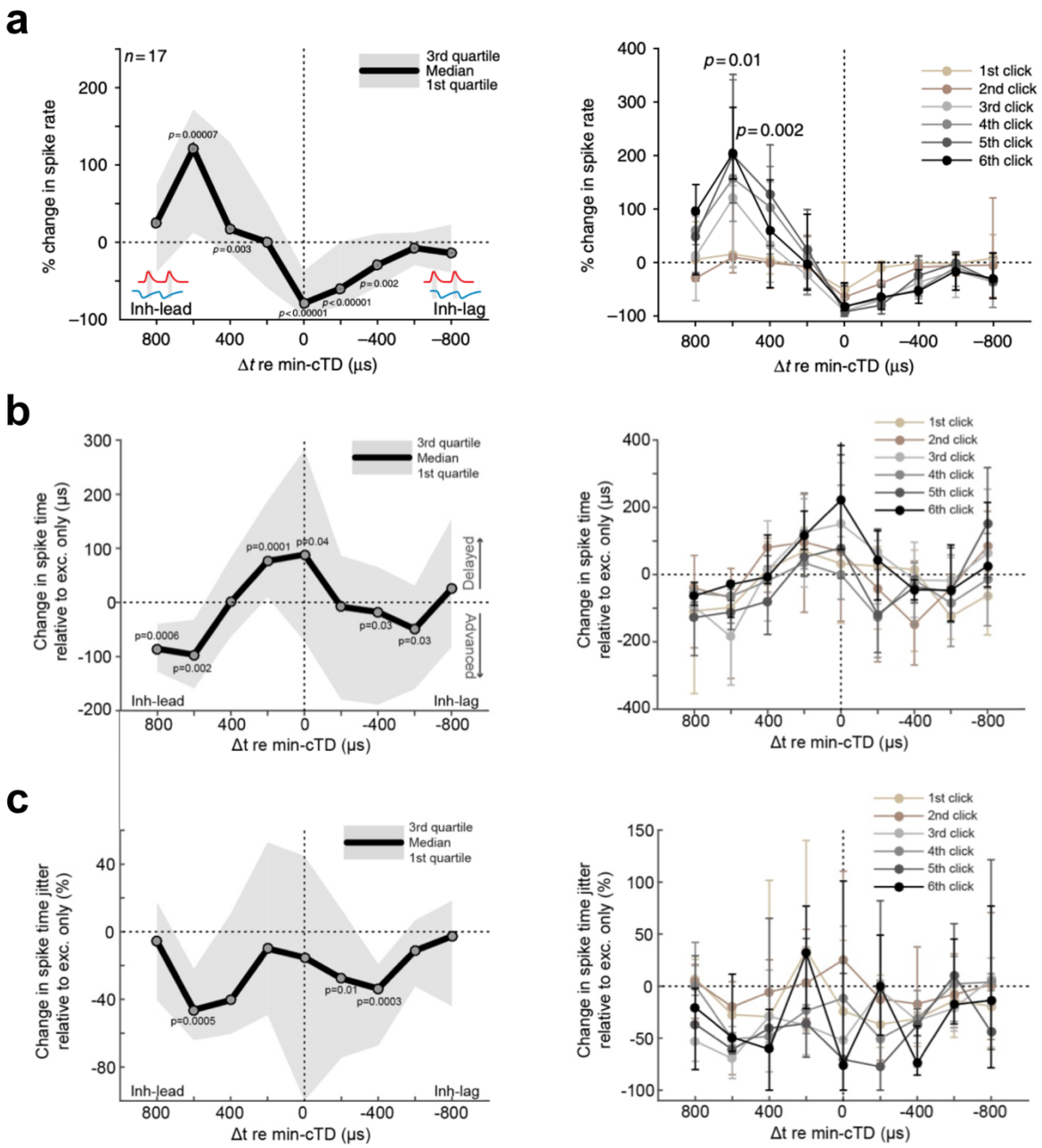

Figure 10: Effects of precisely timed inhibition *in vivo* across *Δt*. Left panel (a-c): Median changes to the entire click train relative to median responses during monaural-only (ipsilateral) stimulation (median ± 25th and 75th percentile). Right panel (a-c): Mean changes ± s.e.m. to individual clicks (color-coded) relative to mean responses during monaural-only (ipsilateral) stimulation **a** Median change in spike rate. Left: Spike rates were significantly increased when inhibition was functionally leading excitation by 400 or 600 µs (n = 17 neurons from 12 animals; median increase: 120.6 and 16.3%, P = 0.00007 and P = 0.003 respectively; Wilcoxon signed rank test). Right: Spike enhancement was preserved throughout the entire click train with more pronounced increase in spiking for subsequently later clicks of the click train (n = 15 neurons from 11 animals, P = 0.01 at *Δt* = 600 µs and P = 0.002 at *Δt* = 400 µs, Friedman's test). **b** Left: Spikes occurred significantly earlier when inhibition was functionally leading excitation by 600 µs (n = 15 neurons from 11 animals; median: 96.6 µs, p=0.002; Wilcoxon signed rank test;) or 800 µs (median: 85.7 µs, p=0.0006; Wilcoxon signed rank test). Right: Trends for bidirectional spike timing shifts as a function of *Δt* were also observed for individual clicks. **c**

Left: Temporal jitter varied across *Δts* with highest reduction at *Δt* = 600 µs (n = 15 from 11 animals; median: -46.2%, p=0.0005; Wilcoxon signed rank test). Right: Jitter reduction tended to be higher for later clicks in the train. (Adapted from (Beiderbeck et al. 2018); Modified. *Nature Communications* articles are published open access under a CC BY license (Creative Commons Attribution 4.0 International License). The CC BY license allows for maximum dissemination and re-use of open access materials. Under Creative Commons, authors retain copyright in their articles.)

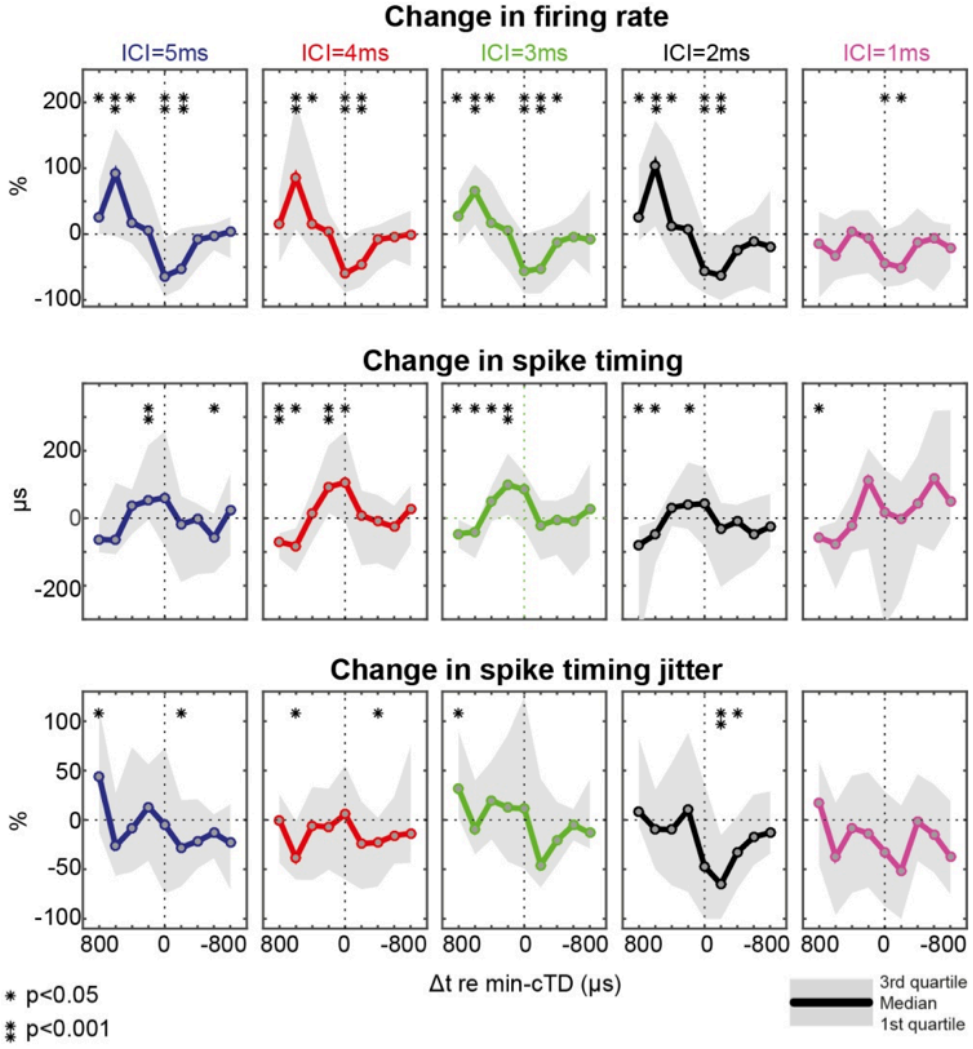

Figure 11: Effects of precisely timed inhibition *in vivo* across *Δt* and across ICIs. Data are presented as Median changes to the entire click train at individual ICIs (1-5 ms; 1 ms steps; color-coded) relative to median responses during monaural-only (ipsilateral) stimulation (median ± 25th and 75th percentile). Top Panel: Change in firing rate. Middle panel: Change in spike timing. Bottom panel: Change in spike timing jitter. Significant changes are denoted by asterisk(s) (paired Wilcoxon signed rank test; * for p-values < 0.05; ** for p-values < 0.005. (Adapted from (Beiderbeck et al. 2018); Modified. *Nature Communications* articles are published open access under a CC BY license (Creative Commons Attribution 4.0 International License). The CC BY license allows for maximum dissemination and re-use of open access materials. Under Creative Commons, authors retain copyright in their articles.)

3.1.3 Inhibition facilitates spiking and alters its timing *in vitro*

In vitro whole-cell recordings in 3.1.3 were conducted by Prof. Dr. Michael Myoga and Dr. Alexander Callan and Dr. Nicolas Müller). The below section is a summary of the most relevant findings for this study. Additional figures and information are available in (Beiderbeck et al. 2018). *In vivo* (3.1.2), we were able to observe changes in spike rates, spike timing and temporal precision of spikes in dependence of the temporal relationship between excitatory and inhibitory inputs. More specifically, well-timed functionally leading inhibition seems to provide a sweet spot for LSO neurons that reduces latencies and promotes spiking. It has previously been shown in juvenile MSO neurons *in vitro* that precisely timed preceding synaptic inhibition can enhance spiking through post-inhibitory facilitation (PIF) (Dodla, Svirskis, and Rinzel 2006) and we sought to test if similar properties may be present in LSO neurons. To gain a mechanistic understanding of these effects acute in vitro brain slice preparations in adult gerbils (postnatal days 31-38) have been developed to examine temporal interactions between excitation and inhibition at LSO somata using conductance clamp. Stimulus design involved measuring excitatory and inhibitory synaptic conductance waveforms in voltage-clamp to obtain conductance templates reflecting natural synaptic kinetics of adult LSO neurons. In accordance to these templates and relative to a set reversal potential for excitation (+5 mV) and inhibition (-85 mV) calculated currents could be injected (Fig. 12a). To mimic the stimulus of six consecutive clicks presented *in vivo,* six-event stimulus trains of excitatory synaptic conductance templates with a fixed amplitude for each event (G_e) were applied with an inter-stimulus-interval (ISI) of 5 ms. Initial results of an example neuron revealed a consistent spike in response to the first event, however, spiking to subsequent events was rarely observed (Fig. 12 b, grey traces). When pairing an excitatory conductance train with a corresponding inhibitory conductance train at a relative time difference (rTD) of +2.5 ms (inhibition leading excitation) spiking was successfully suppressed

(Fig. 12b top panel, red traces). However, at rTDs of +3.5 ms spiking was promoted throughout the entire event-train (Fig. 12b bottom panel, red traces).

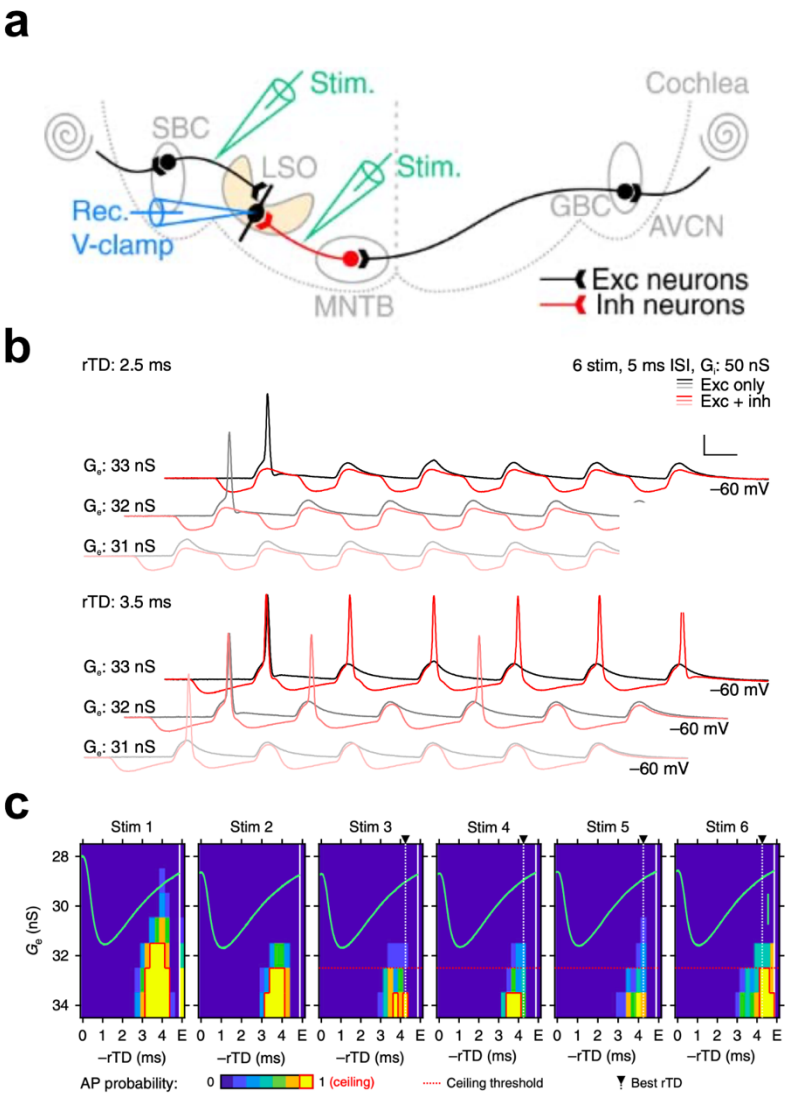

Figure 12: Experimental design and example for spike enhancement through well-timed inhibition *in vitro*. a Schematic of the recording and stimulus design. **b** Voltage traces from an example conductance-clamp recording in response to six-event trains with an ISI of 5 ms. Excitation alone (grey traces) generated at most one spike at the onset. The same protocol performed with an identical inhibitory train (peak conductance (Gi) = 50 nS) at an rTD of –2.5 ms suppressed spiking (top panel; red traces), but at an rTD of –3.5 ms promoted spiking not only at the onset but also throughout the event-train (bottom panel; red traces). Scale bar: 20 mV, 2 ms. **c** Probability heat maps as a function of G_e vs. rTD for subsequent events (left to right) for the experiment shown in (b) with corresponding IPSP trace overlaid (green, scale bar: 5 mV). Red border outlines G_e conditions that resulted in 100% spike probability on more than one rTD (ceiling). At higher G_e values, PIF saturates (yellow area with red outline) in particular for the first two stimulus events. Dotted red line indicates the ceiling threshold for this recording. Spike probability from excitation alone is shown at the right of each plot. Dotted white line and arrowhead indicates the calculated "Best rTD" for the last 4 events for this recording. (Adapted from (Beiderbeck et al. 2018); Modified. *Nature Communications* articles are published open access under a CC BY license (Creative Commons Attribution 4.0 International License). The CC BY license allows for maximum dissemination and re-use of open access materials. Under Creative Commons, authors retain copyright in their articles.)

For better comparability to our *in vivo* recordings where spike enhancement was significant only for the last 4 clicks of the click-train (Fig. 10a), *in vitro* analysis of the population sample (n=9 recordings) was concentrated on the last 4 stimulus-events where PIF was shown to be a sizeable and robust phenomenon that occurs within a precise temporal window during the repolarization phase of inhibition that matches our *in vivo* findings (Fig. 10a; Fig. 12c, Fig. 13a). In addition, based on our *in vivo* findings where functionally leading inhibition was shown to decrease spike latency, single AP timing (using suprathreshold G_e values without inhibitory stimulation) was compared to single AP-timing imposed by preceding inhibitory stimulation at various rTDs. Consistent with our *in vivo* findings, the relative timing of inhibition and excitation generates a sizeable modulation in AP-timing, with AP latencies being decreased within a temporally precise positive rTDs (preceding inhibition) (Fig. 13c, $P = 6.53 \times 10–6$, one-way ANOVA). Moreover, it was examined whether well-timed and preceding inhibition also decreases temporal jitter as observed *in vivo*. It was found that that PIF *in vitro* in fact led to a general decrease in AP jitter (Fig. 13d; $P = 7.38 \times 10–7$, one-sample t-Test). Thus, our findings in adult LSO slices *in vitro* successfully recapitulated the inhibitory effects identified *in vivo*.

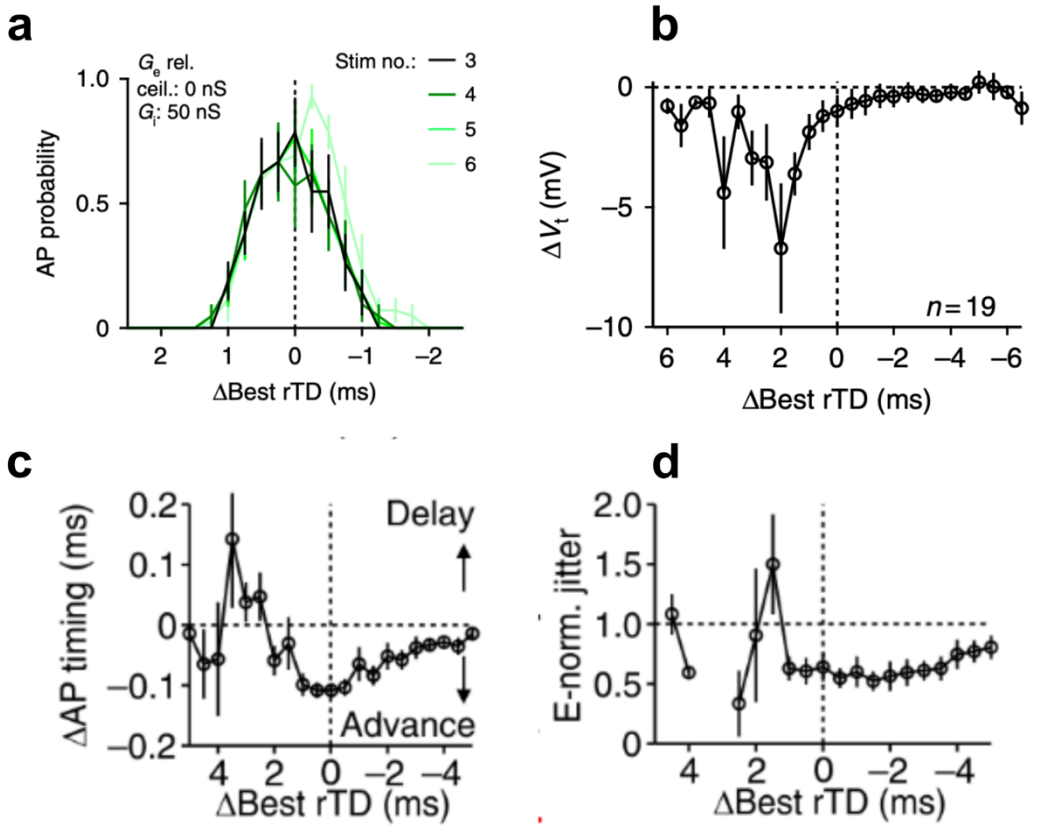

Figure 13: Inhibition modulates spike generation, spike timing and precision of spike timing in vitro in adult LSO slices. Population analysis (n = 9 in (a); n = 19 in (a-d)). All average data represent mean ± s.e.m. **a** Event-wise, population averaged spike probability at ceiling threshold G_e and G_i = 50 nS as a function of ΔBest rTD (ms) (Best rTD represents the temporal relation of excitation and inhibition that generates maximal spike suppression) **b** Quantification of the relative change of spike voltage threshold as a function of ΔBest rTD (ms) **c** Average AP onset timing with inhibition relative to excitation alone plotted against relative Best rTD reveals timing conditions that advance and delay APs. **d** Average jitter, normalized to excitation alone (E-norm) show a generalized reduction in spike timing jitter (P = 7.38 × 10–7, one-sample t-Test). (Adapted from (Beiderbeck et al. 2018); Modified. *Nature Communications* articles are published open access under a CC BY license (Creative Commons Attribution 4.0 International License). The CC BY license allows for maximum dissemination and re-use of open access materials. Under Creative Commons, authors retain copyright in their articles.)

During AP generation, voltage-gated sodium channels first open (activate) following depolarization of the membrane which drives the upstroke. Then, these sodium channels close again (deactivate) during repolarization (enabling repolarization to the resting potential). Mechanistically, PIF could be a result of Na_v channels being relieved from inactivation, which is indicated by the decrease in the AP threshold (V_t) under the influence of well-timed inhibition (Fig. 13b). This hypothesis was examined by mimicking an IPSP waveform in voltage-clamp and at varying times during IPSP presentation the neurons were abruptly brought to a suprathreshold potential in order to evoke an inward AP current (Fig. 14a). The peak current was slightly increased at

particular times during inhibition and this increase declined reliably with the time course of the IPSP (Fig. 14b top). This boost in inhibition induced AP current was significant across cells (Fig. 14b bottom; n = 10; P = 0.002, Wilcoxon signed rank test). These findings suggest that well-timed inhibition could enable repetitive spiking (Fig. 12b,c) through the relief of Na_v channels from inactivation during the repolarization phase which lowers the effective threshold for AP generation. Theoretically, also hyperpolarization-activated cyclic nucleotide-gated (HCN) channels could contribute to PIF. The inward current through opening of HCN-channels (I_h) promotes rebound spiking which has been observed in the superior paraolivary nucleus (Cornelia Kopp-Scheinpflug et al. 2011; Felix et al. 2011). By definition PIF is not identical to rebound spiking as it requires additional excitation and the temporal window in which inhibition promotes spiking is much sharper than the relatively long inhibitory stimulus that is required for rebound spiking. Nevertheless, potential contribution to PIF by I_h was examined by blocking HCN-channels with the selective antagonist ZD 7288 (ZD; data not shown; see (Beiderbeck et al. 2018)) for review). It was shown that under ZD, PIF-function half-widths were increased but PIF persisted in the absence of I_h, which suggests that I_h might sharpen PIF, however, HCN-channels are not required for the generation of PIF (data not shown; see (Beiderbeck et al. 2018) for review).

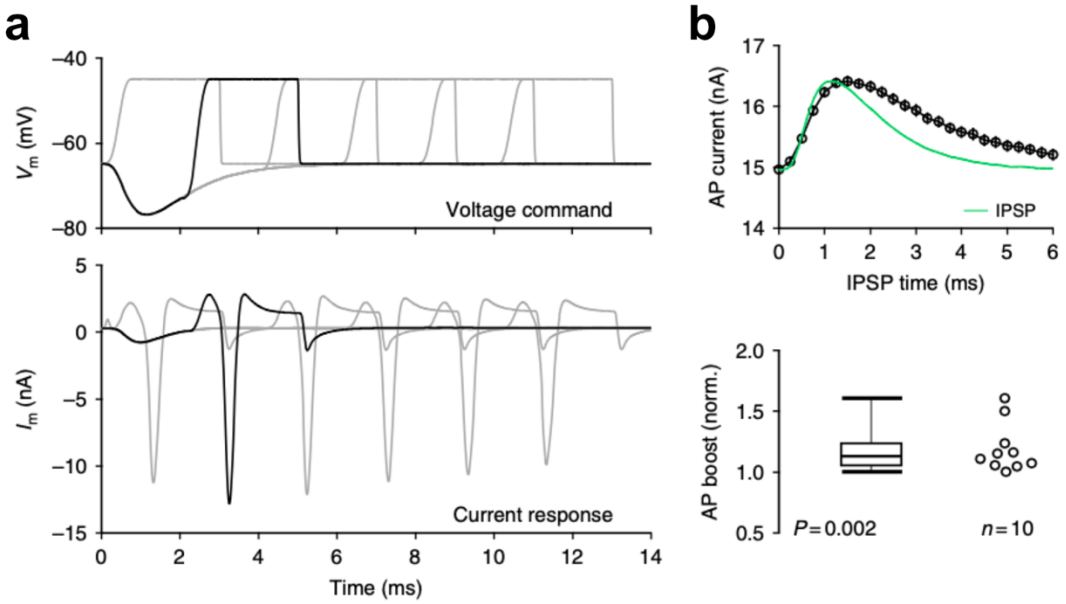

Figure 14: Changes in membrane excitability as a potential mechanism for PIF. a Example traces from a voltage-clamp recording where the voltage command (top) as IPSP waveform was interluded by a suprathreshold value (3 ms duration) at various different starting points (black trace: starting point at

2.5 ms). The resulting inward current (bottom) shows transients of sodium currents that are associated with an AP. **b** Top panel: mean amplitude of the AP current as a function of IPSP time for the recording in (a). The green trace depicts the decay time course of the IPSP. Bottom: box plot shows the median and 25th / 75th percentiles of the distribution of AP boost for all recordings (n = 10). (Adapted from (Beiderbeck et al. 2018); Modified. *Nature Communications* articles are published open access under a CC BY license (Creative Commons Attribution 4.0 International License). The CC BY license allows for maximum dissemination and re-use of open access materials. Under Creative Commons, authors retain copyright in their articles.)

3.1.4 PIF boosts ILD coding

Well-timed and preceding inhibition decreases firing thresholds and therefore enables spiking to otherwise subthreshold excitatory inputs. Subthreshold PSPs could be a result of weak acoustic signals. For contralateral sound source locations, ipsilateral stimuli might eventually not be loud enough to evoke spiking in the LSO. We hypothesize that PIF contributes to the maintenance of the dynamic range (i.e., the slope) of the ILD function in cases where ipsilateral (excitatory) inputs are weak by coupling of subthreshold excitation with strong – and therefore potentially preceding – inhibition (Fig. 15a,b). To test our hypothesis, I performed further extracellular single-cell recordings in the LSO and recorded sets of binaurally correlated noise ILD functions, each set having a progressively weaker fixed ipsilateral sound intensity paired with an unchanged range of contralateral stimuli. Interestingly, when the ipsilateral intensity was lowered by 5 dB, response rates to a particular contralateral intensity (along the slope of the ILD function) remained comparable (Fig. 15d; n=7 neurons; −0.37% median change, interquartile range −2.75–0.24%; P = 0.22, Wilcoxon signed rank test) and tended to be only marginally lower when the ipsilateral intensity was lowered by 10 dB (at same contralateral intensity) (Fig. 15d; n = 7 neurons; −13.0% median change, interquartile range −21.5 to −5.9%; P = 0.03, Wilcoxon signed rank test). As a result, the different sets of ILD-response functions displayed a robust dynamic range (slope) that was not significantly altered (Fig. 15e; n = 7 neurons; −5dB: −3.1% median change, interquartile range: −16.6–9.8%, P = 0.81, Wilcoxon signed rank test; −10 dB: −4.7% median change, interquartile range −19.6–11.4%, P = 0.81, Wilcoxon signed rank test). This slope consistency maintains separability between ILDs across various ipsilateral intensities (standard separability measure, see figure legend and 2.2.5.1 for additional information). Therefore, the functional significance of PIF in the LSO could include preserving spatial separability across sound intensities which suggests that sub-millisecond precision of the relative timing of excitation and inhibition plays a crucial role in binaural integration in the LSO.

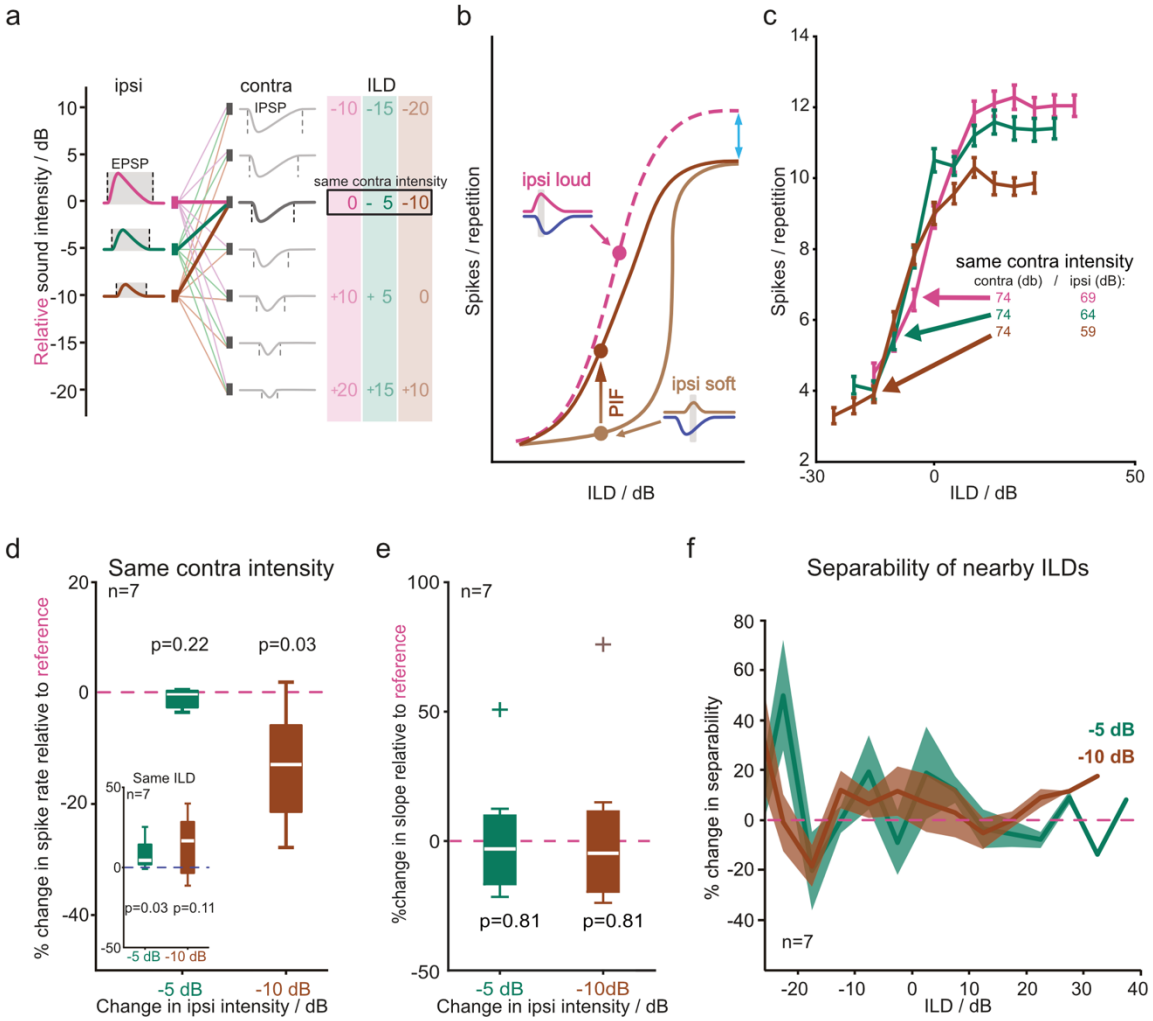

Figure 15: The functional role of PIF in the LSO. a Schematic illustration of the stimulus design. ILD functions of correlated noise stimuli: Three distinct ipsilateral sound intensities (left panel) were paired with a fixed cassette contralateral sound intensities (middle panel) resulting in 3 different ILD functions (right panel; color-coded relatively to ipsilateral stimulus strength). Black box depicts the ILD for an individual contralateral stimulus level at 3 different ipsilateral intensity levels. **b** Schematic illustration of our hypothesis: ILD functions that are based on weak ipsilateral levels might have steeper slopes (and therefore the separability of nearby ILDs might be decreased; light brown trace) than ILD functions that are based on loud ipsilateral levels (dashed pink trace). However, since PIF could potentially promote spiking of otherwise subthreshold excitatory inputs it could potentially recover the slope of the ILD function (dark brown trace). Insets depict the relative timing between EPSPs and IPSPs (EPSPs color-coded as per schematic traces; weak excitation = light brown; strong excitation = pink; blue traces depict the relative timing of the unchanged IPSP to a respective weak or strong EPSP). **c** Distinct ILD-response functions of an example neuron (CF: ~16.2 kHz) color-coded as per stimulus protocol illustrated in (a). Data are presented as mean ± s.e.m.; color-coded arrows point at the mean response rates at a fixed contralateral level of 74 dB paired with ipsilateral levels of either 69, 64 or 59 dB SPL (which equals to ILDs of -5, -10 and -15 dB respectively) **d** Changes in spike rates along the slopes of the ILD function were either comparable or only marginally (and not significantly) affected by decreased ipsilateral levels (Wilcoxon signed rank tests (n = 7 neurons): −5 dB: −0.37% median change, interquartile range −2.75–0.24%; P = 0.22; −10 dB: 13.0% median change, interquartile range −21.5 to −5.9%; P = 0.03). Inset: spike rates at identical ILDs were increased during reduced ipsilateral stimulus

intensities (−5 dB: 4.4% median change, interquartile range: 1.9–14.3%, P = 0.03; −10 dB: 16.6% median change, interquartile range: −3.5–28.4%, P = 0.11, n = 7 cells). White horizontal bars display respective medians, interquartile range is displayed by box plot size; whiskers extend to most extreme data points). **e** Slopes remained comparable between the three different ILD response functions (as per stimulus protocol in (a); −5 dB: −3.1% median change, interquartile range: −16.6–9.8%, P = 0.81; −10 dB: −4.7% median change, interquartile range −19.6–11.4%, P = 0.81, n = 7 cells). Same color-coding as in (d). **f** Separability of adjacent ILDs was comparable across ipsilateral intensities (p > 0.05 (t-test) for all tested ILDs as per protocol in (a); solid lines and shaded areas represent mean ± s.e.m.) (Figure adapted from (Beiderbeck et al. 2018); Modified. *Nature Communications* articles are published open access under a CC BY license (Creative Commons Attribution 4.0 International License). The CC BY license allows for maximum dissemination and re-use of open access materials. Under Creative Commons, authors retain copyright in their articles.)

3.2 Study 2:

Pushing the envelope – The impact of the effective envelope on low frequency MSO neurons

I performed *in vivo* experiments and histology, analyzed the *in vivo* data and wrote the manuscript presented in this thesis. Dr. Jason Mikiel-Hunter analyzed the *in vivo* data and contributed to the design of the experiments.
PD Dr. Michael Pecka, Prof. Dr. David McAlpine, and Prof. Dr. Benedikt Grothe designed and conceived *in vivo* experiments (see 13.2 for signatures and affiliations).

3.2.1 Evidence of envelope sensitivity in low-CF MSO neurons

In study 1 we have investigated how the temporal relationship between inputs can affect neuronal output in the LSO. Such changes in temporal input composition can result from naturally occurring ILDs that independently affect the relative strength, latency and duration of excitatory and inhibitory inputs. However, neurons in the MSO are tuned to low frequencies for which naturally occurring ILDs are negligible. Under the assumption that relative input strengths are therefore likely to remain constant studies in the MSO are usually conducted using either pure tone stimuli or single frozen noise tokens representing only a subset of naturally occurring stimulus varieties. Noteworthy, MSO neurons are known to be slope-detectors (Mikiel-Hunter, Kotak, and Rinzel 2016; Meng, Huguet, and Rinzel 2012), hence response rates are highest at the rising slope (the rate of increased displacement of the basilar membrane within the critical frequency band) of any complex signal. This allows for phase locking to both, TFS and envelope of the stimulus. In fact, the MSO has been assessed with regard to its envelope sensitivity, however, these studies have mainly been conducted using high carrier frequencies (Batra and Fitzpatrick 1997; McFadden and Pasanen 1976). Nonetheless, as outlined in 1.3.8, cochlear filtering decomposes complex broadband signals into a series of narrowband signals with dynamic and nonlinear $envelope_{effect}$ patterns. As outlined in 1.3.2 and 1.3.3, ITD sensitivity in the MSO relies on relative excitatory and inhibitory inputs. How these individual inputs are affected by

such dynamic $envelopes_{effect}$ patterns and therefore to what extent $envelopes_{effect}$ affect ITD sensitivity in the MSO has not yet been fully assessed, in particular for low frequency stimuli where neurons in the MSO are still able to phase-lock to the TFS of the stimulus as well (Kiang 1965; Johnson 1980; Palmer and Russell 1986). To study the functional impact of $envelopes_{effect}$ on low frequency ITD sensitivity, I conducted extracellular single-cell recordings *in vivo* of 16 low frequency neurons in the MSO of anesthetized Mongolian gerbils (n = 12 animals, 3-7 months of age with CFs ranging from 267-1600 Hz). Via headphones, I presented a set of 10 distinct frozen and binaurally correlated white noise tokens for which the spectral content of the stimulus remains unchanged whilst applying a different envelope to each noise token (duration: 100 ms, 5 ms cos-ramps, spectral content unchanged with cut-off at 10 kHz). Individual white noise tokens were presented binaurally at various ITDs from -1.75 ms to +1.75 ms (50 µs resolution; 3 repetitions per noise token per ITD; 30 dB above threshold) (Fig. 16).

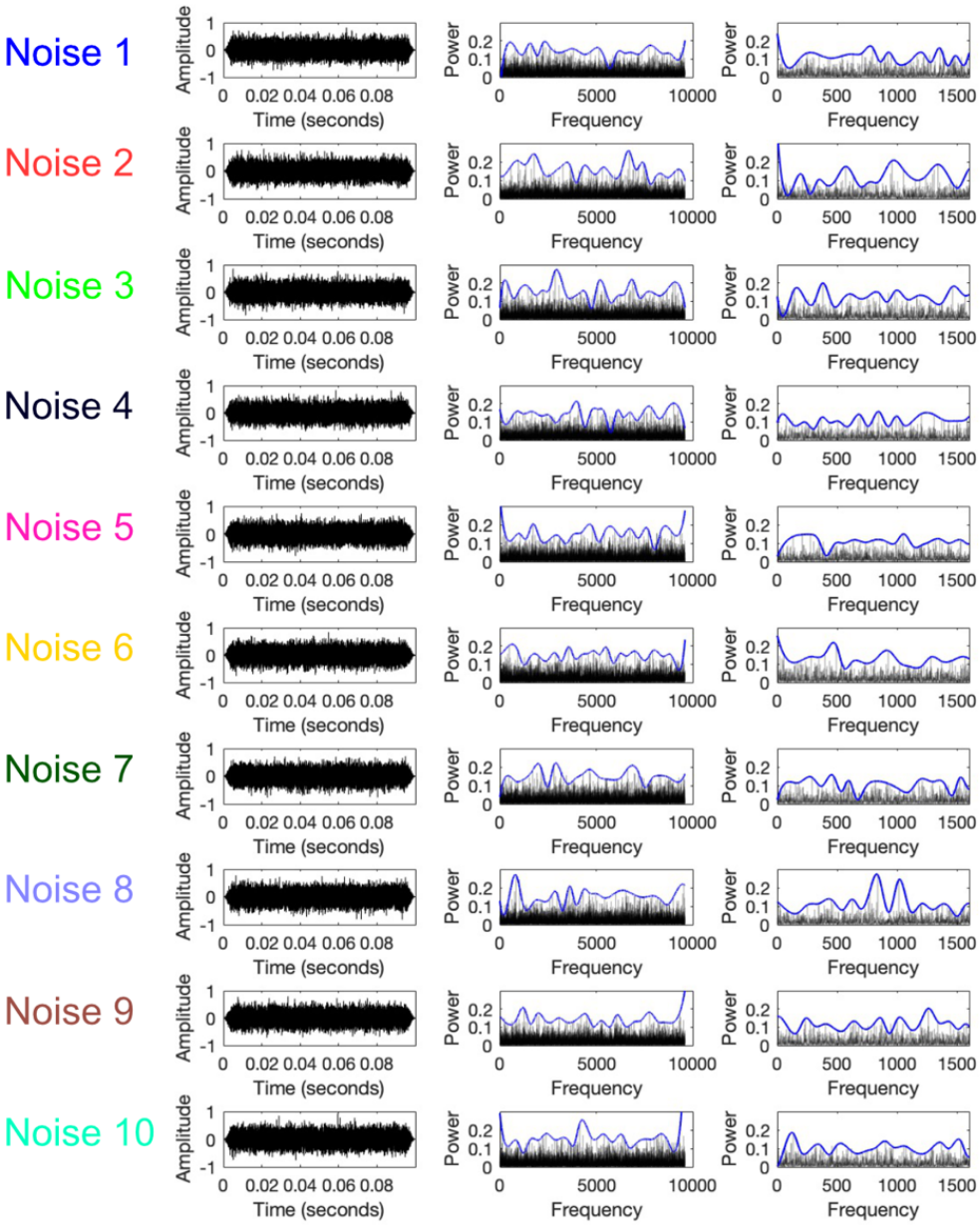

Figure 16: Noise Library. Left column: 10 frozen white noise tokens with different envelopes (color-coded; duration: 100 ms; spectral content unchanged, cut-off at 10 kHz). Middle column: Individual power spectra of noise tokens shown on the left. Blue traces depict individual envelopes. Right column: Same concept as in the middle column; zoomed in for greater spectral resolution up to 1600 Hz (covering the CF range of recorded MSO neurons).

Resulting NDFs were analyzed for each individual noise token. Figure 17c shows the individual NDFs of an example neuron (CF: 267 Hz) for each single noise protocol (mean spike rates ± standard deviation (s.d.)). Individual NDFs of this example neuron varied in overall magnitude with Noise#5 generating most spiking (mean = 8 spikes ± 0 spikes s.d.) at the peak of the ITD function (best ITD) compared to Noise#4 eliciting the least spikes at best ITD (mean = 4 spikes ± 1 spike s.d.). This difference in spike rate can be explained in basilar membrane displacement in the frequency band that

generates spiking in the MSO neuron (example neuron's CF: 267 Hz) varying across noises, i.e., spike magnitude depends on the overall spectral energy (envelope) of the stimulus in the specific frequency band of a neuron (compare Fig. 16 Noise#4 vs. Noise#5 around the neuron's CF). If this displacement is little it will naturally limit activity in ANFs and – more importantly – the ability to phase-lock to specific transient events in the stimulus (envelope), which represents a prerequisite for ITD computations in the MSO. In other words, the $envelope_{effect}$ of the noise token within a neuron's frequency band may affect its ITD sensitivity. Accordingly, across the population tested (n = 16 neurons) neuronal responses were individually modulated by both ITD and noise sample (for each individual neuron: ITD: $p < 0.001$; noise sample: $p < 0.001$; two-way ANOVA) with significant interaction (combination of both ITD and noise) in 50% of the tested population (two-way ANOVA; $p < 0.05$). In addition, we applied a Gaussian fit to each individual ITD function and examined the potential shifts of best ITD per noise sample for individual neurons. We observed that best ITDs in fact vary in dependence of the $envelope_{effect}$ (Fig 18, paired Student's t-tests re mean best ITD (over all noise samples); p-values (per cell, per noise) < 0.05). On top of that, for some neurons individual noise tokens led to a decrease in overall ITD sensitivity (blue stars, Fig. 18). These unexpected findings suggest stimulus dependent changes in input strength on top of the phasic ITD-sensitivity associated with the CF that can be attributed to the $envelope_{effect}$.

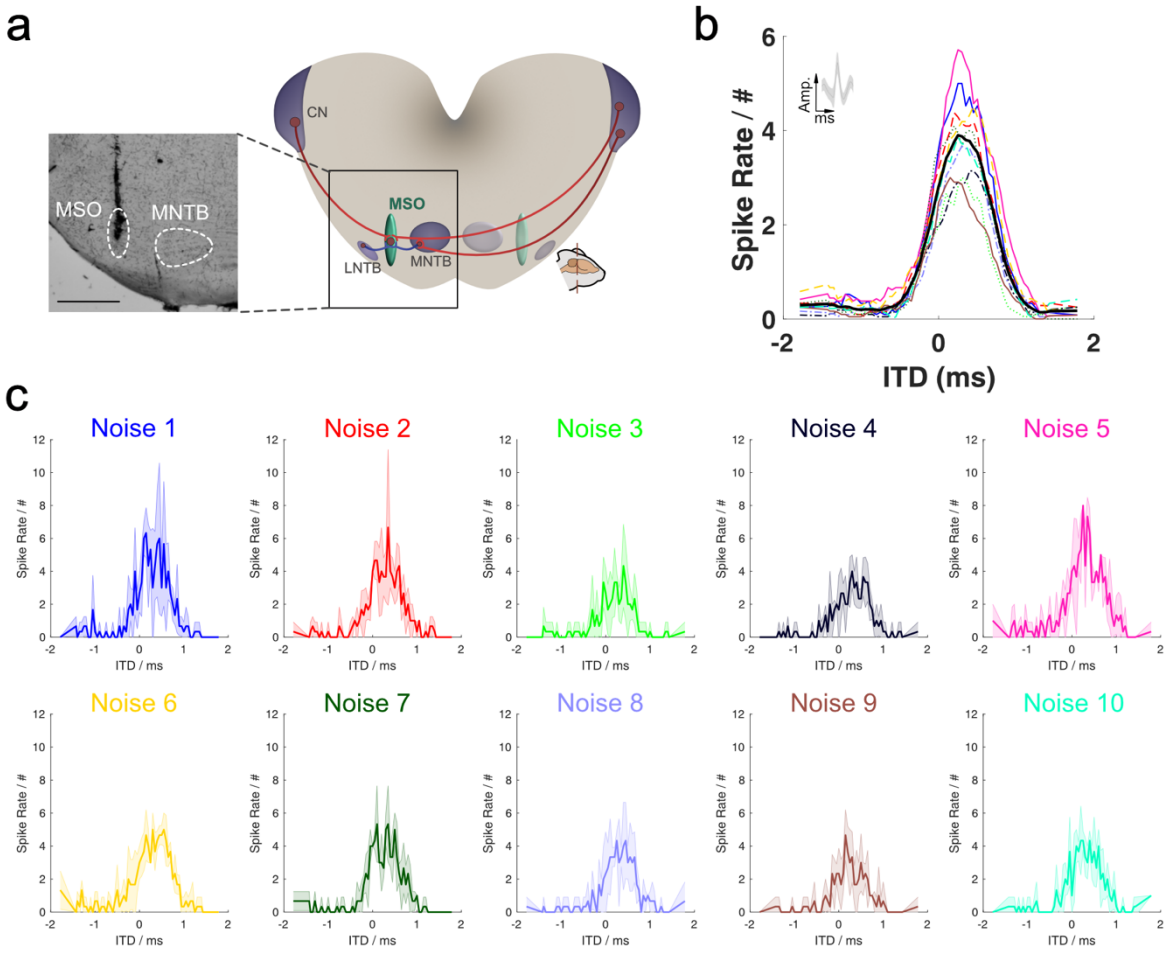

Figure 17: Individual ITD-response functions to 10 sets of frozen correlated white noise tokens. **a** Left: Histologically, the recording site of the example neuron in (b) and (c) has been located in the MSO, scale bar; 500 µm. Right: Schematic: Neurons in the MSO receive excitatory inputs from the ipsilateral and contralateral CN. Inhibitory inputs are received from the ipsilateral LNTB and indirectly from the contralateral CN via the ipsilateral MNTB. **b** Mean ITD-response functions (repetitions: 3, moving average) of an example neuron (CF: 267 Hz). Individual traces represent color-coded ITD-response functions to individual noise tokens as per legend inset and Fig. 16. Bold black trace represents the mean ITD function over all tested noise protocols. Inset displays the spike shape of the recorded example neuron. **c** Individual color-coded ITD-response functions for each tested noise protocol (as per Fig. 16) for the same neuron as in (b). Data are presented as mean (solid trace) ± standard deviation (s.d.; shaded area).

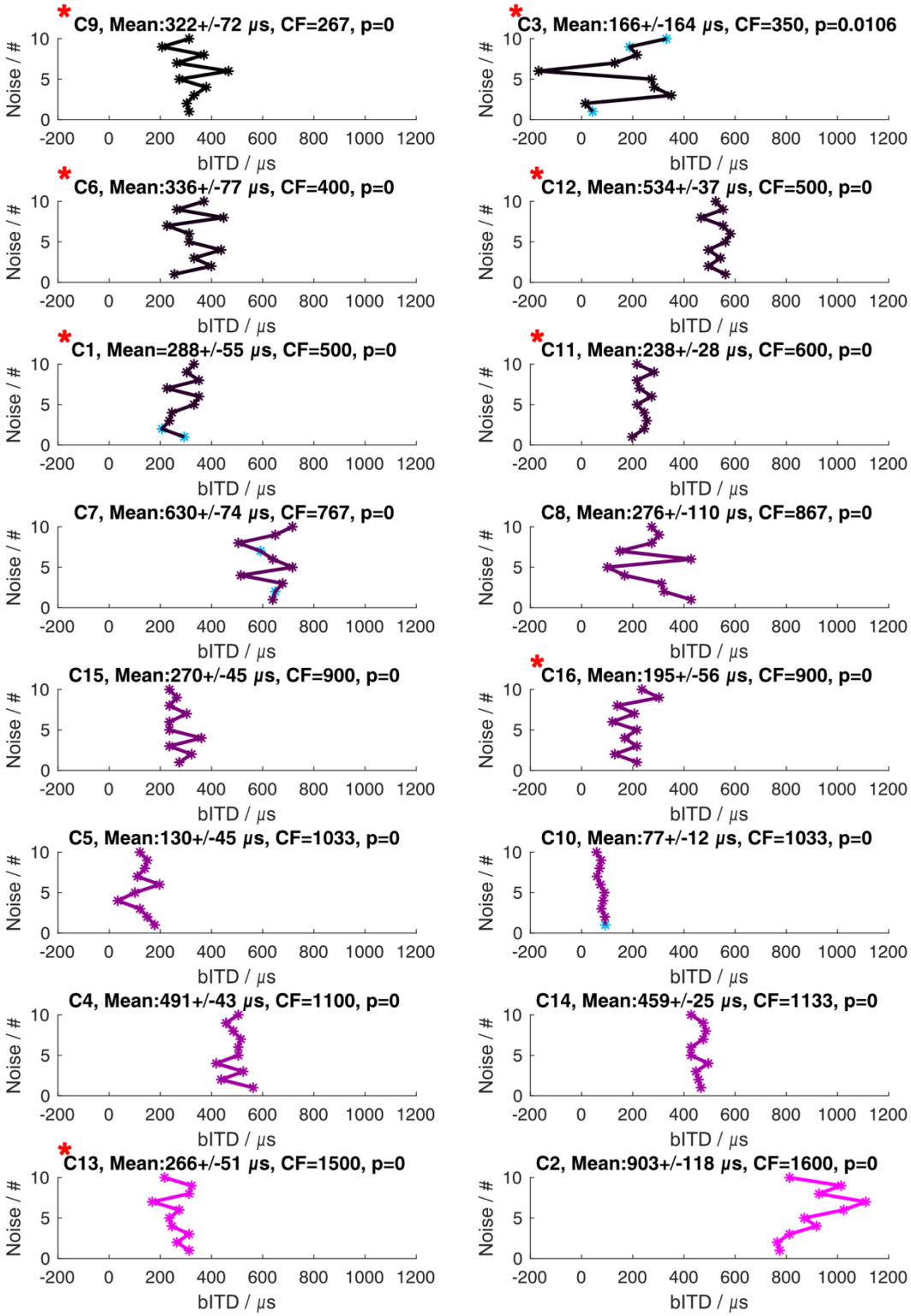

Figure 18: Absolute change of best ITD per noise sample. Each subplot depicts the mean best ITD of an individual MSO neuron (n = 16) per noise sample (y-axis; 3 repetitions/per noise); color-gradient highlights CFs from as low as 267 Hz (subplot 1, black trace) to 1600 Hz (subplot 10, pink trace). Light blue data points reflect noise protocols for which individual cells did not show significant ITD sensitivity. Red stars reflect cells for which neuronal responses were significantly modulated by a combination of both ITD and noise ((two-way ANOVA; $p < 0.05$)). All neurons showed significant shifts in best ITD with

varying noise samples (t-test re mean best ITD per cell; individual p-values are displayed in the title of each subplot; “p = 0” indicates p<0.0001). Cell “C9” is the same cell as in Fig. 17b and 17c.

Since the different noise tokens in our study setting have different envelopes (i.e. different rising slopes) phase-locking in the MSO might reflect the temporal pattern of the underlying $envelope_{effect}$. Hence, evidence for $envelope_{effective}$ sensitivity can be identified by looking at the spike timing in each NDF of individual noise samples. Fig. 19a (upper left panel) displays a heatmap with spikes that occur within the first 30 ms (x-axis; spike histograms are displayed for the first 30 ms for improved visibility of individual event columns) in response to Noise#1 at various ITDs (y-axis). The spike raster heatmap reveals particular events across the stimulus where the neuron tended to fire. Collapsing this information along the timeline (x-axis) will read-out the underlying NDF for this time frame (Fig. 19a; middle panel). On the other hand, collapsing the heatmap across ITD (y-axis), will provide a spike histogram across ITDs (in response to Noise#1 over 3 repetitions, Fig. 19a; lower left panel, black trace) that depicts the accumulated spikes across ITDs at a given time along this time frame. Since the MSO by its nature shows phasic response patterns, we can assume that these event columns in the heatmap reflect the neuron’s phase-locking to either the TFS, the $envelope_{effect}$, or a combination thereof. We can assess its underlying driving element by presenting the same stimulus protocol with inverted stimulus polarity. If the neuron is phase-locking solely to the TFS, flipping the polarity of the underlying carrier will ultimately change the occurrence of the rising slopes of the TFS and hence event columns should appear at different points in time (out-of phase to the original stimulus). On the other hand, if the neuron is phase-locking solely to the $envelope_{effect}$, changing the polarity of the carrier will not affect the temporal occurrence of individual slopes of the $envelope_{effect}$, hence the occurrence of event columns should not vary in time using an inverted stimulus paradigm. A comparison of the spike histogram in response to the original stimulus (Fig. 19a left bottom panel; black trace (original polarity)) with the spike histogram in response to the same stimulus setting but with inverted polarity (Fig. 19a left bottom panel; red traces (inverted polarity)) reveals a temporal overlap of respective accumulated spikes across ITD. This suggests that the temporal window in which the neuron was most likely to fire action potentials was orchestrated by the $envelope_{effect}$.

Unexpectedly, we noticed that the spike histogram in Fig. 19a (bottom panel) reveals rather smeared peaks despite there being particular events where the neuron tended to fire (compare to diagonal spike traces in Fig. 19a; left panel). This “smearing” or diagonality seems to be caused by a temporal bias that expands from negative to positive ITDs. Usually, we would expect the neuron to follow the stimulus that is temporally leading at a given ITD, i.e., we would expect that spike latencies match the ipsilateral stimulus for negative ITDs and the contralateral stimulus for positive ITDs (Fig. 19b; left panel). Unexpectedly, however, the delay in spike timing neatly matches the temporal displacement of the monaural ipsilateral $envelope_{effect}$ that was introduced experimentally to generate ITDs (compare Methods and Fig. 19b; right panel). This can be demonstrated by compensating spike times for the prior introduced ipsilateral stimulus delays, i.e., by artificially (and post-hoc) advancing the spikes for positive ITDs and delaying them for negative ITDs. This generated a spike histogram with clearly defined event peaks (Fig. 19a; lower right panel, black trace), demonstrating that spiking (more specifically spike timing) of this MSO neuron was determined by the ipsilateral input. In addition, the compensated spike histogram in response to the original stimulus and the compensated spike histogram in response to the inverted stimulus (Fig. 19a bottom right panel) remains highly correlated. Cross-correlating (CC) the compensated spike histograms of the neuron’s response to different noises with original and inverted polarity result in CC-coefficients in the range of 0.68-0.85 for the first 30 ms of the stimulus ($p < 0.0000$ apart from Noise#5 where $p = 0.84$) and 0.65-0.79 for the entire stimulus ($p < 0.0000$ apart from Noise#5 where $p = 0.21$) (Fig. 19c; right panel). Similar CC-coefficients can be observed across the sample tested (n = 7 MSO neurons with available inverted ITD-response functions (CFs ranging from 500-1600 Hz): Median $CC\text{-}coefficient_{0\text{-}30ms} = 0.70$; Median $CC\text{-}coefficient_{0\text{-}100ms} = 0.45$) suggesting high correlation for the first 30 ms of the stimulus that only slightly decreases along the entire stimulus length implying that the neuron’s temporal firing pattern was dominated by the temporal displacement of the monaural ipsilateral $envelope_{effect}$. Interestingly, this rather unexpected finding of monaural dominance can per se not be explained under the classical Jeffress model given perfect equality of the two excitatory inputs. Together, our initial analysis suggests that event peaks can be associated with either the onset or the ongoing amplitude fluctuations of the $envelope_{effect}$ which could potentially be used to isolate spikes associated with $envelope_{effect}$ or carrier components of the stimulus.

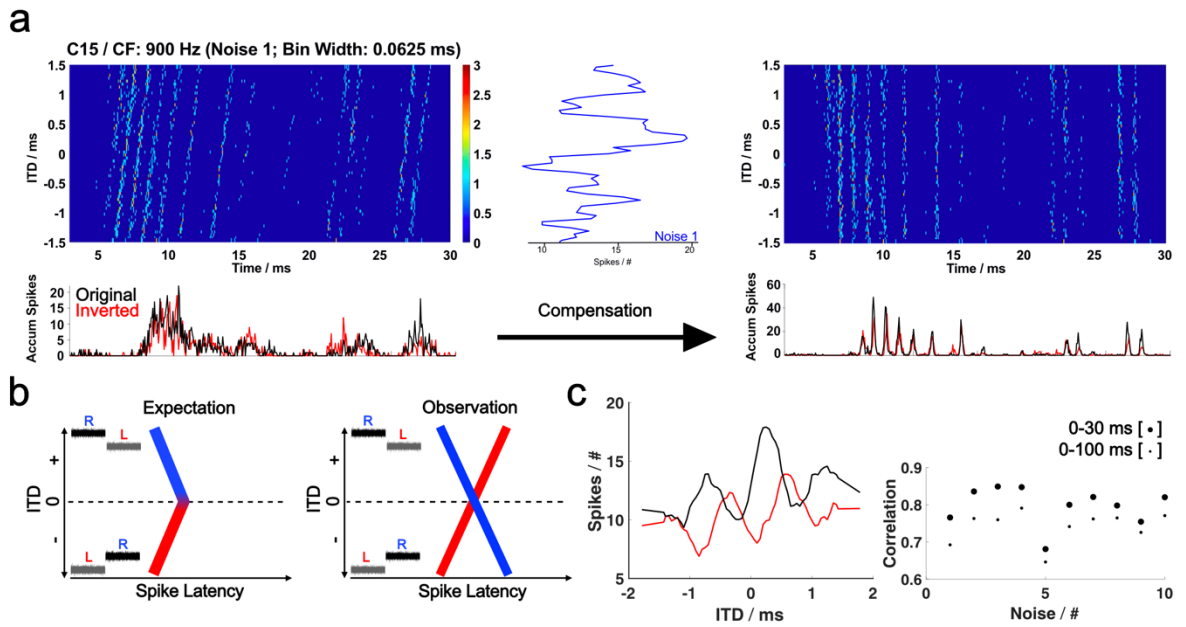

Figure 19: Envelope sensitivity in low-frequency MSO neurons. a Example neuron: CF: 900 Hz (cell 15 in Fig. 18). Left panel: Top: Heatmap of spikes (bin width: 0.0625 ms) that occur within the first 30 ms in response to Noise#1 at various ITDs (y-axis; 3 repetitions per ITD) before (left panel) and after (right panel) compensation of the temporal monaural (in this case: ipsilateral) envelope$_{effect}$-bias. Top middle panel depicts the mean spike rate in response to Noise#1 at various ITDs which can be obtained by collapsing the heatmap across the time dimension (x-axis). Bottom: Accumulated spike histograms of responses to Noise#1 (with original polarity (black trace) and inverted polarity (red trace)) across ITDs (3 repetitions) before and after compensation of the temporal monaural envelope-bias (bottom left vs. bottom right panel). Note: Compensation reveals precisely timed event peaks in which the neuron was inclined to fire. **b** Left: Schematic of expected temporal bias caused by the stimulus design: We would expect the neuron to follow the stimulus that is temporally leading at a given ITD, i.e., that spike latencies match the ipsilateral envelope for negative ITDs and the contralateral envelope for positive ITDs. Right: Schematic of the observation found in a subset of neurons: the delay in spike timing matches the temporal shift of the monaural ipsilateral or contralateral envelope. **c** Same example neuron as in (a) Left: Mean response rates to ITD functions using 10 different noise tokens (as in Fig. 16) with original polarity (black trace) and inverted polarity (red trace). Note, despite tuning functions being anti-correlated, occurrence of event peaks in the uncompensated and compensated accumulated spike histogram remains similar in time (see Fig. 19a; bottom panel). Right: Cross-correlation coefficients between event peaks (in the accumulated spike histograms) in response to original (with original polarity) and inverted NDFs for the first 30 ms (large circles) and for the entire stimulus-length (100 ms; small circles).

3.2.2 Epoch vs. non-Epoch components

The question arises to what extent spikes within such event peaks, i.e., spikes that appear to be monaurally dominated in their timing, influence overall ITD-sensitivity. To identify their impact on overall ITD sensitivity, we separated spikes at and tightly around the event peaks of the accumulated spike histogram after monaural timing compensation as introduced in Fig. 19 (Fig. 20a). The threshold for separation was

set in a way that at least 90% of the summed coincident spikes across ITDs are considered to be spikes that are aligned with monaural timing of the $envelope_{effect}$ (Fig. 20b). This definition will thus subdivide neuronal responses into two groups: “epoch-spikes” which will presumably reflect a less ITD-sensitive response to the monaural $envelope_{effect}$ of the stimulus and the remaining “non-epoch-spikes” which we assume might leave us with the responses that are predominantly driven by a binaural coincidence mechanism. Fig. 20c depicts the disaggregation of the NDFs of an example neuron (CF: 867 Hz) into epoch and non-epoch components. The original NDF that contains all spikes (NDF_{all}; Fig. 20c; left panel; mean NDFs per noise; color-coded as in Fig.16/17) is modulated by ITD with mean best ITDs of +249 µs ± 90 µs (across noise samples) and a general rate asymmetry between negative (ipsi-leading) and positive (contra-leading) ITDs. Such a DC-offset (which we have observed in 17 of 21 MSO neurons including additional MSO neurons from 3.2.4) has been previously observed in the IC (an upstream target of the MSO) and was linked to envelope-sensitive components that cannot be predicted from linear interaural integration (Agapiou and McAlpine 2008b). In line with this explanation, this rate asymmetry becomes even more pronounced for NDFs that are limited to the epoch-spikes (NDF_{Epoch}; Fig. 20c; middle panel) which results in a nearly sigmoid shape of the NDF_{Epoch} that is reminiscent to ILD-functions in the LSO (compare with Fig. 15c). Noteworthy, despite the spike timing being heavily driven by the monaural input, ITD sensitivity is not lost in these epoch-components, suggesting it is still influenced by a binaural mechanism. NDFs that only contain non-epoch spikes (NDF_{NEpoch}), on the other hand, display ITD-sensitive components without DC-offset that are more typically associated with phasic ITD response functions to pure tone stimulation (Fig. 20c; right panel). Noteworthy, their average best ITD seems to be slightly shifted towards less positive ITDs (average best $ITD_{NonEpoch}$ = 150 µs ± 91.3 µs; One-way ANOVA (best $ITD_{NonEpoch}$ vs. ITD_{Epoch}); p = 0.0713; population n= 16 MSO neurons: average best $ITD_{NonEpoch}$ = 334 µs ± 137 µs; average best ITD_{Epoch} = 351 µs ± 124 µs). Taken together, on top of the phasic ITD sensitivity associated with the CF there is an additional slower modulation of the tuning function that is heavily influenced by the $envelope_{effect}$.

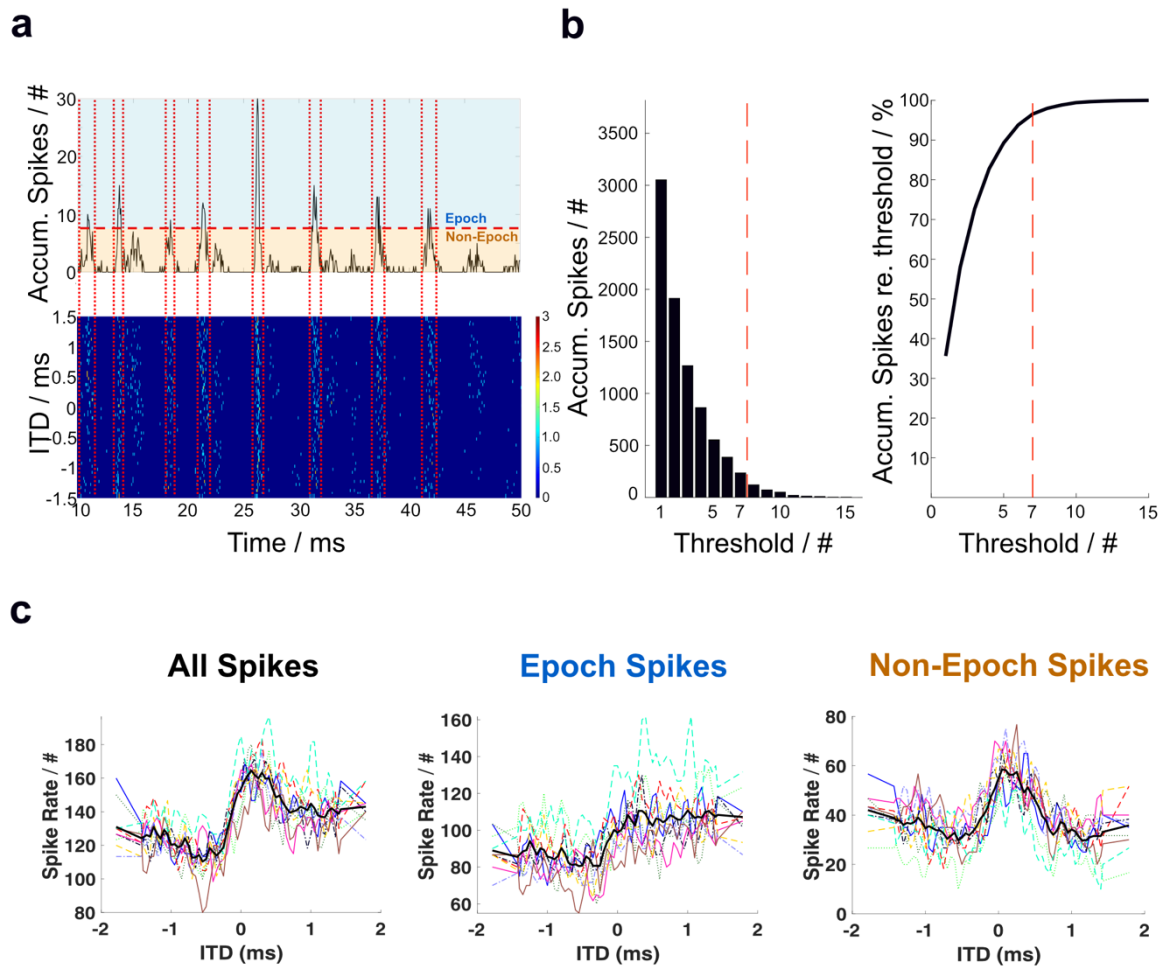

Figure 20: Disentangling NDFs into asymmetric epoch-components and periodic non-epoch components. Epoch and non-epoch analysis of an example neuron (CF 867 Hz). **a** Lower panel: Heatmap of spikes that occur within the first 50 ms in response to Noise#1 across various ITDs (y-axis; 3 repetitions per ITD). Epoch-spikes have been compensated for ipsilateral monaural dominance (as described in Fig. 19). Compensated heatmaps are then collapsed across ITDs and reveal a spike histogram with event peaks (upper panel; as described in Fig. 19). Event peaks are then binned (bin width: 0.0625 ms; indicated by red vertical lines). Horizontal dashed line in red indicates the epoch-threshold further explained in (b). Event peaks that exceed this threshold are classed as 'epoch'-components (light-blue area); event peaks that lie below this threshold are classed as 'non-epoch'-components (orange area). **b** Accumulated spikes as a function of spike threshold (left panel) are translated into a probability graph (right panel) to display the required threshold to define >=90 % of accumulated spikes in event peaks as epoch-components. Vertical dashed line in red displays actual threshold chosen for the displayed example neuron (threshold: 7 spikes in event peak). c Mean NDFs across all noise samples (black trace; 30 repetitions (3 reps per noise)) as well as individual NDFs per noise sample (color-coded as in Fig. 16/17; 3 reps per noise) are shown for all spikes (NDF_{All}; left panel), epoch-spikes (NDF_{Epoch}; middle panel) and non-epoch spikes (NDF_{NEpoch}). Note spike rate asymmetry in NDF_{All} that is preserved in NDF_{Epoch} but not in the more oscillatory NDF_{NEpoch}.

3.2.3 The impact of dynamic changes in input dominance on ITD sensitivity

As shown in 3.2.2, despite the monaural dominance in the spike timing of epoch-components, both, NDF_{Epoch} and NDF_{NEpoch} display ITD sensitivity. However, whilst non-epoch spikes display the classic phasic responses that are associated with the MSO, it is unclear how and to what extent the observed monaural dominance of the $envelope_{effect}$ on spike timing impacts ITD-sensitivity. Importantly, we found that the observed monaural dominance (Fig. 19) can eventually swap over time within the same noise token (switch between ipsilateral and contralateral dominance): Figure 21a depicts the heatmap of an example neuron for which monaural dominance varies for individual "epoch events" along the stimulus which suggests that monaural $envelope_{effect}$ sensitivity is dynamically altered over time. A potential underlying mechanism for this phenomenon could root in neural adaptation at preceding levels of the auditory pathway (e.g. rapid adaptation / recovery from adaptation in auditory nerve fibers (Yates, Cody, and Johnstone 1983; Yates, Robertson, and Johnstone 1985; Westerman and Smith 1987; Dietz et al. 2014) or at the level of the MSO itself (Stange et al. 2013). Hence, activity-dependent adaptation (i.e., the stimulus history) can lead to different input strengths at a given time which manifests neuronal output in the MSO in different ways. Therefore, we sought to compare ITD sensitivity of NDF_{Epoch} and NDF_{NEpoch} in response to the stimulus onset (0-10 ms) and to the ongoing component of the stimulus (10-115 ms). Figure 21b depicts the (from left to right) NDF_{All}, NDF_{Epoch} and NDF_{NEpoch} of an example neuron (CF: 600 Hz; cell 11 in Fig. 16) in response to the stimulus onset (red trace; 0-10 ms) and in response to the ongoing stimulus component (blue trace; 10-115 ms; mean ± s.e.m. across all 10 noise samples (3 reps / noise sample)). Both, onset and ongoing components of NDF_{All}, NDF_{Epoch} and NDF_{NEpoch} are significantly modulated by ITD (2-way ANOVA (noise/ITD): $p<0.005$). For ongoing components, we see the typical differences between NDF_{Epoch} and NDF_{NEpoch}: NDF_{NEpoch} shows the expected classic oscillatory modulation across ITDs typically associated with pure tone ITD sensitivity, whilst NDF_{Epoch} shows a slight DC offset at contra-leading ITDs (compare to Fig. 20c) which has been associated with $envelope_{effect}$ sensitivity (Agapiou and McAlpine 2008). Nonetheless, this neuron still displayed strong ITD sensitivity for the epoch

component, demonstrating that the “classic” binaural coincidence mechanism directly influenced the monaural spike probabilities. Interestingly, despite the differences of NDF_{Epoch} and NDF_{NEpoch} in response to the ongoing stimulus component, both preserve a nearly identical periodicity without DC offset at stimulus onset (Cross-correlation between onsets of NDF_{Epoch} and NDF_{NEpoch}: 0.84, $p<0.0001$). Therefore, whilst the $envelope_{effect}$ can bias ITD sensitivity for ongoing stimulation (Bernstein and Trahiotis 1985), both epoch and non-epoch components in this neuron provide the same combined response to upstream nuclei during the onset of the stimulus which is of particular importance for sound localization in reverberant environments and sound segregation (Franssen 1960; Wallach, Newman, and Rosenzweig 1949). However, this is not necessarily the case in every MSO neuron. As mentioned before, monaural envelope effects on spiking may swap between ipsilateral and contralateral dominance at various epochs within the noise stimuli. Data in Fig. 21c even demonstrated an absence of ITD sensitivity during the first 10 ms of the noise stimulus in both NDF_{Epoch} and NDF_{NEpoch} and the cell only becomes sensitive to ITDs with ongoing stimulation. Potentially, the reason for this evolving ITD sensitivity along the noise stimulus might be a sort of stimulus-dependent adaptation that adjusts the relative tuning of excitatory and inhibitory inputs. This suggests that epoch-spikes in this neuron at the onset of the stimulus were predominantly driven by monaural inputs that override the ITD-sensitive component of its response. Only after the stimulus triggered the aforementioned short-term adaptation of the individual inputs according to the spectral composition of the noise at the respective epoch, a “true” ITD sensitive response is generated by the MSO neuron.

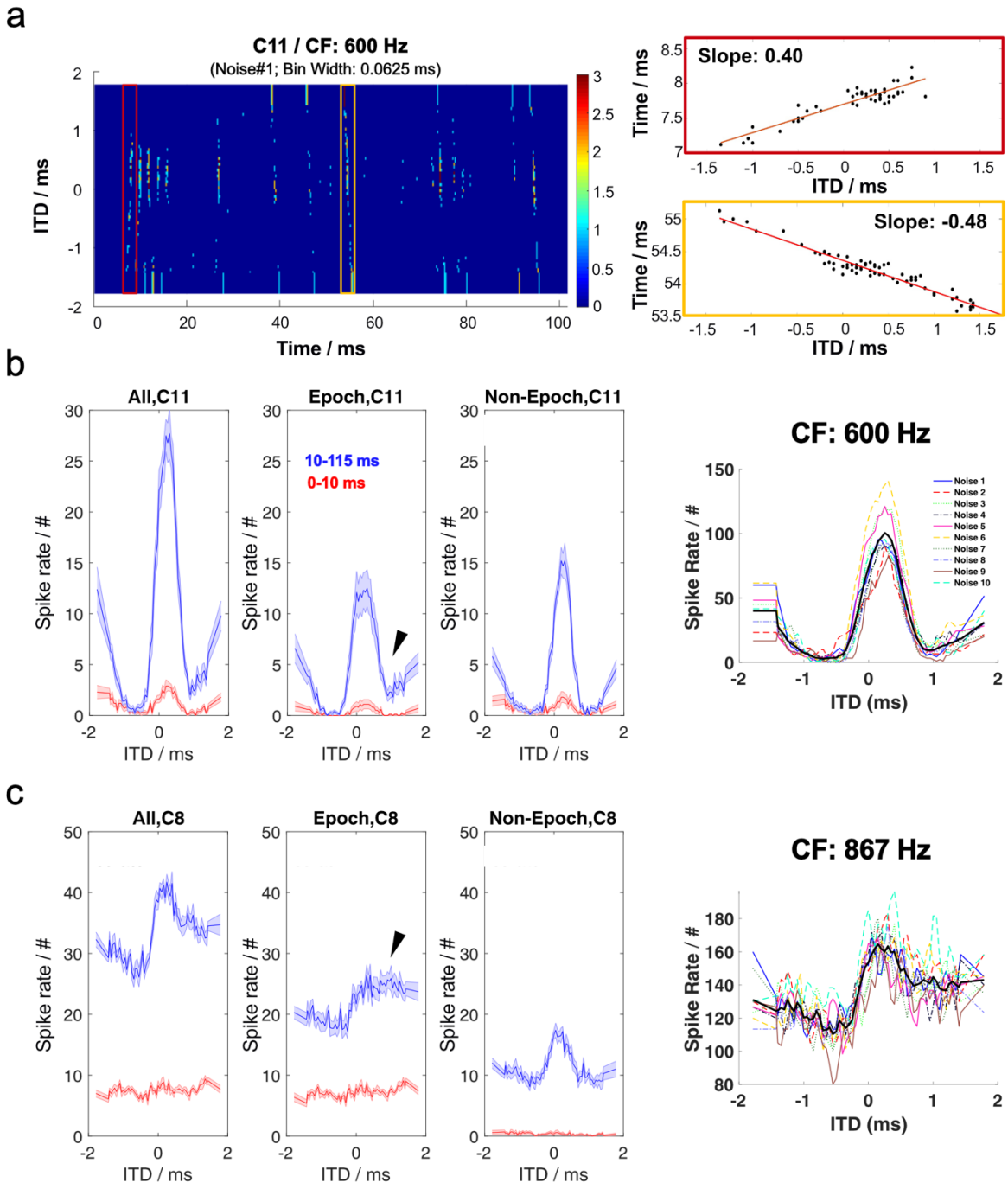

Figure 21: Monaural dominance can vary along the stimulus. a Example Neuron (C11 in Fig. 18; CF: 600 Hz; color-coded as in Fig. 16/17)**.** Left panel: Uncompensated heatmap showing event-peaks in response to Noise#1 (3 repetitions) for various ITDs (as described in Fig. 19). Note that the temporal bias of event-peaks swaps between ipsilateral and contralateral dominance along the stimulus. The red box (upper right panel) accentuates an example for an event peak that neatly follows the ipsilateral envelope across ITDs (ipsilateral dominance; slope +0.40; middle panel). The yellow box (lower right panel) accentuates an example for an event peak that neatly follows the contralateral envelope across ITDs (contralateral dominance; slope -0.48; bottom panel). **b** Same neuron as in (a). NDFs (mean ± s.e.m. (3 reps per noise; 10 noise samples) across all noise samples of the same example neuron (Cell 11 in Fig. 16; CF: 600 Hz) at stimulus onset (0-10 ms; red trace) and during ongoing stimulus presentation (10-115 ms; blue trace) (2-way ANOVA (noise/ITD): $p<0.0001$). Data are presented for NDF_{All} (1st panel from the left), NDF_{Epoch} (2nd panel from the left), NDF_{NEpoch} (3rd panel from the left). Black arrow-heads accentuate rate asymmetries for NDF_{Epoch}. Panel on the far right depicts mean rate

level functions for individual noise samples (NDF_{All}, black trace depicts the average over all noise samples) **c** Same condition as in (b); Example neuron (Cell 8 in Fig. 16; CF: 867 Hz). Significant sensitivity to both noise and ITD (2-way ANOVA (noise/ITD): $p<0.0001$) except for onset spikes in $NDF_{NEpoch/}$ NDF_{Epoch} (across the physiological range).

As mentioned earlier, presenting NDFs using different noise tokens can lead to varying $envelopes_{effect}$ with basilar membrane displacements exhibiting different levels of displacement rates and magnitude at different points in time that can drive individual inputs in different ways. Such highly complex activation patterns can ultimately lead to amplitude-driven imbalances in relative input strength and can therefore influence the binaural coincidence mechanism in the MSO, e.g. through an overbalance of unilateral inputs. On top of that, potential adaptation might have an additional influence on the tuning of individual inputs. To investigate this hypothesis further, we recorded in a small exemplary subset of neurons also composite tonal ITD functions (n = 2 neurons, CF: 500 Hz/267 Hz; pure tone at or closely at CF, ITD range ± 1.3 ms; stimulus length: 50 ms), to assess potential adaptive changes in ITD sensitivity of onset and ongoing components without the presence of a broadband stimulus that contains envelope fluctuations in the ongoing component. Figure 22a depicts the same heatmap analysis that we had developed for the noise token stimuli (compare to Fig. 19) of an example neuron (CF 267 Hz) using a 270 Hz tonal token (10 repetitions). Individual ITD functions were visualized for each individual event peak to assess how ITD sensitivity might change over time potentially through adaptation (Figure 22a; color-coded box relative to subsequent event peaks). Noteworthy, this type of evaluation has not yet been carried out for pure tones. Interestingly, the uncompensated heatmap reveals two rather surprising observations: First, ITD sensitivity is least pronounced in the onset event peak and the onset event peak is monaurally dominated. Second, the best ITD shifts from more contralaterally leading ITDs far outside the physiological range (red box; Fig. 22a right panel, Fig. 22b left panel) towards best ITDs closer to midline for more subsequent event peaks. In another example neuron, best ITDs seem to shift from less contralaterally leading ITDs (still outside the physiological range) during stimulus onset towards even more contralaterally leading ITDs very far outside the physiological range during the ongoing stimulus component (Fig. 22b right panel). This 2nd finding suggests that indeed the ITD sensitivity of MSO neurons is dynamically varying between individual input cycles.

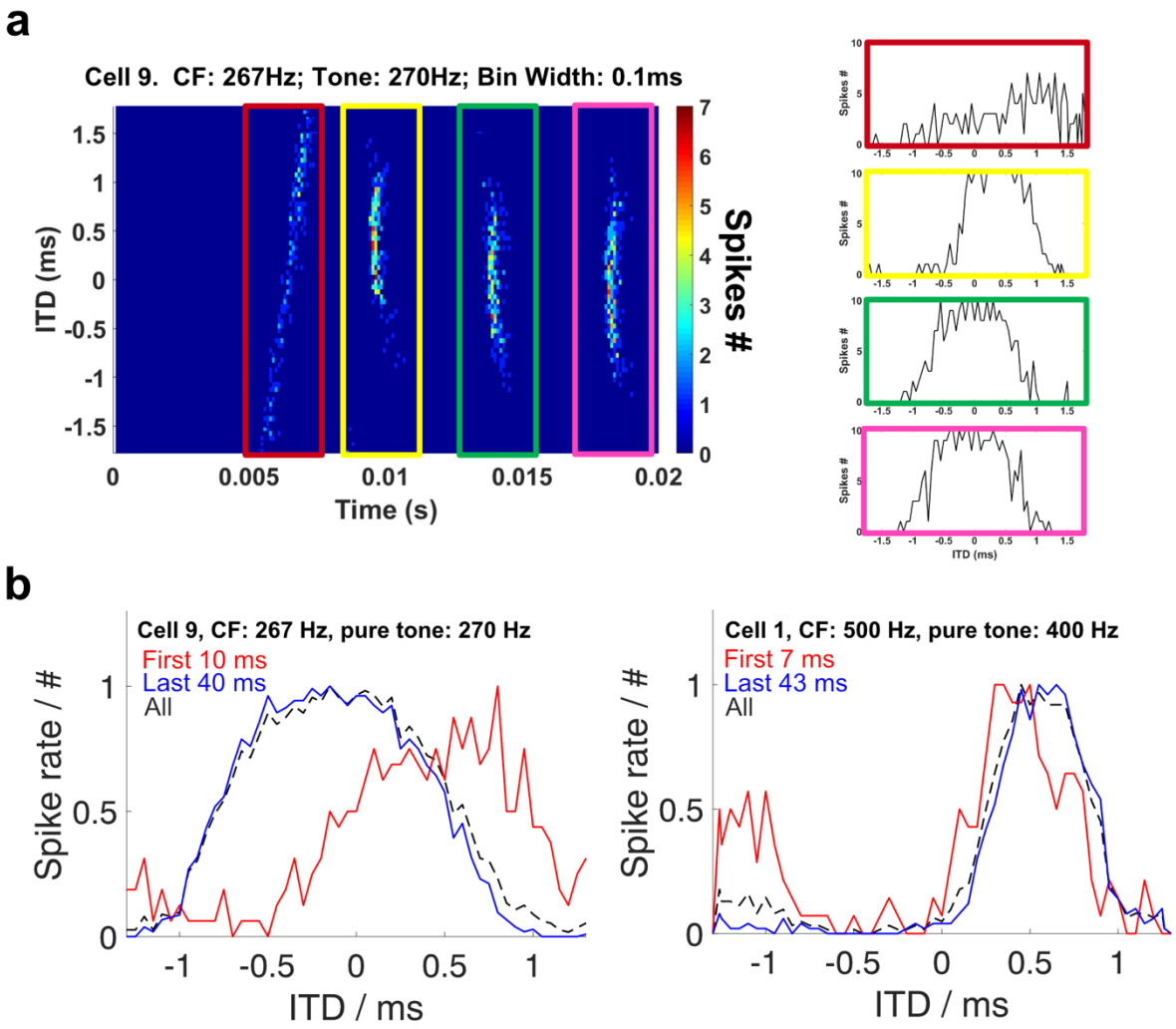

Figure 22: Nonuniformity between onset and ongoing tonal ITD functions. a Example Neuron (C9 in Fig. 18; CF: 267 Hz). Left panel: Uncompensated heatmap showing event-peaks in response to a tonal ITD function (270 Hz, 10 repetitions) for various ITDs in the range of ± 1.8 (as described in Fig. 19). Colored boxes accentuate subsequent binned event peaks (bin width: 0.1 ms). Right panel: Collapsed ITD-functions (as described in Fig. 19) for individual subsequent peaks. Note the decrease in best ITD from onset (red box) to ongoing components (subsequently: yellow box, green box, pink box). **b** Normalized ITD functions re best ITD for stimulus onset (red trace), ongoing components (blue trace), and for the whole stimulus length (50 ms; black trace). Left panel: Same cell as in (a) and Fig. 16. Right panel: Cell 1 in Fig. 18 (CF 500 Hz, tonal stimulus: 400 Hz). Note relative shifts in best ITD between onset and ongoing components.

3.2.4 Monaural dominance is eliminated through pre-adaptation of either side

Our findings strongly suggest that adaptation has a strong influence on the relative tuning of excitatory and inhibitory inputs that drive the coincidence mechanism in the

MSO. However, it is yet unclear how the timing of epoch-spikes can underly varying degrees of monaural dominance. One potential explanation could be that the MSO neuron receives a strong and less adapted input from one side that either requires non or very little input from the other side to elicit spiking, whilst the input from the other side is weaker (or strongly adapted due to prior spectral components in the preceding stimulus) and is unable to drive the MSO neuron by itself. This would naturally cause a temporal bias of spike timing that is monaurally dominated. Hence, if we pre-adapted the side that causes monaural dominance, we would expect less monaurally dominated responses in MSO neurons. In an additional subset of neurons (n = 5 MSO neurons; CFs ranging from 615-900 Hz) we therefore included a preceding monaural or binaural tonal adapter at the neuron's characteristic frequency in our noise-delay protocols (5 different noise protocols, 6 repetitions per noise; 3 ms between tonal adapter (duration: 100 ms) and noise token (duration: 100ms). This so-called forward masking typically reduces neuronal responses which is associated with adaptation in the auditory nerve (Harris and Dallos 1979; R. L. Smith 1977; 1979). Figure 23 depicts the neuronal response of an example neuron (CF: 731 Hz) in response to the aforementioned noise protocols without pre-adapter (Fig. 23a), with preceding ipsilateral adapter (Fig. 23b), with preceding contralateral adapter (Fig. 23c) and with binaural presentation of a preceding adapter stimulus at 0 ITD (Fig. 23 d). Without preceding adapter stimulation, spike latencies in epoch-components neatly follow the "temporal movement" of the contralateral stimulus across ITDs resulting in shorter spike latencies at positive (contra-leading) ITDs compared to longer latencies at negative (ipsi-leading) ITDs. The resulting NDF shows spike rate modulation as a function of ITD that slightly varies for different noise protocols (as described in Fig. 18). Collapsing the spike raster heatmap across ITDs will reveal the uncompensated accumulated spike histogram which shows a rather broad peak of accumulated spikes around stimulus onset (< 10ms) which is naturally the case due to the observed monaural dominance (as explained in Fig. 19). Across the tested sample (n = 5) all neurons showed contralateral monaural dominance and as expected, forward masking of the contralateral side diminishes contralateral monaural dominance. This is also reflected in the more defined and sharp peaks of the uncompensated accumulated spike histograms (Fig. 23/24c). Interestingly, monaural dominance was also diminished through ipsilateral forward masking. In this case, spiking is enhanced resulting in more repetitive epoch-components in this neuron, suggesting that pre-

adaptation might have affected the inhibitory input most in this cell. However, spike enhancement was not consistently present in all tested neurons (n = 5) after ipsilateral forward masking. In individual cases it was caused by contralateral adaptation and in other cases, provoked adaptation in either ear restricted spiking to the very onset (Fig. 24 b-d). In all cases, however, adaptation of either ear reduced overall ITD sensitivity and in addition, whilst our data reveal different effects following monaural or binaural forward masking across neurons, in all tested neurons monaural dominance was eliminated by adaptation to either ear which suggests monaural dominance being dependent on the relative strength of each of the binaural inputs given the spectral composition of the stimulus.

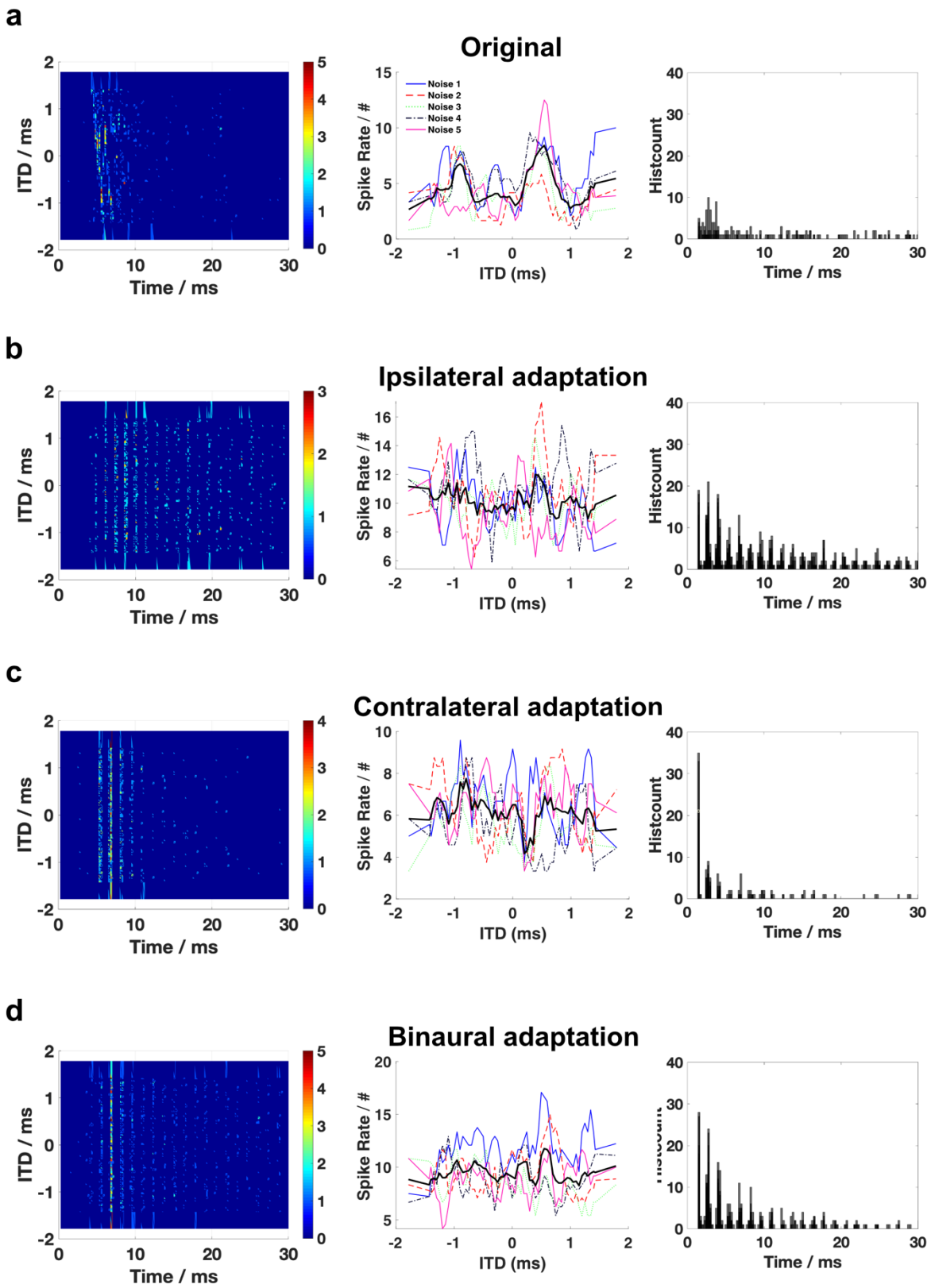
a
Original
ITD / ms
Time / ms
Spike Rate / #
ITD (ms)
Noise 1
Noise 2
Noise 3
Noise 4
Noise 5
Histcount
b
Ipsilateral adaptation
c
Contralateral adaptation
d
Binaural adaptation

Figure 23: Temporal monaural is eliminated by both, ipsilateral and contralateral forward masking. Forward masking stimulus paradigm: NDFs as in 3.2.1-3.2.3 but with 5 different noise tokens (6 repetitions per noise protocol; ITDs in the range of ± 1.78 ms) including a monaural or binaural preceding adapter at the neuron's CF (duration: 100 ms) before binaural presentation of noise tokens (duration 100 ms; 3 ms between adapter stimulus and noise token). Figure depicts the individual responses of an example neuron (CF: 731 Hz; hence tonal adapter was presented at 731 Hz) in response to NDFs with various adapter-conditions (a-d). Left panel: Uncompensated heatmap showing event-peaks of the NDF with ITDs being represented on the y-axis as a function of time (spikes across all 5 noise protocols (6 repetitions each; spike rate color-coded); Middle panel: Mean spike rates for individual noise protocols as a function of ITD (noise tokens color-coded). Black trace shows average spike rate across all noise protocols. Right panel: Uncompensated accumulated spike histogram across all noise protocols and across ITDs. **a** NDF without the presentation of a preceding tonal adapter. **b** NDF including preceding tonal adapter (731 Hz) presented to the ipsilateral ear only. **c** NDF including preceding tonal adapter (731 Hz) presented to the contralateral ear only. **d** NDF including preceding tonal adapter (731 Hz) presented binaurally.

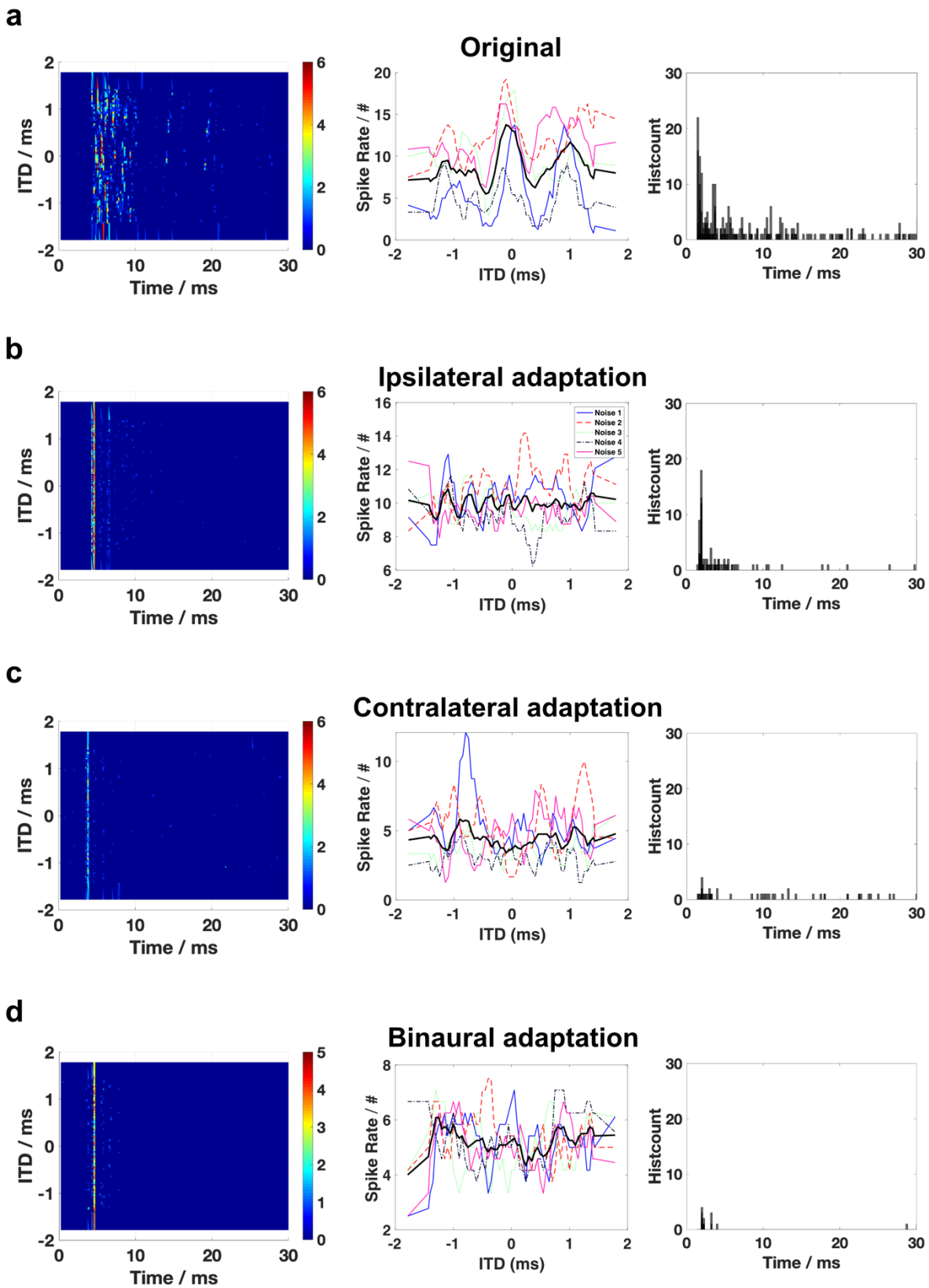
a
Original
ITD / ms
Time / ms
Spike Rate / #
ITD (ms)
Histcount
Time / ms
b
Ipsilateral adaptation
Noise 1
Noise 2
Noise 3
Noise 4
Noise 5
c
Contralateral adaptation
d
Binaural adaptation

Figure 24: Temporal monaural is eliminated by both, ipsilateral and contralateral forward masking. Forward masking stimulus paradigm: NDFs as in 3.2.1-3.2.3 but with 5 different noise tokens (6 repetitions per noise protocol; ITDs in the range of ± 1.78 ms) including a monaural or binaural preceding adapter at the neuron's CF (duration: 100 ms) before binaural presentation of noise tokens (duration 100 ms; 3 ms between adapter stimulus and noise token). Figure depicts the individual responses of an example neuron (CF: 900 Hz; hence tonal adapter was presented at 900 Hz) in response to NDFs with various adapter-conditions (a-d). Left panel: Uncompensated heatmap showing event-peaks of the NDF with ITDs being represented on the y-axis as a function of time (spikes across all 5 noise protocols (6 repetitions each; spike rate color-coded); Middle panel: Mean spike rates for individual noise protocols as a function of ITD (noise tokens color-coded). Black trace shows average spike rate across all noise protocols. Right panel: Uncompensated accumulated spike histogram across all noise protocols and across ITDs. **a** NDF without the presentation of a preceding tonal adapter. **b** NDF including preceding tonal adapter (900 Hz) presented to the ipsilateral ear only. **c** NDF including preceding tonal adapter (900 Hz) presented to the contralateral ear only. **d** NDF including preceding tonal adapter (900 Hz) presented binaurally.

3.2.5 From eardrum to conundrum – Evidence for changes in relative spike timing in dependence of ITD

We have seen so far that the $envelope_{effect}$ (i.e., the instantaneous effective level differences in relative energy within a certain frequency band), may trigger monaural dominance and potential subsequent adaptation during ongoing stimulation, which can individually impact the tuning of relative inputs to the MSO. As a consequence, relative inputs can either be monaurally driven and hence ITDs will have little impact on spiking (e.g., see the onset of NDF_{Epoch} in Fig. 21c for reference) or binaural inputs are tuned in a way that still allows for binaural coincidence mechanisms through the TFS (e.g., see NDF_{Epoch} in Fig. 21b for reference). Binaural coincidence, i.e., should naturally also affect the spike timing around the point of functional coincidence (Myoga et al. 2014; Beiderbeck et al. 2018). Hence, in MSO neurons that (despite monaural dominance) are still sensitive to differences in the TFS within epoch components should still reflect changes in relative spike timing around its best ITD for this particular noise token (compare LSO results in this thesis for a detailed explanation how interaction of inhibition and excitation affects spike timing in specific ways). This sensitivity, however, might (due to adaptation) change over time. Figure 25 shows the change in spike timing of epoch-spikes (mean ± s.e.m.; non-epoch spikes have not been included in this analysis) of an example neuron ((CF: 900 Hz; Cell 15 in Fig. 18) relative to the best ITD (y-axis) for varying ITDs (x-axis) using individual noise tokens

(individual subplots color-coded as in Fig. 16). Note that spike times were compensated for individual monaural dominance to disentangle monaural from binaural effects on relative spike timing. Relative changes in spike timing (compensated) are shown for original (Fig. 25a) and inverted (Fig. 25b) stimulus polarities. The relative spike timing in response to the inverted NDF_{Epoch} allows us to identify whether the changes can be linked to TFS sensitivity (as spike timing would shift out-of phase in alignment with anticorrelated changes in spike rates). Note, this example neuron is the same neuron as in Fig. 19 (Fig. 19c shows the anticorrelated NDF functions over all noises for original and inverted stimulus polarities).

Individual best ITDs per noise token protocol have been identified through the peak of each individual Gauss-fitted NDF_{Epoch} per noise token. Relative spike timing is displayed for the onset (first 10 ms; black traces) or for the whole stimulus duration (0-100 ms; overlaid color-coded traces) to identify potential shifts between onset and ongoing components that could be associated with adaptation.

Remarkably, despite monaural dominance of envelope-associated epochs, spike-timing within such epochs is anticorrelated for inverted stimulus polarities (compare Fig. 25a/ b) suggesting that despite monaural dominance (see Fig. 19), this neuron is still highly sensitive to differences in the TFS (which is also reflected in the anticorrelated NDF functions in Fig. 19c). Across noise protocols, spike timing is significantly modulated by ITD (One-way ANOVA; $p<0.05$) with spike timing being delayed (positive values) at the rising slope of the NDF_{Epoch} function and advanced (negative values) from the peak to the baseline of the NDF_{Epoch}. Note, the delay at the rising slope could be explained by preceding inhibition (compare to 3.1.2) (Myoga et al. 2014; Beiderbeck et al. 2018). At stimulus onset (cutoff: 10 ms; black sub-traces), this change in relative spike timing does not significantly vary in shape across tested $NDFs_{Epoch}$ (Noise#1-10) but varies in magnitude between onset and entire stimulus length, which suggests potential short-adaptation in the ongoing stimulus component. Whilst this neuron remained highly sensitive to differences in TFS, on a populational level we would expect higher variation in spike timing due to different levels of monaural dominance and adaptation.

To gain further insight on a populational level, we normalized relative best ITDs of each neuron in response to each individual $NDFs_{Epoch}$ per noise protocol (resulting in a new relational ITD axis: Delta ITD re best ITD / ms) to display the change in relative

spike timing per noise protocol (color-coded; for the entire stimulus length) across the tested population (Fig. 26a; n = 16 MSO neurons).
On a populational level, changes in spike times (median ± 25/75 percentiles) and the magnitude of spike time modulation varies with different noise protocols (Fig. 26a) suggesting a change in relative input tuning across noise tokens. A comparison of the relative change in spike timing for each individual neuron (n = 16 MSO neurons) across all noises is shown in Fig. 26b. Note, the color-code accentuates the neuron's monaural dominance across noise tokens (red: ipsilateral monaural dominance; blue: contralateral dominance; white: no overall dominance). Interestingly, a systematic change in spike timing is only detectable in a few neurons, but not consistently across the population.

Taken together, our data provide strong evidence for $envelope_{effect}$ sensitivity in low frequency MSO neurons that dynamically affects the neurons' ITD sensitivity. Importantly, each event within the $envelope_{effect}$ that the neuron responds to (i.e., fast energy rise within the relevant sound spectrum with regard to the neuron's tuning) can contain a unique spectral composition. Since it is unlikely (being a biological system) that all four functional inputs to the MSO exhibit identical tuning, the strength of individual functional inputs to the MSO and therefore the underlying coincidence mechanism can vary between events. The findings of this study show that $envelopes_{effect}$ play a crucial role for binaural integration in low frequency MSO neurons with strong evidence for its regulation through pre- and short-time adaptation which suggests that the tuning of relative inputs (inhibition/excitation) could be individually adapted throughout the stimulus.

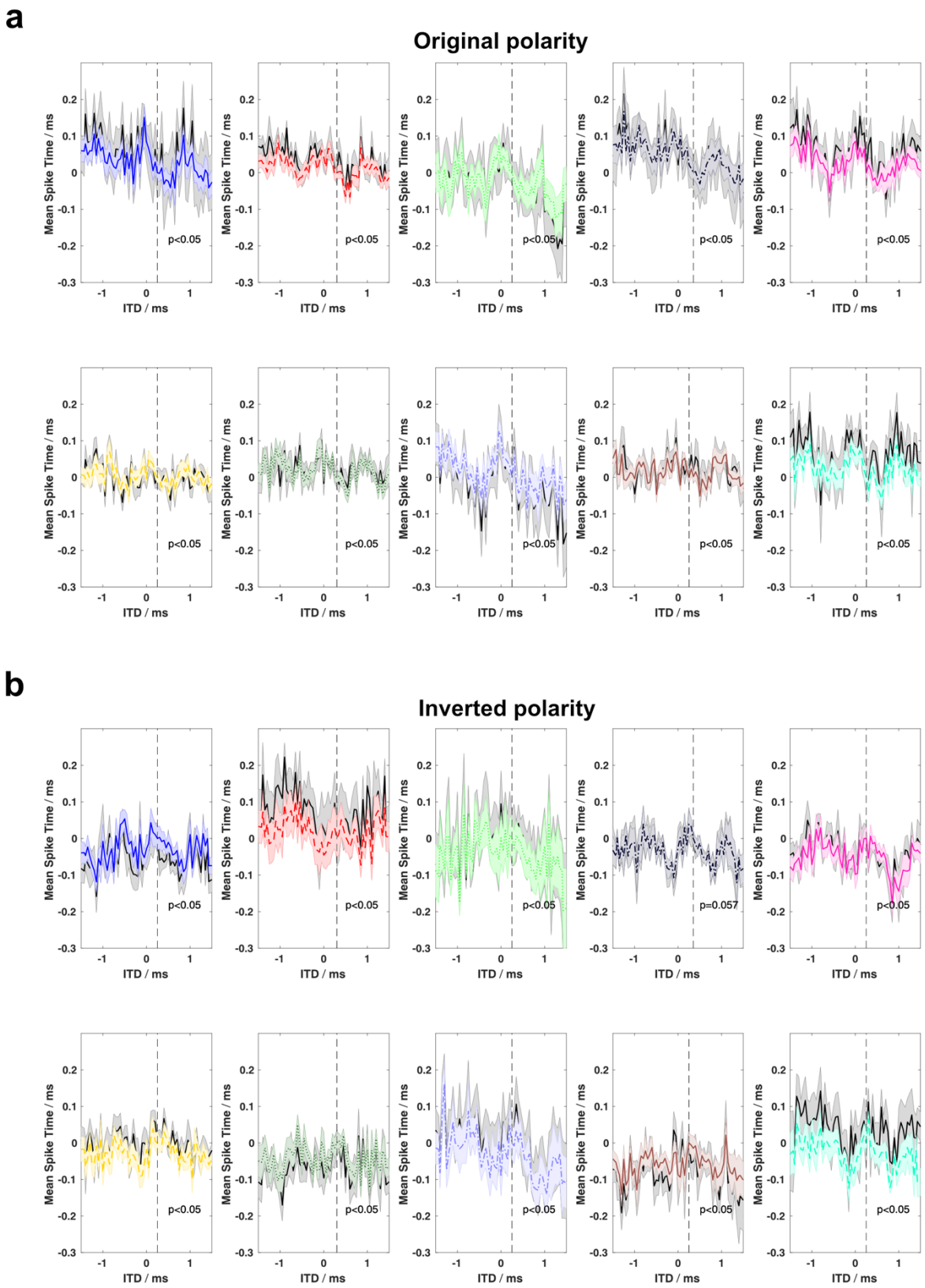
a
Original polarity
b
Inverted polarity
Mean Spike Time / ms
ITD / ms
p<0.05
p=0.057

Figure 25: Changes in relative spike timing in dependence of ITD. a Change in spike timing of epoch spikes of an example neuron (Cell 15 in Fig. 18; CF: 900 Hz) relative to their mean spike times (mean ± s.e.m.) at individual best ITDs for each individual NDF_{Epoch} (Noise#1-10; subplots color-coded as in Fig. 16; individual best ITDs are accentuated by black vertical dashed lines). Spike times for each individual noise protocol are significantly modulated by ITD (One-way ANOVA: $p<0.05$). Black sub-traces in each subplot depict individual changes in relative spike timing at stimulus onset (cutoff: 10 ms). **b** Same figure conventions as in (a) but shows the changes in relative spike timing for $NDFs_{Epoch}$ (Noise#1-10) with inverted stimulus polarity which results in an anticorrelated change in spike timing (see Fig. 19c for individual NDF functions of this neuron in response to the original and inverted stimulus polarity).

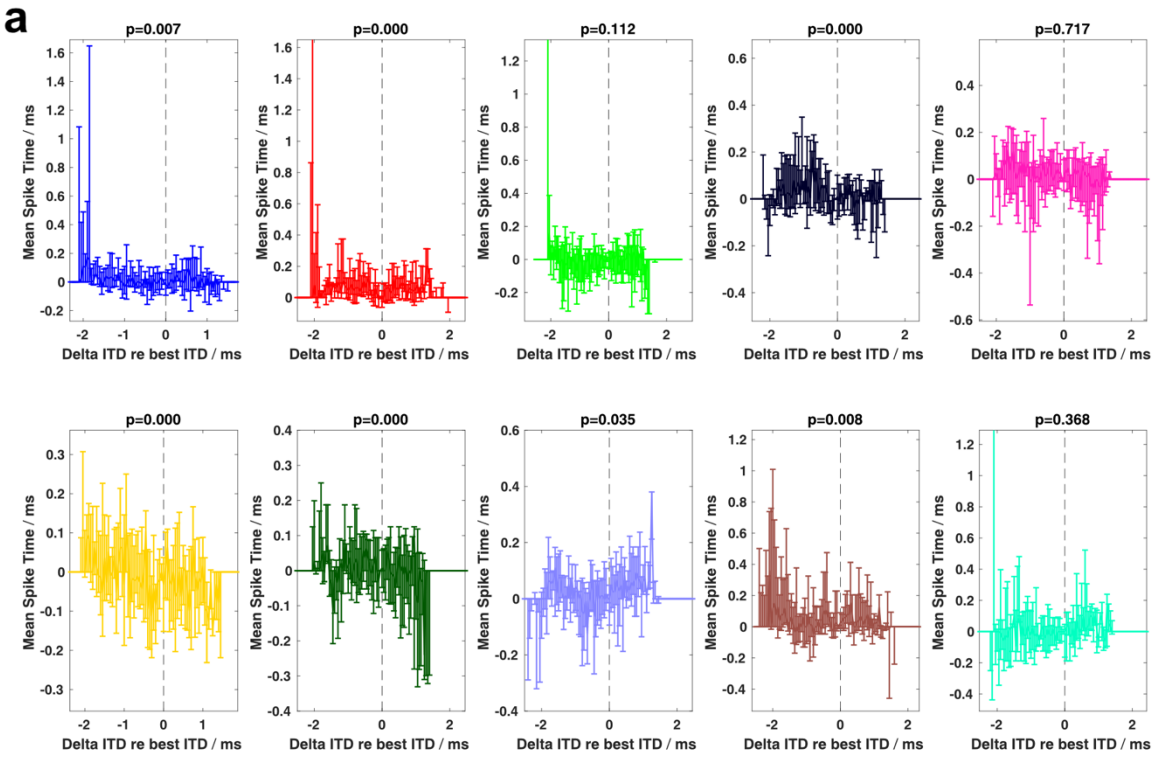
a
p=0.007
p=0.000
p=0.112
p=0.000
p=0.717
p=0.000
p=0.000
p=0.035
p=0.008
p=0.368
Mean Spike Time / ms
Delta ITD re best ITD / ms

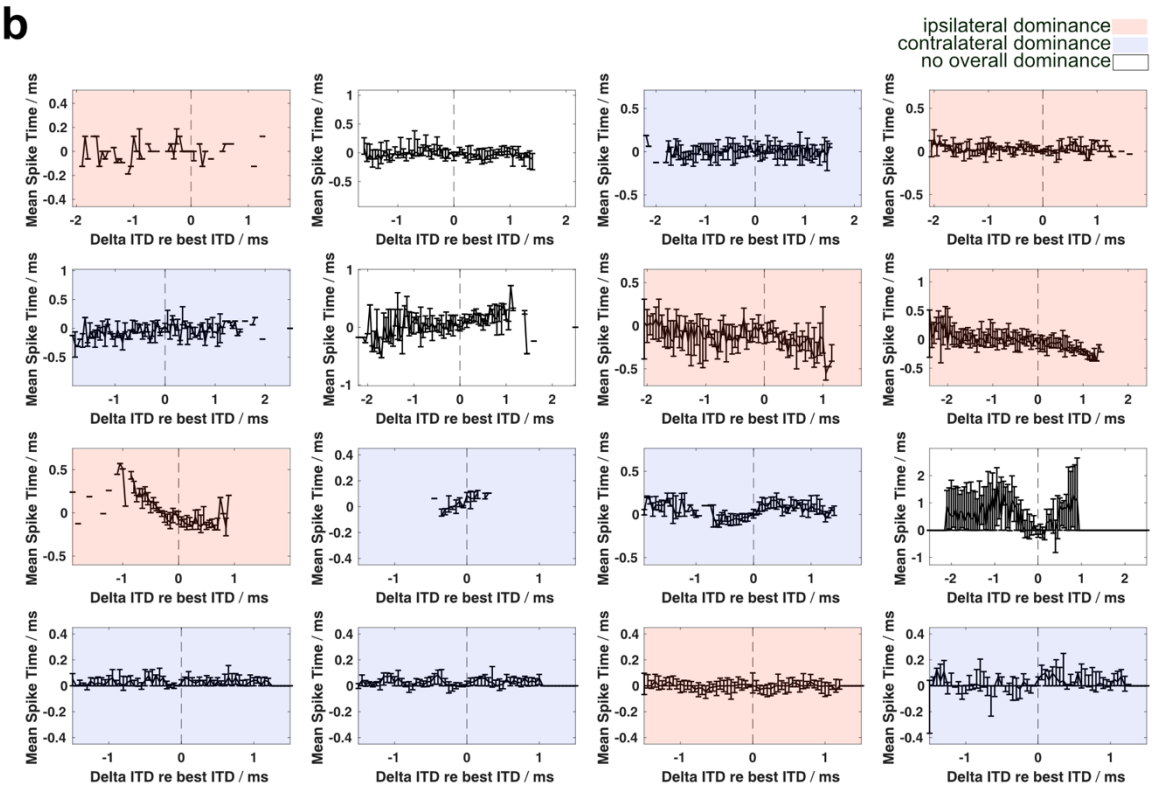
b
ipsilateral dominance
contralateral dominance
no overall dominance
Mean Spike Time / ms
Delta ITD re best ITD / ms

Figure 26: Changes in spike timing in dependence of ITD across noises and across neurons. a Change in spike timing of epoch spikes (median ± 25/75 percentiles) across neurons (n = 16 MSO neurons) per noise relative to their mean spike times at individual best ITDs for each individual NDF_{Epoch} (Noise#1-10; subplots color-coded as in Fig. 16; individual best ITDs are accentuated by black vertical dashed lines). Individual best ITDs per neuron in response to each individual NDF_{Epoch} per noise protocol were normalized (resulting in a new relational ITD axis: Delta ITD re best ITD / ms). **b** Same figure conventions as in (a) but shows the changes in relative spike timing of each individual neuron (n = 16) across noise protocols (Noise#1-10). Color-coded backgrounds accentuate neurons monaural dominance (red: ipsilateral monaural dominance; blue: contralateral dominance; white: no overall dominance)

4 Discussion

Back in 1907, Lord Rayleigh suggested in his pioneering studies that ILDs are used for the localization of high frequency sounds and ITDs are used for localization of low frequency sounds (Rayleigh 1907) which was later termed the 'Duplex theory' in sound localization. Over the last century, whilst it is generally accepted and serves as a backbone for sound localization up to this day, the duplex theory came up against its limits with the presence of ILDs between low frequency sounds in the near-field (Shinn-Cunningham, Santarelli, and Kopco 2000) and ITDs in the envelope of modulated high-frequency sounds (Bernstein and Trahiotis 1985). The goal of this doctoral thesis was to further read between the lines of the Duplex theory by studying the role of precisely-timed inhibition in the LSO, a nucleus in the auditory brainstem of mammals that is equipped to decode ILDs and on the other hand to study the role of $envelope_{effect}$ information (created through non-linear cochlear filtering) in low frequency MSO neurons, another nucleus in the auditory brainstem of mammals that is well-known for its modulation by ITDs. This discussion will outline the general findings in the LSO and MSO of Mongolian gerbils.

4.1 The importance of relative input timing and fast synaptic inhibition in the LSO

As outlined in 1.3.6, the integration of glycinergic inhibitory and glutamatergic excitatory inputs in the LSO was often allegorized as the neural equivalent of a subtraction mechanism which would inherently require a temporal integration window of several milliseconds (Brown and Tollin 2016). Such simple subtraction would go in line with previous suggestions that MNTB-mediated inhibition was insufficiently fast to interact in a timing-dependent manner (Franken et al. 2015; Roberts, Seeman, and Golding 2013; Joris and Yin 2007).

This hypothesis has been shown to be too minimalistic. As indicated in 1.3.6, timing of the excitatory and inhibitory inputs in the LSO is an integral part of ILD computation. Previous studies showed that the potency of inhibition to suppress spiking in response to short stimuli in LSO cells is restricted to specific phases of the IPSP (Park et al. 1996; Sanes 1990; Irvine, Park, and McCormick 2001; Joris and Yin 1995; Wu and Kelly 1991). Hence, inhibitory inputs need to be in precise temporal register relative to

excitation in order to be effective, which is also a prerequisite for ITD computation in its putative descendent, the MSO.

Recently, the outdated 'subtractive image' of the LSO has been further challenged by recent *in vivo* patch clamp data that have shown that LSO principal cells exhibit transient responses with fast membrane kinetics. The authors suggested that LSO principal cells are temporal differentiators rather than integrators, and thus more closely resemble temporal processing in MSO neurons (Franken, Joris, and Smith 2018), as previously assessed by others (Grothe and Pecka 2014).

In addition, ILDs can be regarded as relative energy per time interval. Such instantaneous differences in energy entail a change in the relative arrival times of the respective inputs at the LSO (Grothe and Park 1995; Park et al. 1996; Sanes 1990; Heil and Neubauer 2001) (see 1.3.6 for further information). Thus, under natural free-field conditions in which high frequency sounds are highly influenced by the shadowing effect of the head and therefore give rise to large ILDs, relative intensity-levels and therefore relative inhibitory and excitatory input times will highly influence functional coincidence of inputs in the LSO.

In study 1, we found a fundamental deviation from the aforementioned models on slow and inconsistent inhibitory function (Franken et al. 2015; Joris and Yin 2007; Day and Semple 2011). We provide direct evidence *in vivo* that temporal precision is maintained and effective throughout click-trains even at 500 Hz, which suggests high temporal precision of inhibition that is able to influence excitation on a cycle-by-cycle basis for relatively high click frequencies that shows that temporal acuity in the LSO is not restricted to the initial spike (Franken, Joris, and Smith 2018).

4.2 Precisely timed preceding inhibition facilitates spiking in the LSO through PIF

Besides fast temporal integration of relative inputs in the LSO we demonstrated a 'sweet spot' dependent on the particular sub-millisecond temporal lead (400-600 µs in our *in vivo* setting) of inhibition relative to excitation in which spike generation was promoted. Hence, the temporal integration of excitatory and inhibitory inputs does not only lead to spike suppression but may also promote spike generation depending on the relative input strength and the precise input timing between excitation and inhibition.

It was further established *in vitro* that the increase was mediated by PIF to otherwise sub-threshold excitatory inputs, which was supported by a prior observation of OFF-discharge in the LSO (Tsuchitani 1988). Generally speaking, during PIF, hyperpolarization causes the reduction of an element that is recruited at rest and suppresses excitability. Mechanistically, PIF could be a result of Na_v channels being relieved from inactivation (Svirskis et al. 2004), which our data indicated by the decrease in the AP threshold (V_t) under the influence of well-timed inhibition. Whilst fast sodium channel inactivation might have a dominating impact on PIF in the LSO, additional ion channels might contribute to its mechanism such as HCN channels that are associated with rebound spiking after long-lasting hyperpolarization that does not require an additional excitatory input (Kopp-Scheinpflug et al. 2011; Felix et al. 2011). Whilst respective I_h currents are too slow to account for the facilitation itself, I_h has been shown to modulate the temporal half-widths of PIF which makes the mechanism for PIF in the LSO increasingly complex.

Noteworthy, sub-millisecond PIF has also been identified in slice recordings from juvenile MSO neurons of gerbils (Dodla, Svirskis, and Rinzel 2006) for which the deactivation of low-threshold potassium channels (Gittelman and Tempel 2006; Higgs and Spain 2011; Song et al. 2005) was the dominating factor for PIF. This observation may not be too surprising given the evolutionary heritage of the LSO and MSO (Grothe and Pecka 2014). It further suggests that PIF might also be a contributing mechanism to establish ITD sensitivity in mature MSO and our data in study 2 supports this notion (see 4.7).

4.3 The “Sweet Spot” in the LSO: The functional role of PIF in spatial coding strategies

This bidirectional potential of inhibition to either suppress spiking at a specific phase of the IPSP (which defines the classic ILD-function) or to facilitate spiking of otherwise subthreshold excitatory events can have an enormous impact on spatial coding strategies. Imagine the faint rustling noises or snapping of little twigs generated by a moving prey or an approaching predator. In such a situation, reliable and instantaneous processing of the generated binaural inputs can be essential (every spike counts). For high frequency sounds, where ILDs can be large (Grothe, Pecka, and McAlpine 2010) contralateral sound source locations might generate weak

ipsilateral inputs that might eventually not be strong enough to evoke spiking in the LSO. On the other side, a relatively large ILD would entail stronger, and therefore, potentially preceding inhibition that – given the right timing - lowers the threshold for spike generation and facilitates spiking of otherwise subthreshold excitatory events which could ultimately recover the dynamic range (see LSO study 1 (3.1.4)).

Hence, through PIF, ILD sensitivity could be maintained over a wider range of sound intensities which could account for the observed robust ILD sensitivity against absolute sound level in humans (Hall 1964; Dahmen et al. 2010; Hershkowitz and Durlach 1969).

In addition to facilitation, our *in vitro* and *in vivo* results associate PIF with reduced spike latency and jitter, both of which were generally modulated by the relative timing between excitation and inhibition.

Together, our findings account for fast MNTB-mediated synaptic inhibition that mechanistically, through exquisite temporal precision not only at the onset of stimulation, allows for other functions than 'classic' subtraction over long time periods, and that has the potential to be highly relevant for spatial coding strategies.

4.4 Pushing the envelope of low frequency carrier in the MSO through methodological post-hoc analysis

As outlined in 1.3.7, LSO neurons and its precursors predominantly phase-lock to the envelope of a stimulus and thereby transmit its temporal pattern along the auditory pathway. In study 1 we have investigated how this envelope-driven temporal relationship between binaural inputs can be influenced by external ILDs that independently affect the strength, latency and duration of excitatory and inhibitory inputs and thereby affect neuronal output in the LSO.

It is a well-known phenomenon in the auditory brainstem that neurons can lock their activity to a particular phase of a stimulus, more specifically to the slope of any complex stimulus (Dietz et al. 2014). Neurons in the MSO (the putative 'descendant' of the LSO, see 1.3.7) that are often tuned to low frequencies below 1 kHz are known to be slope-detectors (Mikiel-Hunter, Kotak, and Rinzel 2016; Meng, Huguet, and Rinzel 2012), i.e., action potential firing occurs at moments of fast energy rise within

the relevant sound spectrum that the respective neuron is tuned to. Generally, this allows for phase locking to both, TFS and envelope of the stimulus. In fact, the MSO has been assessed with regard to its envelope sensitivity, however, these studies have mainly been conducted using high carrier frequencies (Batra and Fitzpatrick 1997; McFadden and Pasanen 1976).

Nevertheless, with MSO neurons inherently being tuned to low frequencies that (given the relatively small head of a rodent) give rise to only minuscule ILDs, naturally occurring intensity-to-time conversions that could influence the binaural coincidence mechanism (as observed in the LSO) are negligible in the MSO. As an inherent consequence, under the assumption that relative input strengths are (and remain) constant, most studies in low frequency MSO neurons have been conducted using single pure tone stimuli or single frozen low-pass noise tokens blending out potential energetical differences of the underlying $envelope_{effect}$.

As described in 1.3.8, complex broadband signals, that are typically encountered in a natural setting (e.g., speech), are decomposed by non-linear filtering along the basilar membrane, resulting in a series of instantaneous narrowband signals with unique envelope patterns (Ruggero 1973; Moore 1998; Pickles 1982; Joris 2003; Joris and Yin 1992; Fletcher 1940; Palmer 1987) that can affect the activity in ANFs, specifically its phase-locking. However, to what extent such $envelopes_{effect}$ of low frequency stimuli (for which potential free-field ILD's are marginal, see 1.1) affect ITD sensitivity in the MSO has not yet been systematically assessed.

It was shown that envelope associated epoch components can bias perceptual ITD sensitivity at low frequencies (Bernstein and Trahiotis 1985). Based on acoustic pointing tasks using a 500-Hz narrow-band noise in human listeners, the authors concluded, that lateralization is affected by the envelope but is dominated by ITDs in the TFS.

Following stimulation with low-pass noise subsequent cochlear filtering, each epoch within the $envelope_{effect}$ that the neuron responds to (i.e., fast energy rise within the relevant sound spectrum with regard to the neuron's tuning) can contain a unique spectral composition that can vary over time. For an MSO neuron with 4 functional inputs that exhibit perfectly unisonous frequency tuning and time-intensity trading such dynamics in spectral composition would per se not influence the binaural coincidence mechanism as each functional input would be equally affected. However, being a

biological system, it is unlikely, that all for functional inputs to the MSO share identical frequency tuning.

Hypothetically, such instantaneous differences in spectral energy could individually affect the neuronal drive of the four functional inputs if slight differences in their frequency tuning do exist. Slight differences in frequency tuning could root in different developmental mechanisms that trigger long-term depression and long-term potentiation of inhibitory and excitatory inputs during tonotopic map refinement. Specifically, how inhibitory inputs are established and refined during development is not fully understood (Sanes and Siverls 1991; G. Kim and Kandler 2003; Bach and Kandler 2020).

Moreover, not only changes in frequency tuning might lead to such an effect, but also inherent differences in the gain function between intensity and latency. Furthermore, such differences could individually offset short-time adaptational effects on MSO inputs, i.e., if one input was ‘perfectly’ tuned to the spectral composition in the first epoch, it will undergo stronger adaptation for subsequent epochs than e.g., another input that was weakly tuned to the spectral composition of the first epoch, which might affect coincidence mechanisms for subsequent epochs). Hence, instantaneous integration of the four functional inputs might be dynamic in the MSO not only throughout the duration of the stimulus but also between different complex stimuli (Fig. 27).

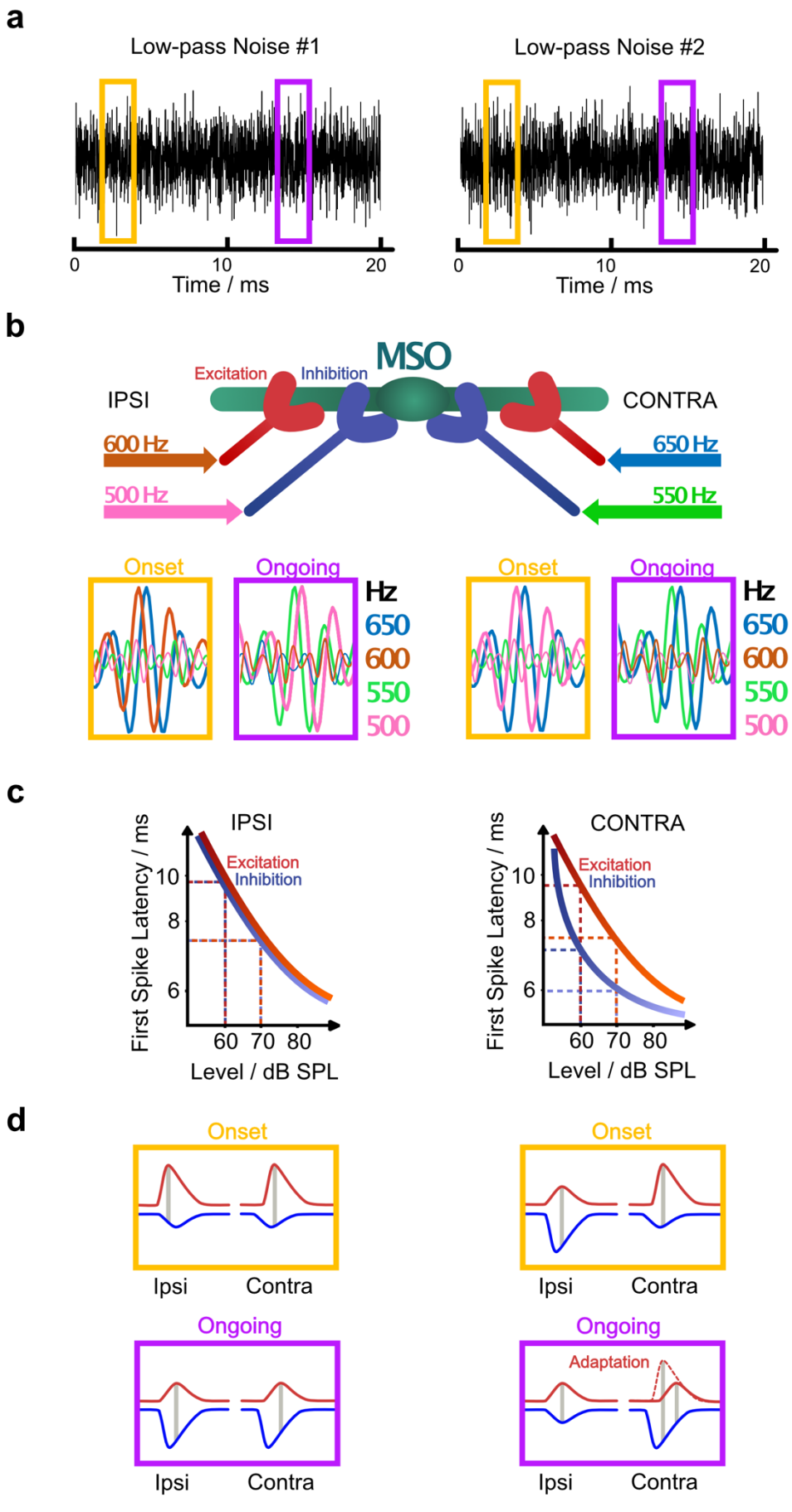
a
Low-pass Noise #1
Low-pass Noise #2
0
10
20
Time / ms
b
MSO
Excitation
Inhibition
IPSI
CONTRA
600 Hz
500 Hz
650 Hz
550 Hz
Onset
Ongoing
Hz
650
600
550
500
c
IPSI
CONTRA
First Spike Latency / ms
Excitation
Inhibition
10
8
6
60 70 80
Level / dB SPL
d
Onset
Ongoing
Ipsi
Contra
Adaptation

Figure 27: Potential dynamics of stimulus-driven binaural inputs through potential unidentical frequency tuning and time-intensity trading. Schematic.
a Illustration of two individual noise tokens that share the same spectral content (i.e., same carrier frequencies) but vary in their respective envelopes (i.e., the amplitude fluctuations across the stimulus). Yellow box depicts an event around stimulus onset; Magenta box depicts an event during the ongoing component of the stimulus. **b** Top panel: Hypothetical illustration of the four functional inputs to the MSO being unidentical in frequency tuning. Being a biological system, it is unlikely that all four functional inputs exhibit fully identical frequency tuning. Slight differences in frequency tuning could root in different developmental mechanisms that trigger long-term depression and long-term potentiation of inhibitory and excitatory inputs during tonotopic map refinement. Bottom panels: Cochlear filtering of complex broadband stimuli can result in unique spectral compositions that can vary over time (illustrational frequencies color-coded; onset and ongoing stimulus events highlighted and color-coded as in (a)). Such differences in spectral energy could drive individual MSO-inputs differently if slight differences in frequency tuning do exist. **c** Hypothetical illustration of potential differences of level-dependent latencies between functional inputs that could impact the binaural coincidence mechanism. For example, a steeper slope in the gain function of contralateral inhibitory inputs could result in preceding inhibition. Differences in gain function of the four functional inputs could further affect binaural coincidence mechanisms in addition to (b). **d** Potential temporal and energetical relationships between the four functional inputs in response to two individual noise tokens (as defined in (a)) at stimulus onset (top panel; color-coded in yellow re (a)) and during ongoing stimulation (bottom panel; color-coded in magenta (re)). Red traces depict excitatory inputs, blue traces depict inhibitory inputs. Note that instantaneous differences in neuronal drive could individually offset short-time adaptational effects adding an additional impact on the instantaneous coincidence mechanism (as illustrated through the dashed line in the bottom right panel. Whilst in this example the contralateral excitatory input would per see underly identical stimulation patterns at the highlighted onset and ongoing event, short-time adaptation might dampen the neuronal drive in the ongoing component.

In study 2, using a cassette of low-frequency broadband stimuli with varying envelopes but unaltered spectral content, our data reveal that $envelopes_{effect}$ not only impact relative spike timing but also affect overall ITD sensitivity in low frequency MSO neurons with CFs ranging from 267-1600 Hz, which represents one of the lowest-frequency datasets that have been recorded in the MSO *in vivo*.

Generally, neuronal responses were individually modulated by both interaural temporal disparities and different noise stimuli that resulted in bidirectional shifts of individual best ITDs, suggesting that sensitivity to the $envelope_{effect}$ individually and differently - drives excitatory and inhibitory inputs on top of the phasic ITD-sensitivity associated with the CF (McAlpine, Jiang, and Palmer 2001; Hancock and Delgutte 2004; Pecka et al. 2008). This notion was corroborated by proof-of-principle experiments using monaural pre-adaptation stimuli.

Despite MSO neurons being able to phase-lock to both, TFS and $envelope_{effect}$ in this stimulus setting, using additional inverted stimulus paradigms we were able to identify individual precisely timed events along individual noise tokens across ITDs that can be attributed to instantaneous elements of the $envelope_{effect}$, potentially the rising slopes within the $envelope_{effect}$ (Dietz et al. 2014).

The post-hoc grouping of individual spikes into envelope-associated epoch components and non-epoch components through compensated spike-timing enabled separate assessment of individual coincidence mechanisms and the impact on overall ITD-sensitivity between groups.

In contrast to the classic methodological reductionism that disentangles a system into its individual elements prior to data collection, our post-hoc reductionist approach enabled both, all-encompassing and individual assessment of spikes associated to the epochs or non-epochs through spike timing without deprivation of their potential mutual impact on each other (van Riel and Van Gulick 2019).

In non-epoch components, spikes displayed classic ITD-sensitive components typically associated with phasic ITD response functions to pure tone stimulation suggesting a harmonic balance of relative inputs.

Unexpectedly, spike timing of envelope-associated (epoch) components appeared to be monaurally dominated by typically either the ipsilateral or contralateral “temporal movement” of the monaural stimulus across ITDs as it was introduced during headphone-based delivery (further discussed in 4.6). Such unilateral dominance is reminiscent to the LSO, the evolutionary blueprint of the MSO, where a monaural excitatory input is modulated through contralateral inhibition.

In epoch-components, despite the unexpected monaural dominance in the spike timing (further discussed in 4.6), ITD sensitivity was generally found in both groups with epoch components displaying a general rate asymmetry between negative and positive ITDs. Our initial findings were coherent with studies in the IC and the DNLL (inter alia upstream targets of MSO neurons) that revealed rate and delay asymmetries in NDFs of low-CF and mid-CF neurons that cannot be exclusively explained by IPD-dependent components (Joris 2003; Agapiou and McAlpine 2008). These components could partially be reflected by cochlear filtering. Whilst this DC offset did per se not diminish ITD-sensitivity (i.e., the ‘classic’ coincidence mechanism) in this group, the overall course of isolated epoch-NDFs eventually took a nearly sigmoid shape that was - again - reminiscent to ILD functions in the LSO.

Our findings from study 2 suggest that on top of the phasic ITD sensitivity associated with the CF there is an additional slower modulation of the tuning function that is heavily influenced by monaural components triggered through the components that are associated with the $envelope_{effect}$. Importantly, such modulations could be explained through indifferent frequency tuning in the MSO. However, since MSO

neurons receive both excitatory and inhibitory inputs from either side disentanglement of individual inputs to record individual tuning functions *in vivo* is challenging and would require additional *in vivo* whole-cell patch recordings using high-resolution sweeps to identify potential tuning differences of MSO inputs.

4.5 Dynamic changes in ITD and the law of the first wave front

It is unclear how and to what extent the observed envelope-mediated monaural dominance on spike timing impacts ITD sensitivity. Importantly, monaural dominance did not seem to be necessarily constant as it could in some instances dynamically swap over time within the same noise stimulus. A potential underlying mechanism for this phenomenon could root in neural adaptation at preceding levels of the auditory pathway. Generally speaking, short-term plasticity typically entails changes in the relative synaptic strength of excitation and inhibition mediated through the history of sensory inputs and can include rapid adaptation / rapid recovery from adaptation in auditory nerve fibers (Yates, Cody, and Johnstone 1983; Yates, Robertson, and Johnstone 1985; Westerman and Smith 1987; Dietz et al. 2014). Nonlinear rapid adaptation in ANFs was observed to be dependent on stimulus intensity and hence could crucially interplay with the aforementioned differences in input tuning and thereof differences in instantaneous input strength. Adaptation time constants were shown to be within as little as 5-25 ms or recovery from adaptation within 25-400 ms (Yates, Robertson, and Johnstone 1985) which falls within the time frame of the stimulus duration we had used (100 ms). On a post-synaptic level, relative changes in input strength and timing can ultimately change coincidence mechanisms that can lead to alterations in firing rate, spike timing and jitter. On a cycle-by-cycle basis, given that the MSO receives both, excitatory and inhibitory inputs, differences in input tuning can also include suppression or post-inhibitory facilitation as shown in study 1 (Beiderbeck et al. 2018; Myoga et al. 2014). Importantly, throughout the timescale of stimulation, we observed changes in overall ITD sensitivity that could be attributed to the effects of short-time adaptation. In individual neurons, envelope-associated components revealed ‘classic’ periodic ITD-sensitivity at stimulus onset and only gradually evolved the typical DC-offset that can be associated with envelope sensitivity (Agapiou and McAlpine 2008). Potentially, during stimulus onset, both envelope-associated

components and non-envelope associated components in this neuron provide the same combined response to upstream nuclei which is of particular importance for sound localization in reverberant environments and sound segregation (Franssen 1960; Wallach, Newman, and Rosenzweig 1949). It is also reminiscent of a previous study by Dietz et. al 2014: With the highest probability for spiking usually at the rising slope of any complex stimulus, it has been found in human subjects that binaural TFS information seems to be preserved during rising components of modulated sound stimuli which could effectively contribute to spatial hearing in complex auditory environments. This study can be seen as an extension to the "law of the first wave front" which was pioneered in 1948 by Lothar Cremer and which was later termed "the precedence effect" by Wallach et al. in 1949 (Cremer 1948; Wallach, Newman, and Rosenzweig 1949). It describes that listeners localize a signal based on the spatial information conveyed by the stimulus part first arriving at the ears and disregard spatial information in the later arriving – i.e., ongoing – stimulus part. In theory, the interplay of short-time adaptation and $envelope_{effect}$ could generate a sweet spot in the tuning of binaural inputs at stimulus onset that allows reliable and combined glimpsing of TFS information throughout the all-encompassing neuronal response in a brief time window at stimulus onset in low frequency broadband noise followed by rapid adaptation that likely removes binaural excitatory and inhibitory inputs from their mutual "sweet spot" tuning.

We were, however, unable to identify consistent all-encompassing glimpsing of TFS information at stimulus onset in every neuron. Sometimes, envelope-associated components did not display TFS-related ITD sensitivity within the physiological range at stimulus onset and evolved ITD sensitivity only during ongoing stimulation. This could be related to the observed monaural dominance (further discussed in 4.6).

Noteworthy, also during pure tone stimulation, we were able to identify dynamic changes in ITD sensitivity of MSO neurons between individual input cycles from the onset and the ongoing stimulation that can be attributed to short-time adaptation. Interestingly, in one neuron, the very first input cycle was also monaurally dominated in its spike timing. Since the precedence effect also holds for short tone pips (Wallach, Newman, and Rosenzweig 1949), the question arises if the observed monaural dominance was an artifact of our stimulation or if it is a functional component that triggers adaptation following onset.

4.6 Monaurally dominated spike timing – Bug or feature?

Our findings strongly suggest that adaptation has a strong influence on the relative tuning of excitatory and inhibitory inputs that drive the coincidence mechanism in the MSO. However, it is yet unclear how the timing of envelope-associated-spikes can underly varying degrees of monaural dominance.

One potential explanation could be that the MSO neuron receives a strong (or less adapted) input from one side that either requires non or very little input from the other side to elicit spiking, whilst the input from the other side is weaker (or strongly adapted due to prior spectral components in the preceding stimulus) and is unable to drive the MSO neuron by itself. This would naturally cause a temporal bias of spike timing that is monaurally dominated. Interestingly, both forward masking of either side diminished monaural dominance of spike timing and reduced overall ITD sensitivity. The findings corroborate the aforementioned hypothesis, and further suggest that the underlying mechanism of monaural dominance still relies on the input from both sides (i.e., a dominating input from one side and at least little input from the other side). Consequently, ITD sensitivity is still observed in monaurally dominated epoch components.

This overly strong single-sided dominance in input tuning could, however, be an artefact of the experimental design, since in the laboratory we work predominantly in anechoic sound chambers where it is completely quiet for considerable time before stimulus onset. In complex natural environments, however, we are constantly being exposed to transients that could possibly attenuate this strong one-sided dominance to some degree, hence it is difficult to say if monaural dominance to the extent we observed it in the MSO is a bug or artifact or a functional feature of sound localization in complex environments.

Monaural dominance is reminiscent of the stereausis model. The ‘classic’ concept of the stereausis hypothesis (that generally includes excitatory inputs only) suggests that differences in wave propagation time along the basilar membrane (due to differences in spectral tuning) of functional inputs systematically determine best ITDs. (Shamma, Shen, and Gopalaswamy 1989). However, we suggest a much more dynamic contribution of individual input tuning of potentially all 4 functional inputs that individually trigger adaptational mechanisms that result in coincidence-dynamics that

cannot account for a systematic change in best ITD (e.g., resulting in bidirectional shifts in best ITD, DC offsets or even diminishes ITD sensitivity).
In addition, studies in the MSO using pure tone stimuli could not account for the contribution of stereausis to ITD tuning (Pecka et al. 2008; Plauška, van der Heijden, and Borst 2017).
Noteworthy, cochlear implant (CI) users lack the experience of natural complex environments. In CIs, a speech processor will pre-analyze the acoustic signal and process it to fit the demands of electrical stimulation (Adunka and Kiefer 2005). Hence, monaural dominance could eventually be excessively overrepresented. In fact, it was shown that ITD sensitivity in CI uses significantly improved by introducing extra pulses to high-rate periodic pulse trains which introduces short inter-pulse-intervals (Lindenbeck et al. 2020; Srinivasan et al. 2018; Buechel et al. 2018; Hancock, Chung, and Delgutte 2012). Potentially, this binaurally introduced 'jitter' could recover from monaural or binaural adaptation (Laback 2012).

4.7 From eardrum to conundrum and why preceding inhibition could contribute to set the beat

Our data suggest that the $envelope_{effect}$ (i.e., which might trigger tuning differences of the individual MSO input types) and short-term adaptation have a strong influence on the relative tuning of excitatory and inhibitory inputs that drive the coincidence mechanism in the MSO.
As a consequence, relative inputs can at some epochs even drive MSO neurons monaurally and hence ITDs will have little impact on spiking. Nonetheless, in most instances the relative binaural input strengths still allowed for binaural coincidence mechanisms through the TFS. We wondered if our data also could provide any clue as to the nature of this mechanism.
We had shown in study 1 that binaural interaction of inhibition and excitation naturally also affects the spike timing around the point of functional coincidence (Myoga et al. 2014; Beiderbeck et al. 2018). Likewise, we found that in MSO neurons that (despite monaural dominance) are still sensitive to differences in the TFS within epoch components, still exhibited changes in relative spike timing around its best ITD for a

particular noise stimulus (compare LSO results in study 1 for a detailed explanation how interaction of inhibition and excitation affects spike timing in specific ways). In individual neurons, spike timing was delayed at the rising slope of the NDF and advanced from the peak to the baseline of the NDF. The delay at the rising slope could be explained by preceding inhibition (compare to study 1) (Beiderbeck et al. 2018), since similar modulations have been observed in the LSO *in vivo* in study 1 and in adult MSO brain slices (Myoga et al. 2014). Thus, our data provided strong evidence that temporal interaction between excitatory and inhibitory inputs on microsecond timescales are critical for binaural processing in the MSO during ITD computation for complex wideband stimuli.

On a populational level, we identified similar modulation in spike timing as a function of ITD (within the epoch-component), however, the modulation in spike timing was highly variable, potentially due to different levels of monaural dominance, difference in individual input tuning within the spectral content and adaptation.

4.8 “Same Same!” - The LSO as the evolutionary blueprint for the MSO

From a conceptual point of view, any air-borne sound that travels from an off-midline sound source to either ear will encounter some level of friction and will generate ILDs to some degree (and sound cannot ‘travel through vacuum’ as there are no vibrating particles). On the other hand, any air-borne sound that travels from a sound source off-midline to either ear will generate ITDs to some degrees. Hence, strictly speaking, ITDs and ILDs are interdependent entities. Along the auditory pathway, any physiologically relevant ILD will generate a relation between inputs with regard to strength and timing and any physiologically relevant ITD will generate a relation between inputs with regard to timing and strength (whilst potential differences in tuning of inputs, and stimulus history can ultimately confuse or fine-tune this relationship; see study 2).

ILD-sensitivity has often been simplified as the ‘gaging of relative sound levels’ which misses a very important term: Timing. As we have learned from previous studies and also from study 1 in this thesis, the relative effects of inhibition (facilitation or suppression) require exquisite temporal register of binaural inputs on a cycle-by-cycle basis (Park et al. 1996; Sanes 1990; Irvine, Park, and McCormick 2001; P. X. Joris

and Yin 1995; Wu and Kelly 1991; Beiderbeck et al. 2018). Timing in the LSO becomes even more relevant, taking into account that it can be confused by relative energy levels that can result in different arrival times of relative inputs (time-intensity trading) (B. Grothe and Park 1995; Sanes 1990; Park et al. 1996) which again can affect the instantaneous functions of inhibition (i.e., suppression / PIF). The relevance of timing in the LSO becomes even more emphasized taking into account that LSO neurons are also sensitive to ITDs (Finlayson and Caspary 1991; Wu and Kelly 1991; P. X. Joris and Yin 1995; Park et al. 1996; Tollin and Yin 2005; Ashida, Kretzberg, and Tollin 2016).

Complementary, the importance of instantaneous strength in the MSO is an inherent part of its mechanism. During pure tone stimulation, the neuron will phase-lock to the rising slope of a single frequency waveform (Dietz et al. 2014). For different ITDs, these rising slopes will either be in- or out of temporal register between the two sides. Hence, with varying ITDs the relative timing of rising slopes and hence the relative instantaneous input strength will vary between sides (which will ultimately result in a 'classic' phasic ITD function (disregarding adaptation effects in this example)). In response to low frequency broadband noise, where MSO neurons can phase-lock to both TFS and to specific events in the $envelope_{effect}$ the relevance of relative instantaneous input strength (and its accompanying dynamics) becomes even more evident (see study 2). Rising slopes within the $envelope_{effect}$ can contain a unique instantaneous spectral composition. As it is a biological system, slight differences in the relative tuning of the 4 functional inputs to the MSO (excitation and inhibition from both sides) are likely and will ultimately generate differences in input strength, depending on how well the individual inputs are tuned to this instantaneous spectral composition. However, most studies in the MSO have been conducted using single pure tone stimuli or single frozen low-pass noise tokens under the assumption that relative input strengths are (and remain) constant. Yet our findings in study 2 show that dynamic $envelopes_{effect}$ can affect the binaural coincidence mechanism and overall ITD sensitivity which could be explained through aforementioned potential differences in frequency tuning of the four functional inputs. Whilst pure tone stimulation allows to study general temporal relationships between excitatory and inhibitory inputs as well as adaptational processes it covers the highly complex capacity of MSO neurons to dynamically encode ITDs in a highly complex natural

environment. The inclusion of complex stimuli in future experimental designs will therefore be essential to understand such dynamics in the MSO.

Ultimately, neurons in the MSO and LSO will both integrate energy per time interval (with the relative timing being as relevant as the relative energy). The MSO having 4 functional inputs rather than 2, does not necessarily change the fundamental mechanisms between LSO and MSO but rather emphasizes additional refinements with regard to 'effective time-intensity trading' (B. Grothe and Park 1995; Sanes 1990; Park et al. 1996). These refinements include an additional inhibitory input from the ipsilateral side which makes it reasonable to speculate that synaptic inhibition plays an essential role in the MSO circuit.

Taken together, when selective pressure on later mammals with larger body (and head) size required adaptation of a coincidence mechanism that enabled significant ITD sensitivity of low frequency sounds (see 1.3.7) (Grothe and Pecka 2014) it is very unlikely that the MSO evolved such a refined mechanism independently given the fact that the LSO is already well equipped for the required mechanism relying on coincidence and relative input strength itself. Our findings provide further evidence for the similarity in MSO- and LSO-mediated binaural processing through spiking phenomena in MSO neurons in study 2 that can be attributed to effects of preceding inhibition as discussed for the LSO in study 1.

4.9 Final conclusions

In general, the number of *in vivo* MSO data is limited due to small somatic action potentials (Scott, Mathews, and Golding 2010) and a large field potential (neurophonic) (Guinan, Guinan, and Norris 1972; Mc Laughlin, Verschooten, and Joris 2010) which makes data collection in MSO neurons in the intact brain particularly challenging. Additionally, the fact that the MSO receives both inhibition and excitation from each side complicates the interpretations of *in vivo* data, resulting in controversial discussions about the underlying mechanisms.

Methodological reductionism which is widely used in science and was therefore an attempted approach to reduce explanations to the smallest possible entities (van Riel and Van Gulick 2019). For studies in the auditory brainstem, reductionism was often restricted to pure tones or single broadband noise tokens typically using high carrier frequencies (Batra and Fitzpatrick 1997; McFadden and Pasanen 1976) that

disentangles phase locking to amplitude modulations from phase-locking to the TFS of the stimulus (due to the aforementioned cut-off for phase-locking at around 2-3 Hz (Johnson 1980)). Importantly, this form of reductionism allows to study the most fundamental capabilities of binaural coincidence detection and ITD sensitivity (Goldberg and Brown 1969; Pecka et al. 2008; Brand et al. 2002).

In particular the underlying mechanism that enables the compensation for external ITDs was found to be related to the CF of the neuron (McAlpine, Jiang, and Palmer 2001; Hancock and Delgutte 2004; Pecka et al. 2008). For pure tone stimulation, this manifests in systematically increasing best ITDs with decreasing characteristic frequencies typically at contra-leading ITDs outside the physiological range. How this underlying mechanism can be explained is a matter of debate (Brand et al. 2002; Pecka et al. 2008; Roberts, Seeman, and Golding 2013; van der Heijden et al. 2013; Franken, Bremen, and Joris 2014; Myoga et al. 2014; Plauška, Borst, and van der Heijden 2016). Importantly, it has been suggested that the functional meaning for this manifestation was the positioning of the slope in the center of the physiological range (Harper and McAlpine 2004).

One potential explanation for the underlying mechanism was suggested through preceding inhibition (Brand et al. 2002; Pecka et al. 2008):

It was shown that contralateral IPSPs can develop at MSO cell somata slightly earlier than contralateral excitatory postsynaptic potentials (EPSPs) despite the longer anatomical pathway and the additional synapse at the MNTB (Grothe and Sanes 1994; Grothe and Park 1998; Dodla, Svirskis, and Rinzel 2006; Roberts, Seeman, and Golding 2013). By iontophoretically blocking glycinergic inputs *in vivo*, firing rates in fact increased at the left-hand slope of the ITD function, shifting the maximal firing rates towards zero and moving the slope away from the physiological range (Brand et al. 2002; Pecka et al. 2008). It was therefore suggested that the temporal margin of inhibition is able to delay the net excitation (Myoga et al. 2014), therefore setting a delayed time window for neuronal excitability.

This explanation seems to impose high temporal demands on the MNTB input, but as indicated in 1.3.4 and shown *in vivo* in study 1 (LSO) contralateral inhibition can be functional on a cycle-by-cycle basis and *in vitro* studies have confirmed that IPSPs can precede EPSPs at MSO cell somata (Grothe and Sanes 1994; Roberts, Seeman, and Golding 2013). However, it was suggested, that contralateral inhibition alone cannot account for the degree of modulation that has been observed *in vivo* (Zhou,

Carney, and Colburn 2005; Jercog et al. 2010; Roberts, Seeman, and Golding 2013; van der Heijden et al. 2013).

In the LSO, by disentangling amplitude effects from effects specifically related to input timing, we demonstrate that inhibition controls spiking with microsecond precision throughout high frequency click trains, resulting in input timing-specific modulation of neuronal output. Furthermore, our data reveal that spiking is facilitated when contralateral inputs are functionally leading excitation within a precise time window. Importantly, our data suggest that post-inhibitory facilitation (PIF) can support ILD maintenance when excitatory inputs are weak. In addition*, in vitro* whole-cell recordings in mature LSO neurons confirm a reduction in the firing threshold due to prior hyperpolarization giving rise to PIF of otherwise sub-threshold synaptic events. This facilitatory effect based on microsecond precise differences between excitation and inhibition could therefore promote spatial sensitivity of faint sounds. In study 2, since low frequency neurons in the MSO are sensitive to both TFS and $envelopes_{effect}$ (as described in 1.3.8), our goal in study 2 was to disentangle the contribution of $envelopes_{effect}$ and stimulus TFS on ITD sensitivity through methodological post-hoc reductionism.

In order to identify the impact of $envelopes_{effect}$ I presented a battery of frozen broadband noise stimuli at various ITDs. Specifically, these stimuli share the same spectral contents (i.e., same carrier frequencies) but vary in their respective envelopes (i.e., their amplitude fluctuations across the stimulus). The post-hoc grouping of individual spikes into components that are highly influenced by the $envelope_{effect}$ and components that reflect a more balanced input relationship and ITD sensitivity that is reminiscent to TFS-mediated coincidence mechanisms enabled separate assessment of individual integrational mechanisms and the impact on overall ITD-sensitivity between groups.

Our data reveal that the interplay of $envelopes_{effect}$ and TFS of the stimulus not only impacts relative spike timing but also dynamically affects overall ITD sensitivity in low frequency MSO neurons. Interestingly, within each stimulus, we were able to identify specific events where spike timing was neatly matching the displacement of the monaural envelope across ITDs as it was introduced during headphone-based delivery. The findings of this study show that $envelopes_{effect}$ play a crucial role for binaural integration in low frequency MSO neurons. Specifically, we detected spiking phenomena in MSO neurons in study 2 that can be attributed to effects of preceding

inhibition as discussed for the LSO in study 1. These findings are in line with the aforementioned suggestions that the temporal margin of inhibition is able to delay the net excitation (Myoga et al. 2014), therefore setting a delayed time window for neuronal excitability (Pecka et al. 2008; Brand et al. 2002).

On top of that, we presented strong evidence for the regulation of ITD sensitivity through individual input tuning of functional excitatory and inhibitory inputs to the MSO within the spectral content ($envelopes_{effect}$) and through pre- and short-time adaptation which could mechanistically contribute to the law of the first wave front (Cremer 1948; Wallach, Newman, and Rosenzweig 1949). In this sense, mechanistically, our findings suggest the existence of “dynamic individual input stereausis”, i.e., potential differences in input tuning that affect the ITD detection mechanism which can include triggering of individual short-time adaptational processes. Hence both, study 1 and study 2 in this thesis provide strong evidence for the functional relevance of relative strength and timing of both, excitatory and inhibitory inputs which comprises a fundamental mechanism in any neural system.

5 Bibliography

Adams, J. C., and E. Mugnaini. 1990. 'Immunocytochemical Evidence for Inhibitory and Disinhibitory Circuits in the Superior Olive'. *Hearing Research* 49 (1–3): 281–98. https://doi.org/10.1016/0378-5955(90)90109-3.

Adunka, O., and J. Kiefer. 2005. 'Wie funktioniert der Sprachprozessor von Cochlea-Implantaten?' *Laryngo-Rhino-Otologie* 84 (11): 841–51. https://doi.org/10.1055/s-2005-870454.

Agapiou, J. P., and D. McAlpine. 2008. 'Low-Frequency Envelope Sensitivity Produces Asymmetric Binaural Tuning Curves'. *Journal of Neurophysiology* 100 (4): 2381–96. https://doi.org/10.1152/jn.90393.2008.

Ashida, G., J. Kretzberg, and D. J. Tollin. 2016. 'Roles for Coincidence Detection in Coding Amplitude-Modulated Sounds'. *PLoS Computational Biology* 12 (6): e1004997. https://doi.org/10.1371/journal.pcbi.1004997.

Bach, E. C., and K. Kandler. 2020. 'Long-Term Potentiation of Glycinergic Synapses by Semi-Natural Stimulation Patterns during Tonotopic Map Refinement'. *Scientific Reports* 10 (1): 16899. https://doi.org/10.1038/s41598-020-73050-y.

Banks, M. I., and P. H. Smith. 1992. 'Intracellular Recordings from Neurobiotin-Labeled Cells in Brain Slices of the Rat Medial Nucleus of the Trapezoid Body'. *The Journal of Neuroscience: The Official Journal of the Society for Neuroscience* 12 (7): 2819–37.

Batra, R., and D. C. Fitzpatrick. 1997. 'Neurons Sensitive to Interaural Temporal Disparities in the Medial Part of the Ventral Nucleus of the Lateral Lemniscus'. *Journal of Neurophysiology* 78 (1): 511–15. https://doi.org/10.1152/jn.1997.78.1.511.

Batra, R., S. Kuwada, and T. R. Stanford. 1993. 'High-Frequency Neurons in the Inferior Colliculus That Are Sensitive to Interaural Delays of Amplitude-Modulated Tones: Evidence for Dual Binaural Influences'. *Journal of Neurophysiology* 70 (1): 64–80. https://doi.org/10.1152/jn.1993.70.1.64.

Beiderbeck, B., M. H. Myoga, N. I. C. Müller, A. R. Callan, E. Friauf, B. Grothe, and M. Pecka. 2018. 'Precisely Timed Inhibition Facilitates Action Potential Firing for Spatial Coding in the Auditory Brainstem'. *Nature Communications* 9 (1): 1771. https://doi.org/10.1038/s41467-018-04210-y.

Békésy, G. von. 1947. 'The Variations of Phase along the Basilar Membrane with Sinusoidal Vibrations'. *J Acoust Soc Am* 19: 452–60.

Bernstein, L. R., and C. Trahiotis. 1985. 'Lateralization of Low-Frequency, Complex Waveforms: The Use of Envelope-Based Temporal Disparities'. *The Journal of the Acoustical Society of America* 77 (5): 1868–80. https://doi.org/10.1121/1.391938.

Blauert, J., and W. Lindemann. 1986. ‘Spatial Mapping of Intracranial Auditory Events for Various Degrees of Interaural Coherence’. *The Journal of the Acoustical Society of America* 79 (3): 806–13. https://doi.org/10.1121/1.393471.

Blauert, J. 1997. *Spatial Hearing: The Psychophysics of Human Sound Localization*. MIT Press.

Borst, J. G., and B. Sakmann. 1996. ‘Calcium Influx and Transmitter Release in a Fast CNS Synapse’. *Nature* 383 (6599): 431–34. https://doi.org/10.1038/383431a0.

Borst, J. G. G., and J. Soria van Hoeve. 2012. ‘The Calyx of Held Synapse: From Model Synapse to Auditory Relay’. *Annual Review of Physiology* 74: 199–224. https://doi.org/10.1146/annurev-physiol-020911-153236.

Boudreau, J. C., and C. Tsuchitani. 1968. ‘Binaural Interaction in the Cat Superior Olive S Segment’. *Journal of Neurophysiology* 31 (3): 442–54. https://doi.org/10.1152/jn.1968.31.3.442.

Brand, A., O. Behrend, T. Marquardt, D. McAlpine, and B. Grothe. 2002. ‘Precise Inhibition Is Essential for Microsecond Interaural Time Difference Coding’. *Nature* 417 (6888): 543–47. https://doi.org/10.1038/417543a.

Brawer, J. R., and D. K. Morest. 1975. ‘Relations between Auditory Nerve Endings and Cell Types in the Cat’s Anteroventral Cochlear Nucleus Seen with the Golgi Method and Nomarski Optics’. *The Journal of Comparative Neurology* 160 (4): 491–506. https://doi.org/10.1002/cne.901600406.

Brown, A. D., and D. J. Tollin. 2016. ‘Slow Temporal Integration Enables Robust Neural Coding and Perception of a Cue to Sound Source Location’. *The Journal of Neuroscience: The Official Journal of the Society for Neuroscience* 36 (38): 9908–21. https://doi.org/10.1523/JNEUROSCI.1421-16.2016.

Brownell, W. E., C. R. Bader, D. Bertrand, and Y. de Ribaupierre. 1985. ‘Evoked Mechanical Responses of Isolated Cochlear Outer Hair Cells’. *Science (New York, N.Y.)* 227 (4683): 194–96. https://doi.org/10.1126/science.3966153.

Browner, R. H., and D. B. Webster. 1975. ‘Projections of the Trapezoid Body and the Superior Olivary Complex of the Kangaroo Rat (Dipodomys Merriami)’. *Brain, Behavior and Evolution* 11 (5–6): 322–54. https://doi.org/10.1159/000123643.

Buechel, B. D., K. E. Hancock, Y. Chung, and B. Delgutte. 2018. ‘Improved Neural Coding of ITD with Bilateral Cochlear Implants by Introducing Short Inter-Pulse Intervals’. *Journal of the Association for Research in Otolaryngology: JARO* 19 (6): 681–702. https://doi.org/10.1007/s10162-018-00693-0.

Cant, N. B., and J. H. Casseday. 1986. ‘Projections from the Anteroventral Cochlear Nucleus to the Lateral and Medial Superior Olivary Nuclei’. *The Journal of*

Comparative Neurology 247 (4): 457–76. https://doi.org/10.1002/cne.902470406.

Cant, N. B., and R. L. Hyson. 1992. 'Projections from the Lateral Nucleus of the Trapezoid Body to the Medial Superior Olivary Nucleus in the Gerbil'. *Hearing Research* 58 (1): 26–34. https://doi.org/10.1016/0378-5955(92)90005-8.

Cant, N. B., and D. K. Morest. 1984. 'The Structural Basis for Stimulus Coding in the Cochlear Nucleus of the Cat'. *C. Berlin (Ed.), Recent Advances in Hearing Science, College Hill, San Diego*, 371–421.

Caspary, D. M., and C. L. Faingold. 1989. 'Non-N-Methyl-D-Aspartate Receptors May Mediate Ipsilateral Excitation at Lateral Superior Olivary Synapses'. *Brain Research* 503 (1): 83–90. https://doi.org/10.1016/0006-8993(89)91707-1.

Chirila, F. V., K. C. Rowland, J. M. Thompson, and G. A. Spirou. 2007. 'Development of Gerbil Medial Superior Olive: Integration of Temporally Delayed Excitation and Inhibition at Physiological Temperature'. *The Journal of Physiology* 584 (Pt 1): 167–90. https://doi.org/10.1113/jphysiol.2007.137976.

Couchman, K., B. Grothe, and F. Felmy. 2010. 'Medial Superior Olivary Neurons Receive Surprisingly Few Excitatory and Inhibitory Inputs with Balanced Strength and Short-Term Dynamics'. *The Journal of Neuroscience: The Official Journal of the Society for Neuroscience* 30 (50): 17111–21. https://doi.org/10.1523/JNEUROSCI.1760-10.2010.

Couchman, K., B. Grothe, and F. Felmy. 2012. 'Functional Localization of Neurotransmitter Receptors and Synaptic Inputs to Mature Neurons of the Medial Superior Olive'. *Journal of Neurophysiology* 107 (4): 1186–98. https://doi.org/10.1152/jn.00586.2011.

Dahmen, J. C., P. Keating, F. R. Nodal, A. L. Schulz, and A. J. King. 2010. 'Adaptation to Stimulus Statistics in the Perception and Neural Representation of Auditory Space'. *Neuron* 66 (6): 937–48. https://doi.org/10.1016/j.neuron.2010.05.018.

Dallos, P. 1985. 'Response Characteristics of Mammalian Cochlear Hair Cells'. *The Journal of Neuroscience: The Official Journal of the Society for Neuroscience* 5 (6): 1591–1608.

Dallos, P., J. Santos-Sacchi, and A. Flock. 1982. 'Intracellular Recordings from Cochlear Outer Hair Cells'. *Science (New York, N.Y.)* 218 (4572): 582–84. https://doi.org/10.1126/science.7123260.

Day, M. L., and M. N. Semple. 2011. 'Frequency-Dependent Interaural Delays in the Medial Superior Olive: Implications for Interaural Cochlear Delays'. *Journal of Neurophysiology* 106 (4): 1985–99. https://doi.org/10.1152/jn.00131.2011.

De No, L.. 1933. ‘Anatomy of the Eighth Nerve: III.—General Plan of Structure of the Primary Cochlear Nuclei’ The Laryngoscope. https://onlinelibrary.wiley.com/doi/abs/10.1288/00005537-193304000-00014.

Denève, S., and C. K. Machens. 2016. ‘Efficient Codes and Balanced Networks’. *Nature Neuroscience* 19 (3): 375–82. https://doi.org/10.1038/nn.4243.

Denk, W., J. R. Holt, G. M. Shepherd, and D. P. Corey. 1995. ‘Calcium Imaging of Single Stereocilia in Hair Cells: Localization of Transduction Channels at Both Ends of Tip Links’. *Neuron* 15 (6): 1311–21. https://doi.org/10.1016/0896-6273(95)90010-1.

Dietz, M., T. Marquardt, A. Stange, M. Pecka, B. Grothe, and D. McAlpine. 2014. ‘Emphasis of Spatial Cues in the Temporal Fine Structure during the Rising Segments of Amplitude-Modulated Sounds II: Single-Neuron Recordings’. *Journal of Neurophysiology* 111 (10): 1973–85. https://doi.org/10.1152/jn.00681.2013.

Dodla, R., G. Svirskis, and J. Rinzel. 2006. ‘Well-Timed, Brief Inhibition Can Promote Spiking: Postinhibitory Facilitation’. *Journal of Neurophysiology* 95 (4): 2664–77. https://doi.org/10.1152/jn.00752.2005.

Dodson, P. D., M. C. Barker, and I. D. Forsythe. 2002. ‘Two Heteromeric Kv1 Potassium Channels Differentially Regulate Action Potential Firing’. *The Journal of Neuroscience: The Official Journal of the Society for Neuroscience* 22 (16): 6953–61. https://doi.org/20026709.

Dreyer, A., and B. Delgutte. 2006. ‘Phase Locking of Auditory-Nerve Fibers to the Envelopes of High-Frequency Sounds: Implications for Sound Localization’. *Journal of Neurophysiology* 96 (5): 2327–41. https://doi.org/10.1152/jn.00326.2006.

Erulkar, S. D. 1972. ‘Comparative Aspects of Spatial Localization of Sound’. *Physiological Reviews* 52 (1): 237–360. https://doi.org/10.1152/physrev.1972.52.1.237.

Felix, R. A., A. Fridberger, S. Leijon, A. S. Berrebi, and A. K. Magnusson. 2011. ‘Sound Rhythms Are Encoded by Postinhibitory Rebound Spiking in the Superior Paraolivary Nucleus’. *The Journal of Neuroscience: The Official Journal of the Society for Neuroscience* 31 (35): 12566–78. https://doi.org/10.1523/JNEUROSCI.2450-11.2011.

Finlayson, P. G., and D. M. Caspary. 1989. ‘Synaptic Potentials of Chinchilla Lateral Superior Olivary Neurons’. *Hearing Research* 38 (3): 221–28.

Finlayson, P. G., and D. M. Caspary. 1991. ‘Low-Frequency Neurons in the Lateral Superior Olive Exhibit Phase-Sensitive Binaural Inhibition’. *Journal of Neurophysiology* 65 (3): 598–605. https://doi.org/10.1152/jn.1991.65.3.598.

Fischl, M. J., T. D. Combs, A. Klug, B. Grothe, and R. M. Burger. 2012. 'Modulation of Synaptic Input by GABAB Receptors Improves Coincidence Detection for Computation of Sound Location'. *The Journal of Physiology* 590 (13): 3047–66. https://doi.org/10.1113/jphysiol.2011.226233.

Fletcher, H.. 1940. 'Auditory Patterns'. *Reviews of Modern Physics* 12 (1): 47–65. https://doi.org/10.1103/RevModPhys.12.47.

Ford, M. C., O. Alexandrova, L. Cossell, A. Stange-Marten, J. Sinclair, C. Kopp-Scheinpflug, M. Pecka, D. Attwell, and B. Grothe. 2015. 'Tuning of Ranvier Node and Internode Properties in Myelinated Axons to Adjust Action Potential Timing'. *Nature Communications* 6 (August): 8073. https://doi.org/10.1038/ncomms9073.

Forsythe, I. D. 1994. 'Direct Patch Recording from Identified Presynaptic Terminals Mediating Glutamatergic EPSCs in the Rat CNS, in Vitro'. *The Journal of Physiology* 479 (Pt 3) (September): 381–87. https://doi.org/10.1113/jphysiol.1994.sp020303.

Forsythe, I. D., and M. Barnes-Davies. 1993. 'The Binaural Auditory Pathway: Excitatory Amino Acid Receptors Mediate Dual Timecourse Excitatory Postsynaptic Currents in the Rat Medial Nucleus of the Trapezoid Body'. *Proceedings. Biological Sciences* 251 (1331): 151–57. https://doi.org/10.1098/rspb.1993.0022.

Fortune, E. S., and G. J. Rose. 2001. 'Short-Term Synaptic Plasticity as a Temporal Filter'. *Trends in Neurosciences* 24 (7): 381–85. https://doi.org/10.1016/s0166-2236(00)01835-x.

Franken, T. P., P. Bremen, and P. X. Joris. 2014. 'Coincidence Detection in the Medial Superior Olive: Mechanistic Implications of an Analysis of Input Spiking Patterns'. *Frontiers in Neural Circuits* 8. https://doi.org/10.3389/fncir.2014.00042.

Franken, T. P, P. X Joris, and P. H Smith. 2018. 'Principal Cells of the Brainstem's Interaural Sound Level Detector Are Temporal Differentiators Rather than Integrators'. Edited by Catherine Emily Carr. *ELife* 7 (June): e33854. https://doi.org/10.7554/eLife.33854.

Franken, T. P., M. T. Roberts, L. Wei, N. L. Golding, and P. X. Joris. 2015. 'In Vivo Coincidence Detection in Mammalian Sound Localization Generates Phase Delays'. *Nature Neuroscience* 18 (3): 444–52. https://doi.org/10.1038/nn.3948.

Franssen, N. V. 1960. 'Some Considerations on the Mechanism of Directional Hearing'. https://repository.tudelft.nl/islandora/object/uuid%3Aaaf33a05-eb9b-446d-b45e-4009a19b6d2b.

Gittelman, J. X., and B. L. Tempel. 2006. 'Kv1.1-Containing Channels Are Critical for Temporal Precision during Spike Initiation'. *Journal of Neurophysiology* 96 (3): 1203–14. https://doi.org/10.1152/jn.00092.2005.

Glendenning, K. K., R. B. Masterton, B. N. Baker, and R. J. Wenthold. 1991. 'Acoustic Chiasm. III: Nature, Distribution, and Sources of Afferents to the Lateral Superior Olive in the Cat'. *The Journal of Comparative Neurology* 310 (3): 377–400. https://doi.org/10.1002/cne.903100308.

Goldberg, J. M., and P. B. Brown. 1968. 'Functional Organization of the Dog Superior Olivary Complex: An Anatomical and Electrophysiological Study'. *Journal of Neurophysiology* 31 (4): 639–56. https://doi.org/10.1152/jn.1968.31.4.639.

Goldberg, J. M., and P. B. Brown. 1969. 'Response of Binaural Neurons of Dog Superior Olivary Complex to Dichotic Tonal Stimuli: Some Physiological Mechanisms of Sound Localization'. *Journal of Neurophysiology* 32 (4): 613–36. https://doi.org/10.1152/jn.1969.32.4.613.

Goldwyn, J. H., M. McLaughlin, E. Verschooten, P. X. Joris, and J. Rinzel. 2017. 'Signatures of Somatic Inhibition and Dendritic Excitation in Auditory Brainstem Field Potentials'. *The Journal of Neuroscience: The Official Journal of the Society for Neuroscience* 37 (43): 10451–67. https://doi.org/10.1523/JNEUROSCI.0600-17.2017.

Griffin, S. J., L. R. Bernstein, N. J. Ingham, and D. McAlpine. 2005. 'Neural Sensitivity to Interaural Envelope Delays in the Inferior Colliculus of the Guinea Pig'. *Journal of Neurophysiology* 93 (6): 3463–78. https://doi.org/10.1152/jn.00794.2004.

Grothe, B., and T. J. Park. 1995. 'Time Can Be Traded for Intensity in the Lower Auditory System'. *Die Naturwissenschaften* 82 (11): 521–23. https://doi.org/10.1007/bf01134488.

Grothe, B., and D. H. Sanes. 1993. 'Bilateral Inhibition by Glycinergic Afferents in the Medial Superior Olive'. *Journal of Neurophysiology* 69 (4): 1192–96. https://doi.org/10.1152/jn.1993.69.4.1192.

Grothe, B., and D. H. Sanes 1994. 'Synaptic Inhibition Influences the Temporal Coding Properties of Medial Superior Olivary Neurons: An in Vitro Study'. *The Journal of Neuroscience: The Official Journal of the Society for Neuroscience* 14 (3 Pt 2): 1701–9.

Grothe, B., and T. J. Park. 1998. 'Sensitivity to Interaural Time Differences in the Medial Superior Olive of a Small Mammal, the Mexican Free-Tailed Bat'. *Journal of Neuroscience* 18 (16): 6608–22. https://doi.org/10.1523/JNEUROSCI.18-16-06608.1998.

Grothe, B., and M. Pecka. 2014. ‘The Natural History of Sound Localization in Mammals – a Story of Neuronal Inhibition’. *Frontiers in Neural Circuits* 8. https://doi.org/10.3389/fncir.2014.00116.

Grothe, B., M. Pecka, and D. McAlpine. 2010. ‘Mechanisms of Sound Localization in Mammals’. *Physiological Reviews* 90 (3): 983–1012. https://doi.org/10.1152/physrev.00026.2009.

Guinan, J. J., S. S. Guinan, and B. E. Norris. 1972. ‘Single Auditory Units in the Superior Olivary Complex: I: Responses to Sounds and Classifications Based on Physiological Properties’. *International Journal of Neuroscience* 4 (3): 101–20. https://doi.org/10.3109/00207457209147165.

Guinan, J. J., B. E. Norris, and S. S. Guinan. 1972. ‘Single Auditory Units in the Superior Olivary Complex: II: Locations of Unit Categories and Tonotopic Organization’. *International Journal of Neuroscience* 4 (4): 147–66. https://doi.org/10.3109/00207457209164756.

Hall, J. L. 1964. ‘Minimum Detectable Change in Interaural Time or Intensity Difference for Brief Impulsive Stimuli’. *The Journal of the Acoustical Society of America* 36 (12): 2411–13. https://doi.org/10.1121/1.1919372.

Hancock, K. E., Y. Chung, and B. Delgutte. 2012. ‘Neural ITD Coding with Bilateral Cochlear Implants: Effect of Binaurally Coherent Jitter’. *Journal of Neurophysiology* 108 (3): 714–28. https://doi.org/10.1152/jn.00269.2012.

Hancock, K. E., and B. Delgutte. 2004. ‘A Physiologically Based Model of Interaural Time Difference Discrimination’. *The Journal of Neuroscience: The Official Journal of the Society for Neuroscience* 24 (32): 7110–17. https://doi.org/10.1523/JNEUROSCI.0762-04.2004.

Harper, N. S., and D. McAlpine. 2004. ‘Optimal Neural Population Coding of an Auditory Spatial Cue’. *Nature* 430 (7000): 682–86. https://doi.org/10.1038/nature02768.

Harris, D. M., and P. Dallos. 1979. ‘Forward Masking of Auditory Nerve Fiber Responses’. *Journal of Neurophysiology* 42 (4): 1083–1107. https://doi.org/10.1152/jn.1979.42.4.1083.

Harrison, J. M., and W. B. Warr. 1962. ‘A Study of the Cochlear Nuclei and Ascending Auditory Pathways of the Medulla’. *The Journal of Comparative Neurology* 119 (December): 341–79. https://doi.org/10.1002/cne.901190306.

Heijden, M. van der, J. A. M. Lorteije, A. Plauška, M. T. Roberts, N. L. Golding, and J. G. G. Borst. 2013. ‘Directional Hearing by Linear Summation of Binaural Inputs at the Medial Superior Olive’. *Neuron* 78 (5): 936–48. https://doi.org/10.1016/j.neuron.2013.04.028.

Heil, P., and H. Neubauer. 2001. ‘Temporal Integration of Sound Pressure Determines Thresholds of Auditory-Nerve Fibers’. *The Journal of*

Neuroscience 21 (18): 7404–15. https://doi.org/10.1523/JNEUROSCI.21-18-07404.2001.

Held, H. 1893. 'Die Zentrale Gehoerleistung'. *Arch. Anat. Physiol. Anat. Abt. 201–48*.

Hershkowitz, R. M., and N. I. Durlach. 1969. 'Interaural Time and Amplitude Jnds for a 500-Hz Tone'. *The Journal of the Acoustical Society of America* 46 (6): 1464–67. https://doi.org/10.1121/1.1911887.

Higgs, M. H., and W. J. Spain. 2011. 'Kv1 Channels Control Spike Threshold Dynamics and Spike Timing in Cortical Pyramidal Neurones'. *The Journal of Physiology* 589 (Pt 21): 5125–42. https://doi.org/10.1113/jphysiol.2011.216721.

Hornbostel, E. M. von, and M. Wertheimer. 1920. *Über die Wahrnehmung der Schallrichtung*. Berlin: Akademie der Wissenschaften.

Huang, H., and L. O. Trussell. 2011. 'KCNQ5 Channels Control Resting Properties and Release Probability of a Synapse'. *Nature Neuroscience* 14 (7): 840–47. https://doi.org/10.1038/nn.2830.

Hudspeth, A. J. 1982. 'Extracellular Current Flow and the Site of Transduction by Vertebrate Hair Cells'. *The Journal of Neuroscience: The Official Journal of the Society for Neuroscience* 2 (1): 1–10.

Hudspeth, A. J. 1985. 'The Cellular Basis of Hearing: The Biophysics of Hair Cells'. *Science (New York, N.Y.)* 230 (4727): 745–52. https://doi.org/10.1126/science.2414845.

Hudspeth, A. J. 1989. 'How the Ear's Works Work'. *Nature* 341 (6241): 397–404. https://doi.org/10.1038/341397a0.

Irvine, D. R. 1987. 'Interaural Intensity Differences in the Cat: Changes in Sound Pressure Level at the Two Ears Associated with Azimuthal Displacements in the Frontal Horizontal Plane'. *Hearing Research* 26 (3): 267–86. https://doi.org/10.1016/0378-5955(87)90063-3.

Irvine, D. R., V. N. Park, and J. B. Mattingley. 1995. 'Responses of Neurons in the Inferior Colliculus of the Rat to Interaural Time and Intensity Differences in Transient Stimuli: Implications for the Latency Hypotheses'. *Hearing Research* 85 (1–2): 127–41. https://doi.org/10.1016/0378-5955(95)00040-b.

Irvine, D. R., V. N. Park, and L. McCormick. 2001. 'Mechanisms Underlying the Sensitivity of Neurons in the Lateral Superior Olive to Interaural Intensity Differences'. *Journal of Neurophysiology* 86 (6): 2647–66. https://doi.org/10.1152/jn.2001.86.6.2647.

Ishikawa, T., Y. Nakamura, N. Saitoh, W.-B. Li, S. Iwasaki, and T. Takahashi. 2003. 'Distinct Roles of Kv1 and Kv3 Potassium Channels at the Calyx of Held

Presynaptic Terminal'. *The Journal of Neuroscience: The Official Journal of the Society for Neuroscience* 23 (32): 10445–53.

Jeffress, L. A. 1948. 'A Place Theory of Sound Localization'. *Journal of Comparative and Physiological Psychology* 41 (1): 35–39. https://doi.org/10.1037/h0061495.

Jeffress, L. A., H. C. Blodgett, and B. H. Deatherage. 1962. 'Effect of Interaural Correlation on the Precision of Centering a Noise'. *The Journal of the Acoustical Society of America* 34 (8): 1122–23. https://doi.org/10.1121/1.1918257.

Jercog, P. E., G. Svirskis, V. C. Kotak, D. H. Sanes, and J. Rinzel. 2010. 'Asymmetric Excitatory Synaptic Dynamics Underlie Interaural Time Difference Processing in the Auditory System'. *PLoS Biology* 8 (6): e1000406. https://doi.org/10.1371/journal.pbio.1000406.

Johnson, D. H. 1980. 'The Relationship between Spike Rate and Synchrony in Responses of Auditory-Nerve Fibers to Single Tones'. *The Journal of the Acoustical Society of America* 68 (4): 1115–22. https://doi.org/10.1121/1.384982.

Johnston, J., S. J. Griffin, C. Baker, A. Skrzypiec, T. Chernova, and I. D. Forsythe. 2008. 'Initial Segment Kv2.2 Channels Mediate a Slow Delayed Rectifier and Maintain High Frequency Action Potential Firing in Medial Nucleus of the Trapezoid Body Neurons'. *The Journal of Physiology* 586 (14): 3493–3509. https://doi.org/10.1113/jphysiol.2008.153734.

Joris, P. X., L. H. Carney, P. H. Smith, and T. C. Yin. 1994. 'Enhancement of Neural Synchronization in the Anteroventral Cochlear Nucleus. I. Responses to Tones at the Characteristic Frequency'. *Journal of Neurophysiology* 71 (3): 1022–36. https://doi.org/10.1152/jn.1994.71.3.1022.

Joris, P. X., P. H. Smith, and T. C. Yin. 1994. 'Enhancement of Neural Synchronization in the Anteroventral Cochlear Nucleus. II. Responses in the Tuning Curve Tail'. *Journal of Neurophysiology* 71 (3): 1037–51. https://doi.org/10.1152/jn.1994.71.3.1037.

Joris, P. X., and T. C. Yin. 1992. 'Responses to Amplitude-Modulated Tones in the Auditory Nerve of the Cat'. *The Journal of the Acoustical Society of America* 91 (1): 215–32. https://doi.org/10.1121/1.402757.

Joris, P. X., and T. C. Yin. 1995. 'Envelope Coding in the Lateral Superior Olive. I. Sensitivity to Interaural Time Differences'. *Journal of Neurophysiology* 73 (3): 1043–62. https://doi.org/10.1152/jn.1995.73.3.1043.

Joris, P. X. 2003. 'Interaural Time Sensitivity Dominated by Cochlea-Induced Envelope Patterns'. *The Journal of Neuroscience* 23 (15): 6345–50. https://doi.org/10.1523/JNEUROSCI.23-15-06345.2003.

Joris, P. X., D. H. Louage, L. Cardoen, and M. van der Heijden. 2006. 'Correlation Index: A New Metric to Quantify Temporal Coding'. *Hearing Research* 216–217 (July): 19–30. https://doi.org/10.1016/j.heares.2006.03.010.

Joris, P. X., and P. H. Smith. 2008. 'The Volley Theory and the Spherical Cell Puzzle'. *Neuroscience* 154 (1): 65–76. https://doi.org/10.1016/j.neuroscience.2008.03.002.

Joris, P. X., and L. O. Trussell. 2018. 'The Calyx of Held: A Hypothesis on the Need for Reliable Timing in an Intensity-Difference Encoder'. *Neuron* 100 (3): 534–49. https://doi.org/10.1016/j.neuron.2018.10.026.

Joris, P. X., and T. C. Yin. 2007. 'A Matter of Time: Internal Delays in Binaural Processing'. *Trends in Neurosciences* 30 (2): 70–78. https://doi.org/10.1016/j.tins.2006.12.004.

Kiang, N. Y.-S.. 1965. 'Discharge Patterns of Single Fibers in the Cat's Auditory Nerve.' STR-13. Massachusetts Inst of Tech Cambridge Research Lab of Electronics. https://apps.dtic.mil/docs/citations/AD0633419.

Kim, G., and K. Kandler. 2003. 'Elimination and Strengthening of Glycinergic/GABAergic Connections during Tonotopic Map Formation'. *Nature Neuroscience* 6 (3): 282–90. https://doi.org/10.1038/nn1015.

Kim, J. H., C. Kushmerick, and H. von Gersdorff. 2010. 'Presynaptic Resurgent Na+ Currents Sculpt the Action Potential Waveform and Increase Firing Reliability at a CNS Nerve Terminal'. *The Journal of Neuroscience: The Official Journal of the Society for Neuroscience* 30 (46): 15479–90. https://doi.org/10.1523/JNEUROSCI.3982-10.2010.

Klemm, O. 1920. 'Ueber Den Einfluss Des Binauralen Zeitunterschiedes Aud de Localisation'. *Arch. Ges. Psychol.* 40: 123–29.

Kopp-Scheinpflug, C., S. Tolnai, M. S. Malmierca, and R. Rübsamen. 2008. 'The Medial Nucleus of the Trapezoid Body: Comparative Physiology'. *Neuroscience* 154 (1): 160–70. https://doi.org/10.1016/j.neuroscience.2008.01.088.

Kopp-Scheinpflug, C., A. J. B. Tozer, S. W. Robinson, B. L. Tempel, M. H. Hennig, and I. D. Forsythe. 2011. 'The Sound of Silence: Ionic Mechanisms Encoding Sound Termination'. *Neuron* 71 (5): 911–25. https://doi.org/10.1016/j.neuron.2011.06.028.

Kuwabara, N., and J. M. Zook. 1992. 'Projections to the Medial Superior Olive from the Medial and Lateral Nuclei of the Trapezoid Body in Rodents and Bats'. *The Journal of Comparative Neurology* 324 (4): 522–38. https://doi.org/10.1002/cne.903240406.

Laback, B.. 2012. 'Neural Basis of Improved ITD Sensitivity with Jitter'. *Journal of Neurophysiology* 108 (3): 712–13. https://doi.org/10.1152/jn.00422.2012.

Leão, R. M., C. Kushmerick, R. Pinaud, R. Renden, G.-L. Li, H. Taschenberger, G. Spirou, S. R. Levinson, and H. von Gersdorff. 2005. 'Presynaptic Na+ Channels: Locus, Development, and Recovery from Inactivation at a High-Fidelity Synapse'. *Journal of Neuroscience* 25 (14): 3724–38. https://doi.org/10.1523/JNEUROSCI.3983-04.2005.

Lindenbeck, M. J., B. Laback, P. Majdak, and S. Srinivasan. 2020. 'Temporal-Pitch Sensitivity in Electric Hearing with Amplitude Modulation and Inserted Pulses with Short Inter-Pulse Intervals'. *The Journal of the Acoustical Society of America* 147 (2): 777. https://doi.org/10.1121/10.0000610.

Lindsey, B. G. 1975. 'Fine Structure and Distribution of Axon Terminals from the Cochlear Nucleus on Neurons in the Medial Superior Olivary Nucleus of the Cat'. *The Journal of Comparative Neurology* 160 (1): 81–103. https://doi.org/10.1002/cne.901600106.

Lorteije, J. A. M., S. I. Rusu, C. Kushmerick, and J. G. G. Borst. 2009. 'Reliability and Precision of the Mouse Calyx of Held Synapse'. *The Journal of Neuroscience: The Official Journal of the Society for Neuroscience* 29 (44): 13770–84. https://doi.org/10.1523/JNEUROSCI.3285-09.2009.

Lothar C. 1948. 'Die Wissenschaftlichen Grundlagen Der Raumakustik'. *Hirzel-Verlag Stuttgart*, no. Bd. 1.

Magnusson, A. K., C. Kapfer, B. Grothe, and U. Koch. 2005. 'Maturation of Glycinergic Inhibition in the Gerbil Medial Superior Olive after Hearing Onset'. *The Journal of Physiology* 568 (Pt 2): 497–512. https://doi.org/10.1113/jphysiol.2005.094763.

Maki, K., and S. Furukawa. 2005. 'Acoustical Cues for Sound Localization by the Mongolian Gerbil, Meriones Unguiculatus'. *The Journal of the Acoustical Society of America* 118 (2): 872–86. https://doi.org/10.1121/1.1944647.

Mc Laughlin, M., E. Verschooten, and P. X. Joris. 2010. 'Oscillatory Dipoles as a Source of Phase Shifts in Field Potentials in the Mammalian Auditory Brainstem'. *The Journal of Neuroscience: The Official Journal of the Society for Neuroscience* 30 (40): 13472–87. https://doi.org/10.1523/JNEUROSCI.0294-10.2010.

McAlpine, D., D. Jiang, and A. R. Palmer. 2001. 'A Neural Code for Low-Frequency Sound Localization in Mammals'. *Nature Neuroscience* 4 (4): 396–401. https://doi.org/10.1038/86049.

McAlpine, D., and B. Grothe. 2003. 'Sound Localization and Delay Lines--Do Mammals Fit the Model?' *Trends in Neurosciences* 26 (7): 347–50. https://doi.org/10.1016/S0166-2236(03)00140-1.

McFadden, D., and E. G. Pasanen. 1976. 'Lateralization at High Frequencies Based on Interaural Time Differences'. *The Journal of the Acoustical Society of America* 59 (3): 634–39. https://doi.org/10.1121/1.380913.

Meng, X., G. Huguet, and J. Rinzel. 2012. ‘Type III Excitability, Slope Sensitivity and Coincidence Detection’. *Discrete and Continuous Dynamical Systems. Series A* 32 (8): 2729–57. https://doi.org/10.3934/dcds.2012.32.2729.

Mikiel-Hunter, J., V. Kotak, and J. Rinzel. 2016. ‘High-Frequency Resonance in the Gerbil Medial Superior Olive’. *PLoS Computational Biology* 12 (11): e1005166. https://doi.org/10.1371/journal.pcbi.1005166.

Moore, B. C. 1986. ‘Parallels between Frequency Selectivity Measured Psychophysically and in Cochlear Mechanics’. *Scandinavian Audiology. Supplementum* 25: 139–52.

Moore, B. C. J. 1998. *Cochlear Hearing Loss*. Wiley.

Moore, L.T., and H.S. Fry. 1907. ‘On the Appreciation of Differences of Phase of Sound-Waves’,. *Phil Mag* 6: 452–59.

Morest, D. K. 1968. ‘The Collateral System of the Medial Nucleus of the Trapezoid Body of the Cat, Its Neuronal Architecture and Relation to the Olivo-Cochlear Bundle’. *Brain Research* 9 (2): 288–311. https://doi.org/10.1016/0006-8993(68)90235-7.

Myoga, M. H., S. Lehnert, C. Leibold, F. Felmy, and B. Grothe. 2014. ‘Glycinergic Inhibition Tunes Coincidence Detection in the Auditory Brainstem’. *Nature Communications* 5 (May): 3790. https://doi.org/10.1038/ncomms4790.

Naidu, R. C., and D. C. Mountain. 2007. ‘Basilar Membrane Tension Calculations for the Gerbil Cochlea’. *The Journal of the Acoustical Society of America* 121 (2): 994–1002. https://doi.org/10.1121/1.2404916.

Nicol, M. J., and B. Walmsley. 2002. ‘Ultrastructural Basis of Synaptic Transmission between Endbulbs of Held and Bushy Cells in the Rat Cochlear Nucleus’. *The Journal of Physiology* 539 (Pt 3): 713–23. https://doi.org/10.1113/jphysiol.2001.012972.

Oertel, D. 1999. ‘The Role of Timing in the Brain Stem Auditory Nuclei of Vertebrates’. *Annual Review of Physiology* 61: 497–519. https://doi.org/10.1146/annurev.physiol.61.1.497.

Ollo, C., and I. R. Schwartz. 1979. ‘The Superior Olivary Complex in C57BL/6 Mice’. *The American Journal of Anatomy* 155 (3): 349–73. https://doi.org/10.1002/aja.1001550306.

Osen, K. K. 1969. ‘Cytoarchitecture of the Cochlear Nuclei in the Cat’. *The Journal of Comparative Neurology* 136 (4): 453–84. https://doi.org/10.1002/cne.901360407.

Ostapoff, E. M., and D. K. Morest. 1991. ‘Synaptic Organization of Globular Bushy Cells in the Ventral Cochlear Nucleus of the Cat: A Quantitative Study’. *The*

Journal of Comparative Neurology 314 (3): 598–613. https://doi.org/10.1002/cne.903140314.

Palmer, A. R. 1987. 'Physiology of the Cochlear Nerve and Cochlear Nucleus'. *British Medical Bulletin* 43 (4): 838–55. https://doi.org/10.1093/oxfordjournals.bmb.a072221.

Palmer, A. R., and I. J. Russell. 1986. 'Phase-Locking in the Cochlear Nerve of the Guinea-Pig and Its Relation to the Receptor Potential of Inner Hair-Cells'. *Hearing Research* 24 (1): 1–15. https://doi.org/10.1016/0378-5955(86)90002-x.

Palmer, A. R. 1982. 'Encoding of Rapid Amplitude Fluctuations by Cochlear-Nerve Fibres in the Guinea-Pig'. *Archives of Oto-Rhino-Laryngology* 236 (2): 197–202. https://doi.org/10.1007/BF00454039.

Park, T. J., B. Grothe, G. D. Pollak, G. Schuller, and U. Koch. 1996. 'Neural Delays Shape Selectivity to Interaural Intensity Differences in the Lateral Superior Olive'. *The Journal of Neuroscience* 16 (20): 6554–66. https://doi.org/10.1523/JNEUROSCI.16-20-06554.1996.

Pecka, M., A. Brand, O. Behrend, and B. Grothe. 2008. 'Interaural Time Difference Processing in the Mammalian Medial Superior Olive: The Role of Glycinergic Inhibition'. *Journal of Neuroscience* 28 (27): 6914–25. https://doi.org/10.1523/JNEUROSCI.1660-08.2008.

Phillips, D. P., M. B. Calford, J. D. Pettigrew, L. M. Aitkin, and M. N. Semple. 1982. 'Directionality of Sound Pressure Transformation at the Cat's Pinna'. *Hearing Research* 8 (1): 13–28. https://doi.org/10.1016/0378-5955(82)90031-4.

Pickles, J. O. 1982. *An Introduction to the Physiology of Hearing*. Academic Press.

Plauška, A., J. G. Borst, and M. van der Heijden. 2016. 'Predicting Binaural Responses from Monaural Responses in the Gerbil Medial Superior Olive'. *Journal of Neurophysiology* 115 (6): 2950–63. https://doi.org/10.1152/jn.01146.2015.

Plauška, A., M. van der Heijden, and J. G. G. Borst. 2017. 'A Test of the Stereausis Hypothesis for Sound Localization in Mammals'. *Journal of Neuroscience* 37 (30): 7278–89. https://doi.org/10.1523/JNEUROSCI.0233-17.2017.

Pollak, G. D. 1988. 'Time Is Traded for Intensity in the Bat's Auditory System'. *Hearing Research* 36 (2–3): 107–24. https://doi.org/10.1016/0378-5955(88)90054-8.

Rautenberg, P. L., B. Grothe, and F. Felmy. 2009. 'Quantification of the Three-Dimensional Morphology of Coincidence Detector Neurons in the Medial Superior Olive of Gerbils during Late Postnatal Development'. *The Journal of Comparative Neurology* 517 (3): 385–96. https://doi.org/10.1002/cne.22166.

Rayleigh, Lord (J. W. Strutt). 1907. ‘On Our Perception of Sound Direction. Philosophical Magazine Series 6 13, 214-232.’ *Philosophical Magazine Series* 6 (13): 214–32. https://doi.org/10.1080/14786440709463595.

Rhode, W. S., and P. H. Smith. 1985. ‘Characteristics of Tone-Pip Response Patterns in Relationship to Spontaneous Rate in Cat Auditory Nerve Fibers’. *Hearing Research* 18 (2): 159–68.

Rhode, W. S., and P. H. Smith. 1986. ‘Physiological Studies on Neurons in the Dorsal Cochlear Nucleus of Cat’. *Journal of Neurophysiology* 56 (2): 287–307. https://doi.org/10.1152/jn.1986.56.2.287.

Riel, R. van, and R. Van Gulick. 2019. ‘Scientific Reduction’. In *The Stanford Encyclopedia of Philosophy*, edited by Edward N. Zalta, Spring 2019. Metaphysics Research Lab, Stanford University. https://plato.stanford.edu/archives/spr2019/entries/scientific-reduction/.

Roberts, M. T., S. C. Seeman, and N. L. Golding. 2013. ‘A Mechanistic Understanding of the Role of Feedforward Inhibition in the Mammalian Sound Localization Circuitry’. *Neuron* 78 (5): 923–35. https://doi.org/10.1016/j.neuron.2013.04.022.

Roberts, M. T., S. C. Seeman, and N. L. Golding. 2014. ‘The Relative Contributions of MNTB and LNTB Neurons to Inhibition in the Medial Superior Olive Assessed through Single and Paired Recordings’. *Frontiers in Neural Circuits* 8: 49. https://doi.org/10.3389/fncir.2014.00049.

Rose, J. E., J. F. Brugge, D. J. Anderson, and J. E. Hind. 1967. ‘Phase-Locked Response to Low-Frequency Tones in Single Auditory Nerve Fibers of the Squirrel Monkey’. *Journal of Neurophysiology* 30 (4): 769–93. https://doi.org/10.1152/jn.1967.30.4.769.

Rosowski, J. J., and A. Graybeal. 1991. ‘What Did Morganucodon Hear?’ *Zoological Journal of the Linnean Society* 101 (2): 131–68. https://doi.org/10.1111/j.1096-3642.1991.tb00890.x.

Ruggero, M. A. 1973. ‘Response to Noise of Auditory Nerve Fibers in the Squirrel Monkey’. *Journal of Neurophysiology* 36 (4): 569–87. https://doi.org/10.1152/jn.1973.36.4.569.

Ruggero, M. A., N. C. Rich, A. Recio, S. S. Narayan, and L. Robles. 1997. ‘Basilar-Membrane Responses to Tones at the Base of the Chinchilla Cochlea’. *The Journal of the Acoustical Society of America* 101 (4): 2151–63. https://doi.org/10.1121/1.418265.

Russell, I. J., and P. M. Sellick. 1978. ‘Intracellular Studies of Hair Cells in the Mammalian Cochlea’. *The Journal of Physiology* 284 (November): 261–90. https://doi.org/10.1113/jphysiol.1978.sp012540.

Ryugo, D. K., and D. M. Fekete. 1982. ‘Morphology of Primary Axosomatic Endings in the Anteroventral Cochlear Nucleus of the Cat: A Study of the Endbulbs of Held’. *The Journal of Comparative Neurology* 210 (3): 239–57. https://doi.org/10.1002/cne.902100304.

Ryugo, D. K., and S. Sento. 1991. ‘Synaptic Connections of the Auditory Nerve in Cats: Relationship between Endbulbs of Held and Spherical Bushy Cells’. *The Journal of Comparative Neurology* 305 (1): 35–48. https://doi.org/10.1002/cne.903050105.

Sakitt, B. 1973. ‘Indices of Discriminability’. *Nature* 241 (5385): 133–34. https://doi.org/10.1038/241133a0.

Sanes, D. H. 1990. ‘An in Vitro Analysis of Sound Localization Mechanisms in the Gerbil Lateral Superior Olive’. *Journal of Neuroscience* 10 (11): 3494–3506. https://doi.org/10.1523/JNEUROSCI.10-11-03494.1990.

Sanes, D. H., and V. Siverls. 1991. ‘Development and Specificity of Inhibitory Terminal Arborizations in the Central Nervous System’. *Journal of Neurobiology* 22 (8): 837–54. https://doi.org/10.1002/neu.480220805.

Schofield, B. R., and N. B. Cant. 1991. ‘Organization of the Superior Olivary Complex in the Guinea Pig. I. Cytoarchitecture, Cytochrome Oxidase Histochemistry, and Dendritic Morphology’. *The Journal of Comparative Neurology* 314 (4): 645–70. https://doi.org/10.1002/cne.903140403.

Schuller, G., S. Radtke-Schuller, and M. Betz. 1986. ‘A Stereotaxic Method for Small Animals Using Experimentally Determined Reference Profiles’. *Journal of Neuroscience Methods* 18 (4): 339–50. https://doi.org/10.1016/0165-0270(86)90022-1.

Scott, L. L., P. J. Mathews, and N. L. Golding. 2005. ‘Posthearing Developmental Refinement of Temporal Processing in Principal Neurons of the Medial Superior Olive’. *The Journal of Neuroscience: The Official Journal of the Society for Neuroscience* 25 (35): 7887–95. https://doi.org/10.1523/JNEUROSCI.1016-05.2005.

Scott, L. L., P. J. Mathews, and N. L. Golding. 2010. ‘Perisomatic Voltage-Gated Sodium Channels Actively Maintain Linear Synaptic Integration in Principal Neurons of the Medial Superior Olive’. *The Journal of Neuroscience: The Official Journal of the Society for Neuroscience* 30 (6): 2039–50. https://doi.org/10.1523/JNEUROSCI.2385-09.2010.

Shamma, S. A., N. M. Shen, and P. Gopalaswamy. 1989. ‘Stereausis: Binaural Processing without Neural Delays’. *The Journal of the Acoustical Society of America* 86 (3): 989–1006. https://doi.org/10.1121/1.398734.

Shinn-Cunningham, B. G., S. Santarelli, and N. Kopco. 2000. ‘Tori of Confusion: Binaural Localization Cues for Sources within Reach of a Listener’. *The Journal of the Acoustical Society of America* 107 (3): 1627–36. https://doi.org/10.1121/1.428447.

Smith, P. H. 1995. ‘Structural and Functional Differences Distinguish Principal from Nonprincipal Cells in the Guinea Pig MSO Slice’. *Journal of Neurophysiology* 73 (4): 1653–67. https://doi.org/10.1152/jn.1995.73.4.1653.

Smith, P. H., P. X. Joris, L. H. Carney, and T. C. Yin. 1991. ‘Projections of Physiologically Characterized Globular Bushy Cell Axons from the Cochlear Nucleus of the Cat’. *The Journal of Comparative Neurology* 304 (3): 387–407. https://doi.org/10.1002/cne.903040305.

Smith, P. H., P. X. Joris, and T. C. Yin. 1993. ‘Projections of Physiologically Characterized Spherical Bushy Cell Axons from the Cochlear Nucleus of the Cat: Evidence for Delay Lines to the Medial Superior Olive’. *The Journal of Comparative Neurology* 331 (2): 245–60. https://doi.org/10.1002/cne.903310208.

Smith, P. H., P. X. Joris, and T. C. Yin. 1998. ‘Anatomy and Physiology of Principal Cells of the Medial Nucleus of the Trapezoid Body (MNTB) of the Cat’. *Journal of Neurophysiology* 79 (6): 3127–42. https://doi.org/10.1152/jn.1998.79.6.3127.

Smith, P. H., and W. S. Rhode. 1987. ‘Characterization of HRP-Labeled Globular Bushy Cells in the Cat Anteroventral Cochlear Nucleus’. *The Journal of Comparative Neurology* 266 (3): 360–75. https://doi.org/10.1002/cne.902660305.

Smith, R. L. 1977. ‘Short-Term Adaptation in Single Auditory Nerve Fibers: Some Poststimulatory Effects’. *Journal of Neurophysiology* 40 (5): 1098–1111. https://doi.org/10.1152/jn.1977.40.5.1098.

Smith, R. L. 1979. ‘Adaptation, Saturation, and Physiological Masking in Single Auditory-Nerve Fibers’. *The Journal of the Acoustical Society of America* 65 (1): 166–78. https://doi.org/10.1121/1.382260.

Sommer, I., K. Lingenhöhl, and E. Friauf. 1993. ‘Principal Cells of the Rat Medial Nucleus of the Trapezoid Body: An Intracellular in Vivo Study of Their Physiology and Morphology’. *Experimental Brain Research* 95 (2): 223–39. https://doi.org/10.1007/bf00229781.

Song, P., Y. Yang, M. Barnes-Davies, A. Bhattacharjee, M. Hamann, I. D. Forsythe, D. L. Oliver, and L. K. Kaczmarek. 2005. ‘Acoustic Environment Determines Phosphorylation State of the Kv3.1 Potassium Channel in Auditory Neurons’. *Nature Neuroscience* 8 (10): 1335–42. https://doi.org/10.1038/nn1533.

Sonntag, M., B. Englitz, C. Kopp-Scheinpflug, and R. Rübsamen. 2009. ‘Early Postnatal Development of Spontaneous and Acoustically Evoked Discharge Activity of Principal Cells of the Medial Nucleus of the Trapezoid Body: An in Vivo Study in Mice’. *The Journal of Neuroscience: The Official Journal of the Society for Neuroscience* 29 (30): 9510–20. https://doi.org/10.1523/JNEUROSCI.1377-09.2009.

Spirou, G. A., and A. S. Berrebi. 1997. ‘Glycine Immunoreactivity in the Lateral Nucleus of the Trapezoid Body of the Cat’. *The Journal of Comparative Neurology* 383 (4): 473–88.

Spirou, G. A., W. E. Brownell, and M. Zidanic. 1990. ‘Recordings from Cat Trapezoid Body and HRP Labeling of Globular Bushy Cell Axons’. *Journal of Neurophysiology* 63 (5): 1169–90. https://doi.org/10.1152/jn.1990.63.5.1169.

Srinivasan, S., B. Laback, P. Majdak, and B. Delgutte. 2018. ‘Introducing Short Interpulse Intervals in High-Rate Pulse Trains Enhances Binaural Timing Sensitivity in Electric Hearing’. *Journal of the Association for Research in Otolaryngology: JARO* 19 (3): 301–15. https://doi.org/10.1007/s10162-018-0659-7.

Stange, A., M. H. Myoga, A. Lingner, M. C. Ford, O. Alexandrova, F. Felmy, M. Pecka, I. Siveke, and B. Grothe. 2013. ‘Adaptation in Sound Localization: From GABA(B) Receptor-Mediated Synaptic Modulation to Perception’. *Nature Neuroscience* 16 (12): 1840–47. https://doi.org/10.1038/nn.3548.

Stevens, S. S., and E. B. Newman. 1936. ‘The Localization of Actual Sources of Sound’. *The American Journal of Psychology* 48 (2): 297–306. https://doi.org/10.2307/1415748.

Stotler, W. A. 1953. ‘An Experimental Study of the Cells and Connections of the Superior Olivary Complex of the Cat’. *The Journal of Comparative Neurology* 98 (3): 401–31.

Svirskis, G., V. Kotak, D. H. Sanes, and J. Rinzel. 2004. ‘Sodium Along With Low-Threshold Potassium Currents Enhance Coincidence Detection of Subthreshold Noisy Signals in MSO Neurons’. *Journal of Neurophysiology* 91 (6): 2465–73. https://doi.org/10.1152/jn.00717.2003.

Tolbert, L. P., D. K. Morest, and D. A. Yurgelun-Todd. 1982. ‘The Neuronal Architecture of the Anteroventral Cochlear Nucleus of the Cat in the Region of the Cochlear Nerve Root: Horseradish Peroxidase Labelling of Identified Cell Types’. *Neuroscience* 7 (12): 3031–52. https://doi.org/10.1016/0306-4522(82)90228-7.

Tollin, D. J., K. Koka, and J. J. Tsai. 2008. ‘Interaural Level Difference Discrimination Thresholds for Single Neurons in the Lateral Superior Olive’. *The Journal of Neuroscience: The Official Journal of the Society for Neuroscience* 28 (19): 4848–60. https://doi.org/10.1523/JNEUROSCI.5421-07.2008.

Tollin, D. J., and T. C. Yin. 2005. ‘Interaural Phase and Level Difference Sensitivity in Low-Frequency Neurons in the Lateral Superior Olive’. *The Journal of Neuroscience: The Official Journal of the Society for Neuroscience* 25 (46): 10648–57. https://doi.org/10.1523/JNEUROSCI.1609-05.2005.

Tsuchitani, C. 1977. ‘Functional Organization of Lateral Cell Groups of Cat Superior Olivary Complex’. *Journal of Neurophysiology* 40 (2): 296–318. https://doi.org/10.1152/jn.1977.40.2.296.

Tsuchitani, C. 1988. ‘The Inhibition of Cat Lateral Superior Olive Unit Excitatory Responses to Binaural Tone Bursts. I. The Transient Chopper Response’. *Journal of Neurophysiology* 59 (1): 164–83. https://doi.org/10.1152/jn.1988.59.1.164.

Tsuchitani, C. 1997. ‘Input from the Medial Nucleus of Trapezoid Body to an Interaural Level Detector’. *Hearing Research* 105 (1–2): 211–24. https://doi.org/10.1016/s0378-5955(96)00212-2.

Tsuchitani, C., and J. C. Boudreau. 1969. ‘Stimulus Level of Dichotically Presented Tones and Cat Superior Olive S-Segment Cell Discharge’. *The Journal of the Acoustical Society of America* 46 (4B): 979–88. https://doi.org/10.1121/1.1911818.

Wallach, H., E. B. Newman, and M. R. Rosenzweig. 1949. ‘The Precedence Effect in Sound Localization’. *The American Journal of Psychology* 62 (3): 315–36.

Wang, L.-Y., L. Gan, I. D. Forsythe, and L. K. Kaczmarek. 1998. ‘Contribution of the Kv3.1 Potassium Channel to High-Frequency Firing in Mouse Auditory Neurones’. *The Journal of Physiology* 509 (1): 183–94. https://doi.org/10.1111/j.1469-7793.1998.183bo.x.

Wang, Y., and P. B. Manis. 2008. ‘Short-Term Synaptic Depression and Recovery at the Mature Mammalian Endbulb of Held Synapse in Mice’. *Journal of Neurophysiology* 100 (3): 1255–64. https://doi.org/10.1152/jn.90715.2008.

Warr, W. B. 1966. ‘Fiber Degeneration Following Lesions in the Anterior Ventral Cochlear Nucleus of the Cat’. *Experimental Neurology* 14 (4): 453–74. https://doi.org/10.1016/0014-4886(66)90130-0.

Webster, D. B, and M. Webster. 1980. ‘Morphological Adaptations of the Ear in the Rodent Family Heteromyidae’. *American Zoologist* 20 (1): 247–54. https://doi.org/10.1093/icb/20.1.247.

Westerman, L. A., and R. L. Smith. 1987. ‘Conservation of Adapting Components in Auditory-Nerve Responses’. *The Journal of the Acoustical Society of America* 81 (3): 680–91. https://doi.org/10.1121/1.394836.

Wever, E. G., and C. W. Bray. 1930. ‘Present Possibilities for Auditory Theory’. *Psychological Review* 37 (5): 365–80. https://doi.org/10.1037/h0075002.

Wever, E. G., J. G. McCormick, J. Palin, and S. H. Ridgway. 1971. ‘Cochlea of the Dolphin, Tursiops Truncatus: The Basilar Membrane’. *Proceedings of the National Academy of Sciences of the United States of America* 68 (11): 2708–11. https://doi.org/10.1073/pnas.68.11.2708.

Wiener, F. M., R. R. Pfeiffer, and A. S. Backus. 1966. ‘On the Sound Pressure Transformation by the Head and Auditory Meatus of the Cat’. *Acta Oto-Laryngologica* 61 (3): 255–69. https://doi.org/10.3109/00016486609127062.

Wu, S. H., and J. B. Kelly. 1991. ‘Physiological Properties of Neurons in the Mouse Superior Olive: Membrane Characteristics and Postsynaptic Responses Studied in Vitro’. *Journal of Neurophysiology* 65 (2): 230–46. https://doi.org/10.1152/jn.1991.65.2.230.

Yang, H., and M. A. Xu-Friedman. 2008. ‘Relative Roles of Different Mechanisms of Depression at the Mouse Endbulb of Held’. *Journal of Neurophysiology* 99 (5): 2510–21. https://doi.org/10.1152/jn.01293.2007.

Yates, G. K., A. R. Cody, and B. M. Johnstone. 1983. ‘Recovery of Eighth Nerve Action Potential Thresholds after Exposure to Short, Intense Pure Tones: Similarities with Temporary Threshold Shift’. *Hearing Research* 12 (3): 305–22. https://doi.org/10.1016/0378-5955(83)90003-5.

Yates, G. K., D. Robertson, and B. M. Johnstone. 1985. ‘Very Rapid Adaptation in the Guinea Pig Auditory Nerve’. *Hearing Research* 17 (1): 1–12. https://doi.org/10.1016/0378-5955(85)90124-8.

Yin, T. C., and J. C. Chan. 1990. ‘Interaural Time Sensitivity in Medial Superior Olive of Cat’. *Journal of Neurophysiology* 64 (2): 465–88. https://doi.org/10.1152/jn.1990.64.2.465.

Yin, T. C., J. A. Hirsch, and J. C. Chan. 1985. ‘Responses of Neurons in the Cat’s Superior Colliculus to Acoustic Stimuli. II. A Model of Interaural Intensity Sensitivity’. *Journal of Neurophysiology* 53 (3): 746–58. https://doi.org/10.1152/jn.1985.53.3.746.

Yost, W., and R. Dye. 1988. ‘Discrimination of Interaural Differences of Level as a Function of Frequency’. *The Journal of the Acoustical Society of America* 83 (June): 1846–51. https://doi.org/10.1121/1.396520.

Zhang, Y., C. K. Kim, K.-J.-B. Lee, and Y. Park. 2007. ‘Resultant Pressure Distribution Pattern along the Basilar Membrane in the Spiral Shaped Cochlea’. *Journal of Biological Physics* 33 (3): 195–211. https://doi.org/10.1007/s10867-007-9052-1.

Zhou, Y., L. H. Carney, and H. S. Colburn. 2005. ‘A Model for Interaural Time Difference Sensitivity in the Medial Superior Olive: Interaction of Excitatory and Inhibitory Synaptic Inputs, Channel Dynamics, and Cellular Morphology’. *The Journal of Neuroscience: The Official Journal of the Society for Neuroscience* 25 (12): 3046–58. https://doi.org/10.1523/JNEUROSCI.3064-04.2005.

6 List of Figures

7 List of Tables

8 Glossary

ANF	Auditory nerve fiber
AP	Action potential
CC	Cross-Correlation
CF	Characteristic frequency
CN	Cochlear nucleus
cTD	Composite timing delays
DAB	3, 3′-diaminbenzidine
DNLL	Dorsal nucleus of the lateral lemniscus
EE	Excitatory / Excitatory
EI	Excitatory / Inhibitory
EPSP	Excitatory postsynaptic potential
G_e	Excitatory conductance
Gi	Inhibitory conductance
GBC	Globular bushy cell
HCN	Hyperpolarization-activated cyclic nucleotide-gated
HRP	Horseradish peroxidase
IC	Inferior colliculus
ICI	Inter-click interval
I_h	Inward current through opening of HCN-channels
IPD	Interaural phase difference
ISI	Inter-stimulus interval
ILD	Interaural level difference
ISPS	Inhibitory postsynaptic potential
ITD	Interaural time difference

LNTB	Lateral Nucleus of the Trapezoid Body
LSO	Lateral Superior Olive
MNTB	Medial Nucleus of the Trapezoid Body
MSO	Medial Superior Olive
NDF	Noise-delay function
PBS	Phosphate-buffered saline
PFA	Paraformaldehyde
PIF	Post-inhibitory facilitation
rTD	Relative timing difference
SBC	Spherical bushy cells
SOC	Superior olivary complex
TFS	Temporal fine structure

9 List of publications

Presented publications in this thesis:

Beiderbeck, B., M. H. Myoga, N. I. C. Müller, A. R. Callan, E. Friauf, B. Grothe, and M. Pecka. 2018. 'Precisely Timed Inhibition Facilitates Action Potential Firing for Spatial Coding in the Auditory Brainstem'. *Nature Communications* 9 (1): 1771. https://doi.org/10.1038/s41467-018-04210-y.

Additional publications not presented in this thesis:

Keplinger, S., B. Beiderbeck, S. Michalakis, M. Biel, B. Grothe, and L. Kunz. 2018. 'Optogenetic Control of Neural Circuits in the Mongolian Gerbil'. *Frontiers in Cellular Neuroscience* 12: 111. https://doi.org/10.3389/fncel.2018.00111.

Müller, M., B. Beiderbeck, B. Grothe, and M. Pecka. 2018. 'Comparison of Temporal Processing in the Auditory Brainstem Neurons between Acoustic and Electrical Hearing'. *The Journal of the Acoustical Society of America* 143 (3): 1783–84. https://doi.org/10.1121/1.5035838.

10. Acknowledgements

First and foremost, I want to thank my supervisor, mentor and friend PD Dr. Michael Pecka for his constant and enduring believe in me. Over the years and across the planet, you have challenged me on numerous occasions to step outside of my comfort zone and to allow myself to grow. Your critical view inspired me and I have learned so much over the years (not only about good coffee, food and music). With your positive input and motivational speeches to keep on going (and well…to speed up towards the end), I was able to channel my inner PIF to get this thesis completed. And this is exactly why I came to the final conclusion that it was not like a rebound spike after all ;)

I especially want to thank Prof. Dr. Benedikt Grothe:
Whilst Georg von Békésy once said that the selection of his particular field in science was 'pure accident', for me, a dream came true when I was given the opportunity to work in auditory neuroscience under your 'B-wing' on the third floor. Thank you for your trust and support.

I also want to thank my other thesis advisory committee members Dr. Thorsten Marquardt and Prof. Dr.-Ing. Werner Hemmert for their great suggestions and discussions during our TAC-meetings.

Thank you, Prof. Dr. David McAlpine, for inviting me several times to meet the brightest minds in the brightest places in and around Sydney, Australia. And also, for numerous lessons on dry humor which certainly equipped me for a life in the UK.
Thank you, Dr. Jason Mikiel-Hunter, for helping me with the analysis in study 2 and for all your time and numerous inspiring discussions.

In addition, I would like to thank Prof. Dr. Michael Myoga, Dr. Alexander Callen, Dr. Nicolas Müller, and Prof. Dr. Eckhard Friauf for your collaboration on study 1.

I would like to thank the Graduate School of Systemic Neurosciences: Thank you for all your support, flexibility and help especially in these challenging times.

Thank you….
… Ela for all your input, support and help, I was very lucky to have you as my lab buddy, especially during our long CI experiments. I really admire your endurance in anything you do!
… Steffi, Dani, Dieter, Helge, Diana and Shreya. Thank you for ‘chair scooter’, laughter, and a restricted amount of oxygen in our little living room. It was a blast!
… to Hilde, Sven, Todd, Lars, Stefan and all of AG Grothe, it was a pleasure working with you all!

Finally, I would like to express my deep and sincere gratitude to my family for their love and support. To my fiancé, Wayne: Thank you for cooking all the healthy food and making all the coffee when I had no time for anything but sitting at the desk for countless hours. Thank you for doing everything you can to support me, because I could have not finished this without you.

11. Declaration of author contributions

11.1 Study 1 (Published)

These authors contributed equally: Barbara Beiderbeck, Michael H. Myoga.

These authors jointly supervised this work: Benedikt Grothe, Michael Pecka.

Affiliations

1. Department Biology II, Division of Neurobiology, Ludwig-Maximilians-Universität Munich, Planegg-Martinsried, 82152, Germany
   Barbara Beiderbeck, Michael H. Myoga, Alexander R. Callan, Benedikt Grothe & Michael Pecka

2. Graduate School of Systemic Neurosciences, Ludwig-Maximilians-Universität Munich, Planegg-Martinsried, 82152, Germany
   Barbara Beiderbeck & Alexander R. Callan

3. Max Planck Institute of Neurobiology, Am Klopferspitz 18, Martinsried, 82152, Germany
   Michael H. Myoga & Benedikt Grothe

4. Department of Biology, Animal Physiology Group, University of Kaiserslautern, Kaiserslautern, 67653, Germany
   Nicolas I. C. Müller & Eckhard Friauf

Contributions

B.B. performed *in vivo* experiments and histology, analyzed the *in vivo* data and contributed to writing the paper. M.H.M. designed and performed *in vitro* experiments and pharmacology, analyzed *in vitro* data and contributed to writing the paper. N.M. designed and performed *in vitro* experiments. A.R.C. performed *in vitro* experiments. E.F. designed *in vitro* experiments and contributed to writing the paper. B.G. conceived the experiments and contributed to writing the paper. M.P. conceived and designed the experiments, analyzed the *in vivo* data and wrote the paper.

Corresponding authors
Correspondence to B.G. or M.P.

11.2 Study 2 (Not published)

These authors jointly supervised this work: Michael Pecka, David McAlpine, Benedikt Grothe

Affiliations

1. Department Biology II, Division of Neurobiology, Ludwig-Maximilians-Universität Munich, Planegg-Martinsried, 82152, Germany
   Barbara Beiderbeck, Benedikt Grothe & Michael Pecka

2. Graduate School of Systemic Neurosciences, Ludwig-Maximilians-Universität Munich, Planegg-Martinsried, 82152, Germany
   Barbara Beiderbeck

3. Department of Linguistics, Macquarie University, North Ryde, NSW 2109, Australia
   Jason Mikiel-Hunter, David McAlpine

Contributions

B.B. performed *in vivo* experiments and histology, analyzed the *in vivo* data and wrote the manuscript presented in this thesis. J. M.-H. analyzed the *in vivo* data and contributed to the design of the experiments. M.P., D.M.A. and B.G. designed and conceived *in vivo* experiments.

Corresponding authors
Correspondence to M.P.